AD NUMBER: AD0853822

LIMITATION CHANGES

TO:

Approved for public release; distribution is unlimited.

FROM:

Distribution authorized to U.S. Gov't. agencies and their contractors; Administrative/Operational Use; 01 JUN 1969. Other requests shall be referred to Office of Naval Research, Arlington, VA 22203.

AUTHORITY

SAMSO ltr dtd 19 JAN 1972

ADVANCED DECOY TECHNOLOGY PROGRAM
ADTECH IV
FINAL REPORT (U)

APPENDIX III
MATHEMATICAL FORMULATION - OPTIMUM DECOY DESIGN PROGRAM

Prepared by

AVCO GOVERNMENT PRODUCTS GROUP
MISSILE SYSTEMS DIVISION
201 Lowell Street
Wilmington, Massachusetts 01887

AVMSD-0465-68-RR, APP. III
Contract F04701-68-C-0012

June 1969

Prepared for

SPACE AND MISSILE SYSTEMS ORGANIZATION
DEPUTY FOR REENTRY SYSTEMS
AIR FORCE SYSTEMS COMMAND
Norton Air Force Base, California 92409

FOR OFFICIAL USE ONLY

SAMSO TR-69-140, APP. III

This document consists of 150 pages,
126 copies, Series A

ADVANCED DECOY TECHNOLOGY PROGRAM
ADTECH IV
FINAL REPORT (U)

APPENDIX III
MATHEMATICAL FORMULATION - OPTIMUM DECOY DESIGN PROGRAM

Prepared by

AVCO GOVERNMENT PRODUCTS GROUP
MISSILE SYSTEMS DIVISION
201 Lowell Street
Wilmington, Massachusetts 01887

AVMSD-0465-68-RR, APP. III
Contract F04701-68-C-0012

June 1969

Sponsored by

Advanced Research Projects Agency
Department of Defense
ARPA Order No. 441, Amendment No. 12

Prepared for

SPACE AND MISSILE SYSTEMS ORGANIZATION
DEPUTY FOR REENTRY SYSTEMS
AIR FORCE SYSTEMS COMMAND
Norton Air Force Base, California 92409

UNCLASSIFIED ABSTRACT

(U) This technical report describes analyses and techniques used in the design and evaluation of advanced decoy concepts. The work described addresses both the design of specific penetration aid elements and the formulation of techniques for their evaluation. The three major technical areas covered in this report are:

1. Investigation of a penetration aid technique that degrades the measurement capability of the radar sensor.

2. The design of a computer program to solve the decoy design problem with flexibility in the selection of optimization criteria and constraints.

3. Studies of the use of certain discrimination techniques for a hard point defense system.

This appendix to this report contains detailed description of the mathematical and engineering formulation of the optimum decoy design program.

EDITED BY:
EDITORIAL SERVICES SECTION
R. L. Tucker

CONTENTS

CONTENTS (Concl'd)

ILLUSTRATIONS

TABLES

1.0 INTRODUCTION AND PURPOSE OF PROGRAM

1.1 PURPOSE AND GENERAL REMARKS

The Optimum Decoy Design Program selects optimum decoy configurations which meet specified performance, weight, and geometric constraints. Optimum typically means minimum weight for a given set of performance and geometric constraints or minimum value of a performance parameter for a given weight and set of geometric constraints. Mutually exclusive constraints, for which there is no acceptable solution, are identified by the program. The program is capable of operating in a mode which allows it to search for any decoy which meets all the constraints, (solution-finder) as well as the mode where the search is for the optimum decoy within all the constraints. The selection processes involve the minimization of non-linear functions subject to non-linear constraints. The analysis portion of the program includes trajectory calculations (which can include the effects of mass loss, nose blunting, thrust, trailing appendages, and angle of attack), wake RCS and length approximations, and effectiveness operations. The program is designed primarily for sharp and blunt cone decoys and reference reentry vehicles. An option is provided which allows an arbitrary reference reentry vehicle to be utilized provided its performance histories are available for input.

The analysis portion of this program does not represent Avco's most accurate prediction techniques but rather represents a carefully balanced set of engineering approximations which are utilized to maintain the required compromise between accuracy and running time for configuration selection studies. The analysis portion of the program does not explicitly contain calculations for the internal arrangements of the equipment inside the decoys or for the exoatmospheric observables. The effects of these requirements on the decoy configuration selection process have usually been included as geometric constraints on the decoy.

The ADTECH III contract resulted in a computer code which performed the solution-finding operations automatically for constraints based on trajectory matching requirements (Ref. III-1). The objective of the ADTECH IV effort in this area was to develop, document, and deliver a computerized decoy configuration selection program which can select optimum decoys considering trajectory, effectiveness, and wake performance parameters. This objective was achieved by utilizing and extending the results obtained in the ADTECH III computer program. The ADTECH III solution-finding program represents the first steps toward the application of digital machine optimization to the decoy design problem. The analysis portion (function generator) of that program contains the decoy trajectory calculations and the comparison of the physical characteristics of the decoy trajectory with the reference reentry vehicle trajectory. The synthesis portion of the program utilizes a penalty-function equation to transform the constrained design problem into an unconstrained search problem. This penalty-function equation was formulated to be compatible with the later extension of the program to include optimization capability. Optimization techniques are applied to the transformed function until any decoy is obtained which is within all the constraints. During the ADTECH IV effort, the ADTECH III program was extended in the analysis portion to include effectiveness operations and observables approximation and extended in the synthesis portion to include the capability for finding the optimum decoy design which is also within all the constraints.

The program developed during ADTECH IV, when given an initial decoy design, the ranges of interest of the decoy parameters, and the system constraints and optimization criteria, will find the best vehicle which is within all the constraints or will establish that there is no solution to the problem. For example, the program is able to find the minimum weight decoy which is within the geometric and observables constraints and which has a trajectory that matches a reference trajectory within specified tolerances (corridors). The program also is able to find the vehicle which minimizes a parameter related to the Avco effectiveness model (probability of discrimination) and is also within specified weight and geometric constraints.

1.2 SUMMARY OF THE COMPUTER PROGRAM FORMULATION

The major elements of the Optimum Decoy Design Program are outlined in Figure III-1. The key problem in formulating this design program has been the integration of many subroutines into an efficient engineering design program. These subroutines fall into two major categories. The first category includes those subroutines which perform the analysis tasks that generate vehicle configurations and that generate the aerodynamic and trajectory behavior of these configurations. In addition, this portion determines reentry observables, performs a comparison analysis between the decoy and reentry vehicle, and places constraints on the observable behavior of the R/V and decoy. These constraints are generally of a corridor type or of an effectiveness parameter type.

The general decoy conceptual design which can be modeled by this program is defined by the thirteen independent design variables identified in Figure III-2. Besides the normal blunt cone design parameters, provisions are made to consider variable geometry techniques, in which the decoy's geometric and mass characteristics can be changed in flight at a designated altitude. In addition, an ion generator or rocket motor can be incorporated whose operational characteristics are controlled by the analysis portion of the program. The decoy design problem then is the search for the numbers defining a decoy configuration which meets all the systems requirements and constraints and is optimum with respect to some specified payoff quantity. This analysis portion of the optimum decoy program is thus a compendium of many Avco analysis procedures that have been efficiently combined into this program.

The second major portion of the optimum decoy design program is the synthesis section which employs selected optimization techniques to find optimum solutions to the decoy design problem. The optimization techniques chosen for inclusion in this program are the Davidon Variable Metric Technique, the Rosenbrock Rotating Coordinate Technique, and the one- and two-variable Fibonacci techniques. The formulation of the program will be discussed in more detail in the following paragraphs.

As shown in Figure III-1, the analysis and synthesis portions of the program require inputs which define the problem statement and the options required for obtaining a solution.

The inputs to the program include the systems requirements, the starting configuration, and the ranges of allowable parameter variations. A solution to the problem can consist of any decoy configuration which meets all the system requirements and constraints, or it can be an optimum decoy configuration which is within all the constraints, depending on whether the "solution-finding" or "optimum-finding" options are selected.

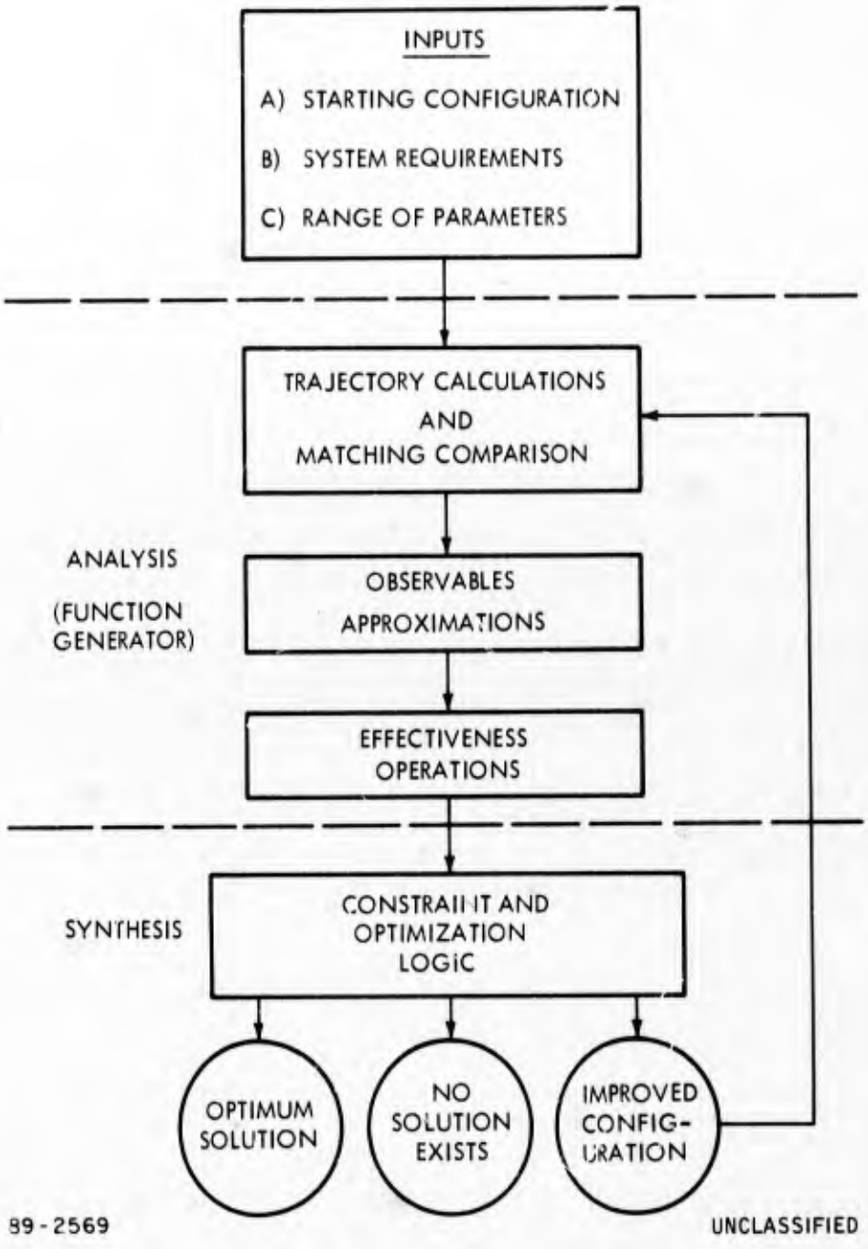

Figure III-1 ADTECH OPTIMUM DECOY DESIGN PROGRAM

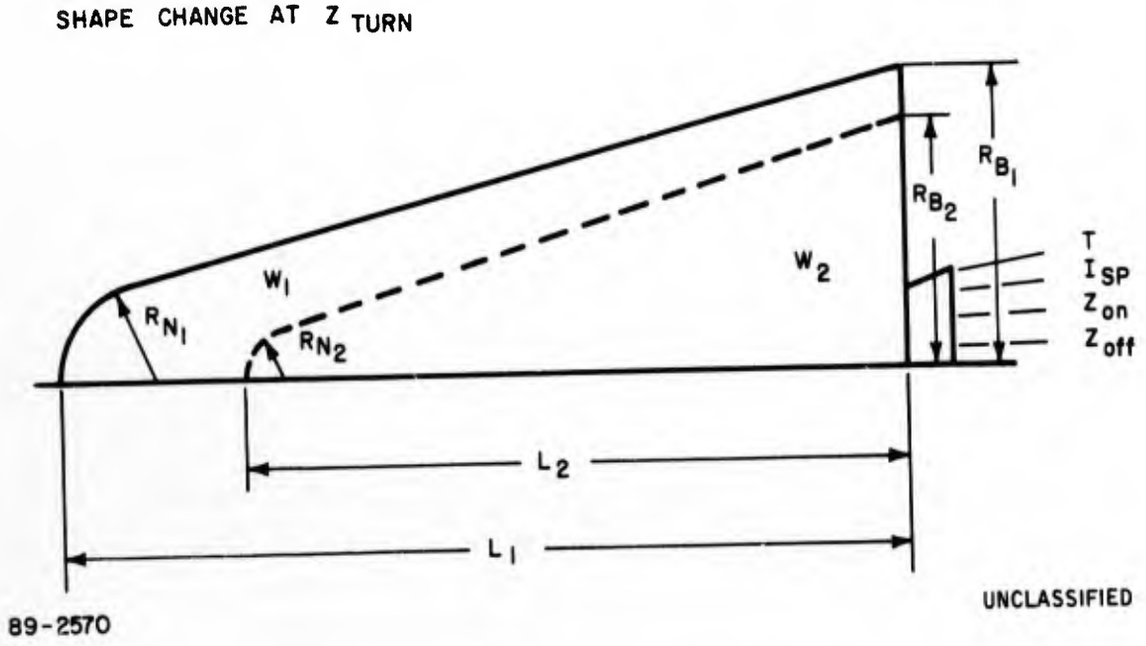

Figure III-2 ILLUSTRATION OF A COMPLEX DESIGN PROBLEM

With the inputs to the problem specified, the trajectory and observables of the initial decoy are calculated in the analysis portion of the program and these data are compared with the reference reentry vehicle data to determine the "performance" of this particular decoy. The effects on the performance as a result of changing the parameters of the decoy configuration slightly are also calculated if required by the synthesis portion of the program. These effects are called influence coefficients or partial derivatives or collectively, the gradient. With this information from the analysis portion of the program, the synthesis portion of the program changes the decoy configuration to make it more acceptable and the analysis is repeated for the new decoy. This process is continued until a decoy is determined which meets all the stated requirements or until it is determined that there is no acceptable decoy. The later case comes about because it is possible to state a problem for which there is no solution. That is, the problem may be over-constrained. The program is designed to identify such a situation and indicate that no solution exists for the stated problem. In addition, the program defines a decoy which is "closest" to being acceptable.

The term configuration in this context implies the specification of the values of the design variables. An example is shown in Figure III-2 where there are thirteen design variables which must be determined. This decoy initially has a weight, W_1, and a shape defined by the nose radius, R_{N_1}, base radius, R_{B_1}, and length, L_1. At some altitude, Z_{TURN}, the outer shape is removed and the decoy immediately after that altitude is defined by the parameters W_2, R_{N_2}, R_{B_2}, and L_2. In addition, there is an ion generator or rocket motor which initiates at some altitude, Z_{on}, and burns out at some altitude, Z_{off}. The thrust is specified at some value, T, and the mass loss due to thrust is determined from the thrust and the specified value of specific impulse, I_{sp}. The decoy design problem then is the search for the numbers defining a decoy configuration which meets all the systems requirements and constraints.

The problems involved with the specification of "suitable" performance or systems requirements is not within the scope of this task. The systems requirements for input to the program must be provided from separate studies. For example, velocity histories for a reentry vehicle and a decoy are shown in Figure III-3. The question of whether or not this "match" allows the decoy to perform its mission in some environment is considered to be a systems problem outside the scope of this computer code. However, once the system requirements are provided, one of the essential features of the program is the capability for determining whether or not a particular decoy meets the stated requirements.

In addition to the requirements which may be placed on the trajectory and the observables there are design constraints which place limits on the weight and geometry of the decoy. For example, the length and base radius might be limited by the design of an existing deployment system.

The search for an acceptable decoy configuration is then typically bounded by a number of constraints, some trajectory related, some observables related, and some related to the size, shape, and mass of the decoy.

Provisions are included to constrain each of the design parameters between lower and upper limits if desired. The program can accept any combination of the constraints which are available in the program.

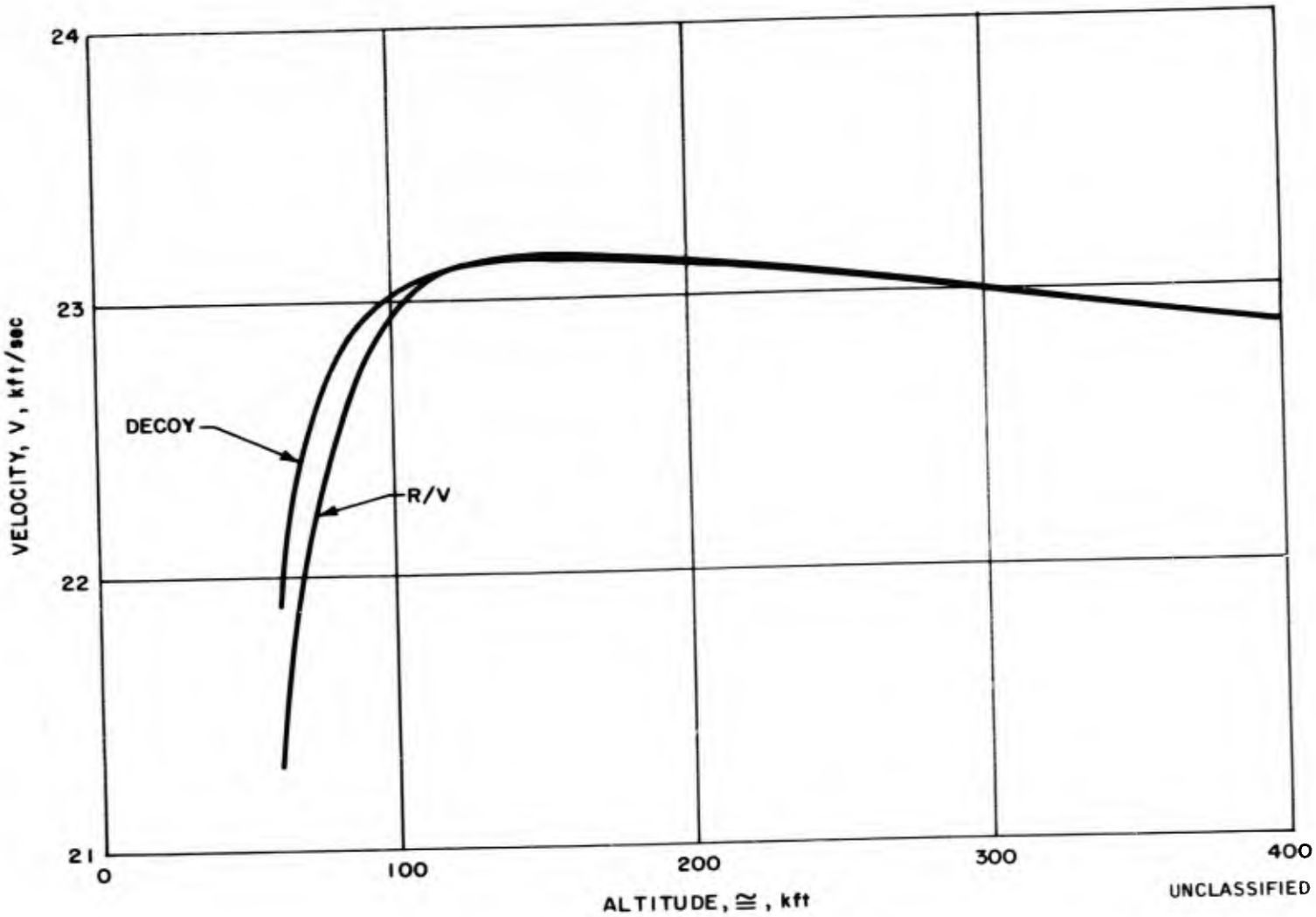

Figure III-3 SAMPLE VELOCITY HISTORIES

The above sections have described the decoy design problem and the general procedures utilized to solve the problem. In the following paragraphs the actual formulation of the computer program will be discussed in terms of its modules or subroutines, starting with the outermost program and proceeding in to the actual trajectory calculations. The main program (Figure III-4) accepts the input quantities, allows the reentry vehicle data to be input or calls the basic function evaluation subroutine (F123) the reentry vehicle data, allows the selection of the desired search subroutines which in turn call the function evaluator (FEV) and provide for the final output.

The function evaluator (Figure III-5) screens the coordinates (decoy design parameters) selected by the optimizer to determine if they are compatible with the capabilities of the trajectory subroutines. If the coordinates are not acceptable, a dummy function is defined to encourage the optimizer to select more reasonable designs. If the coordinates are acceptable, the matching subroutine (F123) is used to compare the reentry vehicle data with decoy data calculated using the trajectory and observables subroutines. The matching subroutine calculates the corridor functions illustrated by the shaded area in Figure III-6. The corridor function immediately indicates whether or not the decoy velocity history is within the allowable corridor. If the function is zero, the velocity aspects of the trajectory are acceptable; if the function is positive, the velocity history is not acceptable. This function also provides a measure of the "amount" the velocity history is out of the corridor. Provisions are made for calculating corridor functions for nine observable histories:

a. Velocity,

b. Deceleration,

c. Ballistic Coefficient,

d. Wake length at the first frequency,

e. Wake length at the second frequency,

f. Wake length at the third frequency,

g. Wake RCS at the first frequency,

h. Wake RCS at the second frequency,

i. Wake RCS at the third frequency.

In addition, nine "effectiveness integrals" are also optionally calculated in the matching subroutine for use in the probability of discrimination calculation in subroutine EFFECT.

The formulation of the miscellaneous subroutine (MISC) includes calculations of the average density of the decoy which may be constrained to aid in obtaining reasonable packaging situations. This average density calculation is a first step toward the possible requirement for internal packaging logic which can be added into this subroutine at some future time. Also provisions are made in this subroutine to allow the parameters describing the decoy after a discontinuous shape

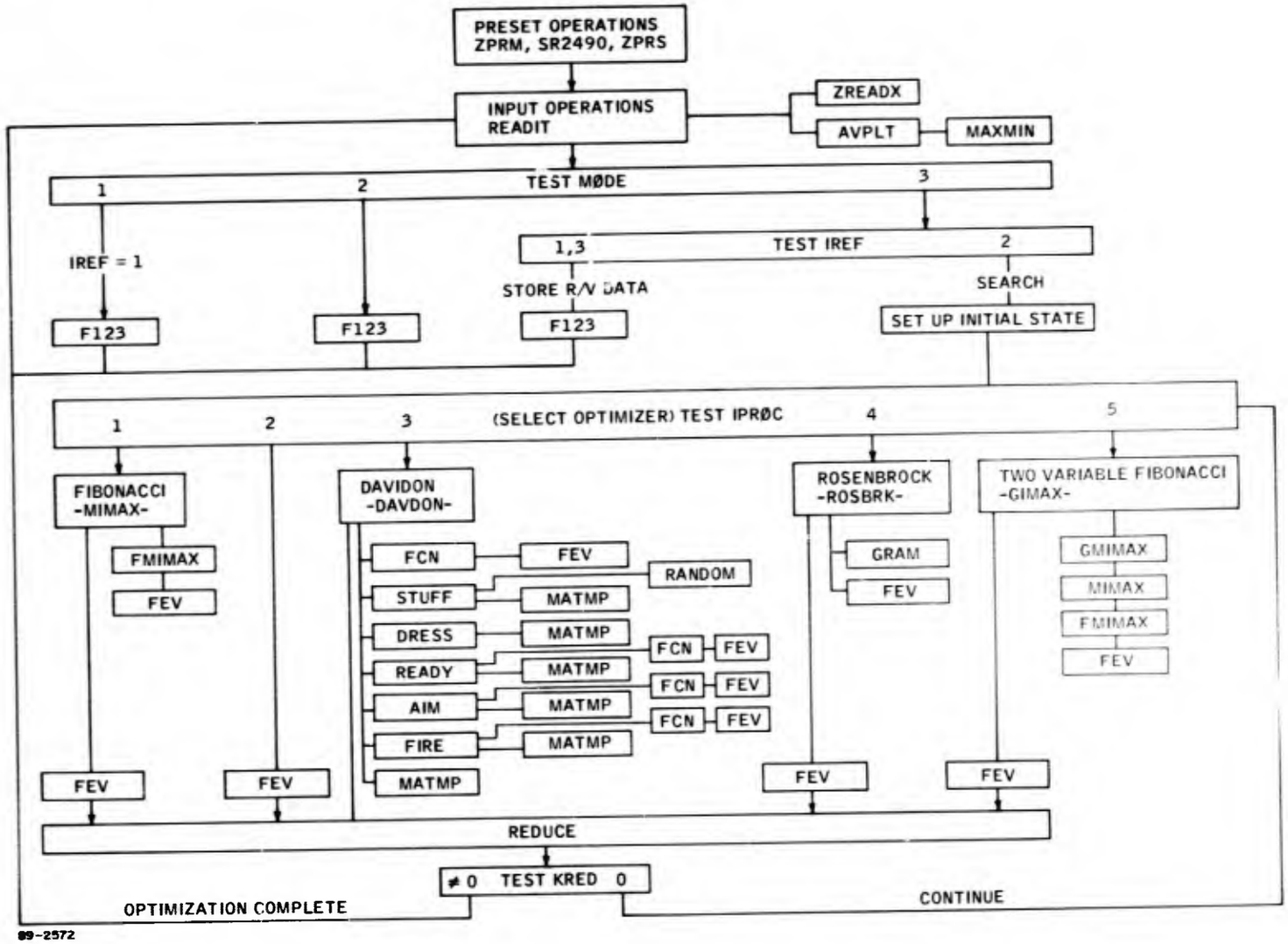

Figure III-4 FLOW CHART OF MAIN PROGRAM AND OPTIMIZATION LOGIC

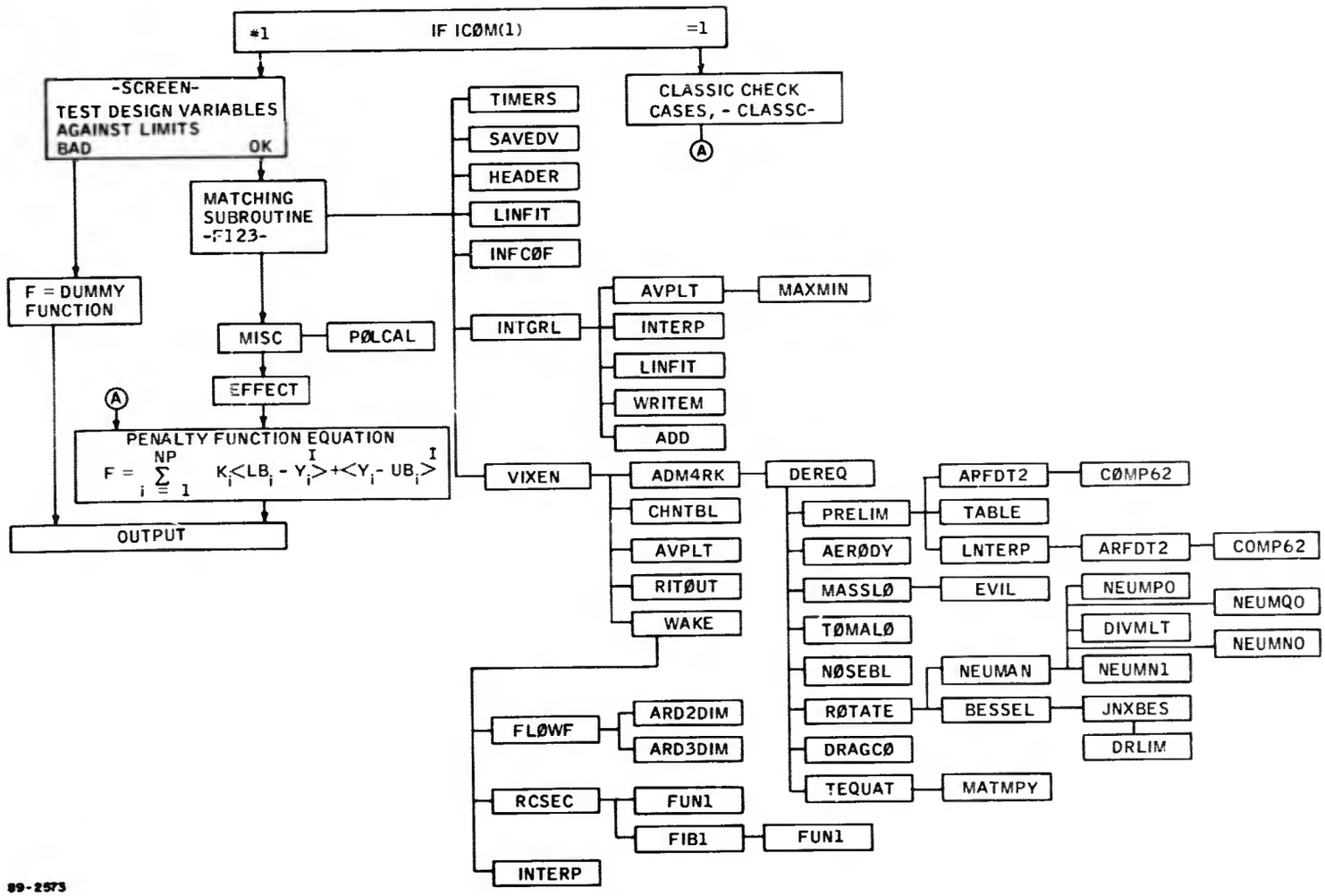

Figure III-5 FLOW CHART OF FUNCTION EVALUATOR (FEV)

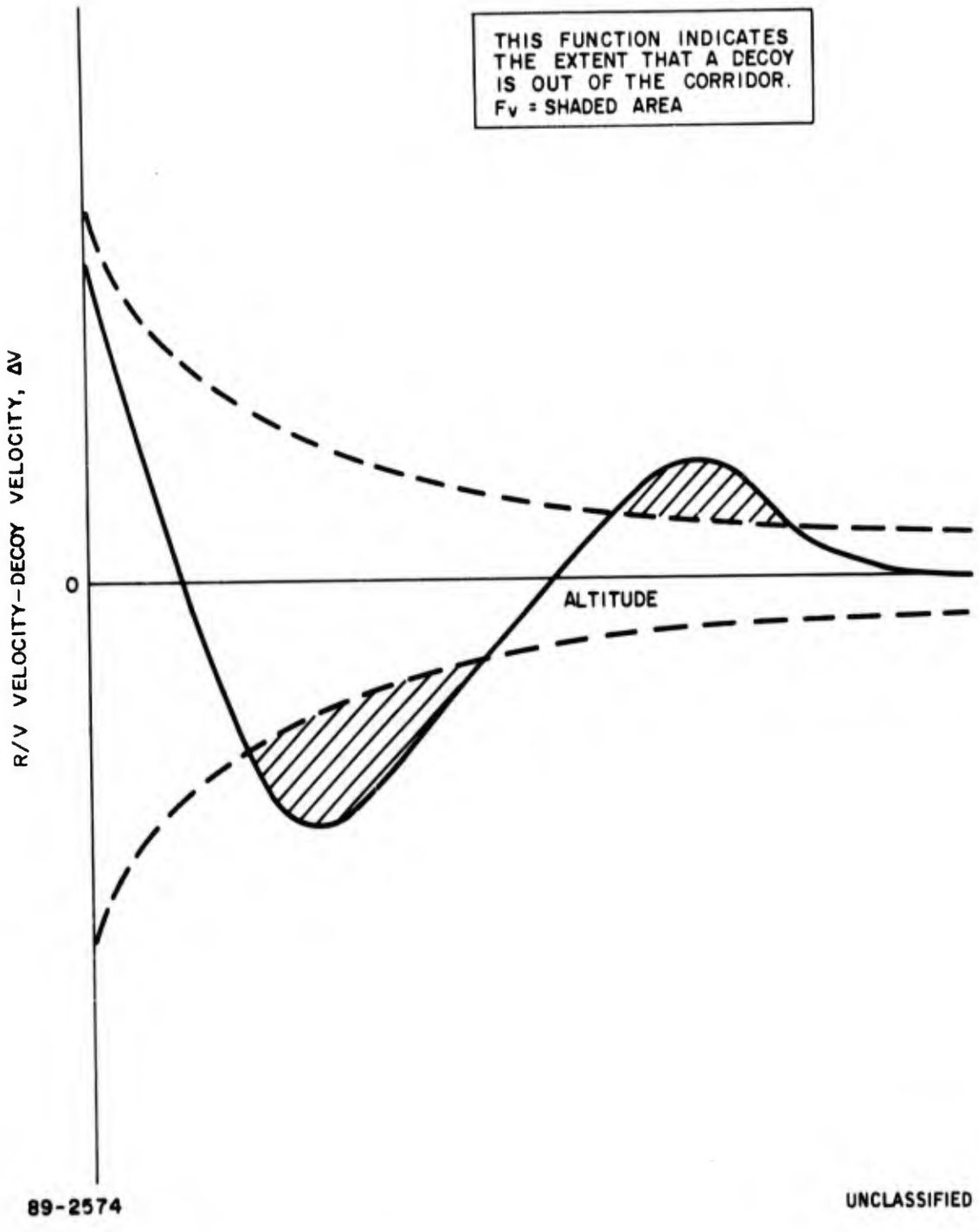

Figure III-6 ILLUSTRATION OF A CORRIDOR FUNCTION

change to be constrained relative to the parameters describing the decoy just before the shape change. For example, the vehicle must not be allowed to gain weight at the shape change.

The subroutine called EFFECT contains the operations for defining a probability of discrimination based on any desired combination of the nine performance functions. This probability of discrimination can then be constrained or minimized, if desired.

The calculation of the penalty function equation is performed in the function evaluator. The penalty function equation provides the fundamental link between the function evaluator calculations and the synthesis operations. The penalty function equation has been developed to handle all the constraints simultaneously. This equation is an adaption of the work of Schmidt and Fox (Ref. III-2). An Avco developed programming technique for this equation allows any combination of quantities which are available in the program to be constrainted.

If the decoy design is within all the constraints, the penalty function will be zero; if not, the penalty function will have some positive value. This formulation immediately provides identification of acceptable designs. Information about the penalty function, F , and its behavior as the decoy design is changed is generated and used to proceed from a starting configuration to an acceptable solution and then to an optimum solution, if desired.

Typically, the behavior of the penalty function is sampled for each of the design variables being considered and all variables are then changed simultaneously to proceed to a new configuration.

An illustration of the use of the penalty function is shown in Figure III-7 for two independent variables. Conceptually, an optimization technique is applied to the penalty function to find decoy designs with smaller values of the function until a design is found where the function is zero. This implies that the final decoy is within the trajectory and observable corridors and is within all stated geometric and other constraints. This process is repeated with a sequence of tighter constraints in order to obtain an optimum solution.

If a minimum is located where the function is not zero, this implies that the stated problem is overconstrained. If multimodel functions are suspected, it may be advisable to start the search from several different starting points to build confidence that there is not a better solution in some other part of the allowable search volume.

The use of this form of penalty function has provided an immediate identification of acceptable solutions, a procedure for identifying impossible problems, and has mathematically transformed a constrained optimization problem into a sequence of unconstrained optimization problems.

The synthesis portion of the program is designed to perform a sequence of searches for decoys which have zero values of the penalty function. As shown in Figure III-4, four techniques have been mechanized for selection by the user of the code depending on the nature of the decoy design problem and on the experience the user has with optimization techniques. The search techniques consist of the Davidon Variable Metric Technique, the Rosenbrock Rotating Coordinate Technique, and the one- and two-variable Fibonacci techniques.

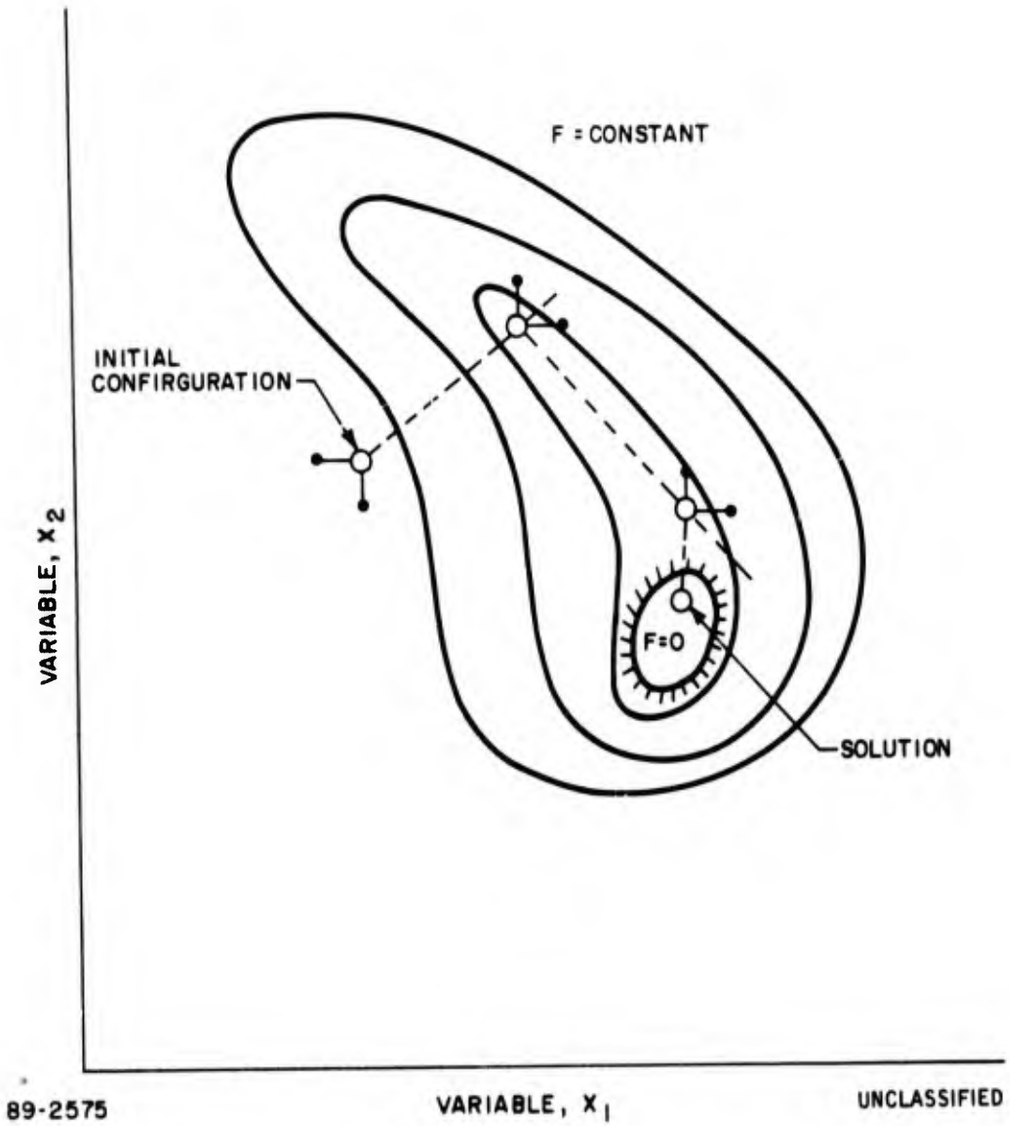

Figure III-7 ILLUSTRATION OF A USE OF THE PENALTY FUNCTION TO IMPROVE THE CONFIGURATION

This optimum decoy design program has been utilized on several programs to design decoys. Its utility has been demonstrated on programs like the Nike-X Targets Program and it is being utilized in examining Tethered Radar Reflector (TRR) designs in the program of that name. As a result of the effort pursued under this task, the penetration aids community now has a tool that economically performs a series of parametric evaluations that normally would take an engineer many months of effort. Unlike most parametric studies, this program rigorously chooses an optimum design and ensures that no configuration has been left out of consideration for a given requirement.

1.3 IDENTIFICATION OF DOCUMENTATION ELEMENTS

The documentation for this code is in three parts. The volume entitled, "Numerical Description of the Optimum Decoy Design Program" (Appendix I) contains descriptions of each subroutine, descriptions of the numerical methods employed, correlation of program segments with their function descriptions and a complete listing of the source program and preset deck. The numerical description volume is primarily intended for the professional programmer who is required to understand the internal detailed operation of the code. The second part is entitled "User's Manual for the Optimum Decoy Design Program" (Appendix II). This manual contains detailed descriptions of the input symbols, input sheets, sample inputs, and corresponding sample outputs, along with descriptions of the output and tests of the correctness of the operation of the program. The user's manual is primarily intended for immediate reference by the personnel preparing inputs for the code. The third part is entitled "Mathematical Formulation of the Optimum Decoy Design Program" (Appendix III) and contains the basic equations and procedures which are mechanized in the code. This part is of use to all personnel involved with the code; however, it is primarily intended to provide a description of the state-of-the-art of the technology utilized in the code which will guide the current users and will serve as a baseline for futher improvement in the code. The three parts of the description overlap in some areas in order to provide more complete explanations; however, it is expected that a careful user of the code would read all three parts to reduce the chance of misunderstanding the description in any one part. In particular, the User's Manual presupposed an understanding of this Mathematical Formulation document. These three parts of the program description are designed to be independent of the task-by-task discussion of the portion of the effort accomplished during ADTECH IV which is included in the main body of the ADTECH IV final report.

The following sections of this volume describe the formulation of the Optimum Decoy Design Program in detail. The material in Sections 2.0 through 6.0 in this volume and in Sections 2.0 through 6.0 of the numerical description volume (Appendix I) are organized in roughly the same order. The breakdowns of the individual sections have been made different in some cases to best serve the needs of each volume.

BLANK PAGE

2.0 OPTIMIZATION TECHNIQUE

The techniques described in this section include the definition and utilization of a penalty function transformation, the calculation of the gradient of the penalty function, and the description of the various search techniques which can be applied to the penalty function.

2.1 PENALTY FUNCTION TRANSFORMATION

The penalty function used in this program allows the constrained optimization problem to be solved as a sequence of unconstrained problems. This section contains descriptions of the penalty function equation, the technique for defining a dummy function if the current search point is outside the capability of the trajectory modules, and the techniques for tightening a constraint after each unconstrained search.

2.1.1 Function Evaluation

The analysis portion of the program (including the calculation of the corridor functions, miscellaneous quantities, and effectiveness parameters) characterizes each decoy by a set of numbers called y_i . The selection of the desired combination of these quantities to be used in the penalty function is made by the user by means of input codes. The penalty function equation is shown in Figure III-5. The notation used will be defined in paragraph 2.1.3 of this volume. An alternate way of describing the calculation of the value of the penalty function, F, is as follows. Let F be the sum of the NP individual constraint terms, f_i :

$$F = \sum_{i=1}^{NP} f_i$$

where each term is:

$$f_i = \begin{cases} 0.0 \text{ if the constrained quantity is within the limits} \\ k_i \left(\left| \text{amount out of the limits} \right| \right)^I \text{ if not within limits} \end{cases}$$

where k_i and I are inputs. If the penalty function, F, is zero, the decoy is within all the constraints. If the penalty function is not zero, then its magnitude represents the "amount" that this decoy is unacceptable. The penalty function thus reduces the entire set of performance histories and design constraint situations to a single number (F). Optimization techniques can then be applied to find the decoys which result in smaller values of the penalty function until a decoy is found which has a penalty function value of zero. This would then complete one "Solution-finding" operation. The detail of the process of utilizing a sequence of solution-finding operations to obtain an optimum solution will be discussed in paragraph 2.1.3.

2.1.2 Screening Operations

It is possible for an optimizer to specify that a decoy be evaluated which is not physically meaningful or which is outside the capability of the trajectory modules. A testing procedure has been set up which "screens" out such situations and defines a value for the penalty function, F, which is equal to the sum of the last calculated value from the penalty function equation, D, to the amount the decoy failed the screening test:

$$F = D + \sum_{i=1}^{15} S_i \left\{ \langle LL_i - X_i \rangle^2 + \langle X_i - UL_i \rangle^2 \right\}$$

where S_i is input; and the parameters, X_i, the lower limits LL_i, and the upper limits, UL_i, are given in Table III-I. It is assumed in this formulation that the reference reentry vehicle and the initial decoy are input so that both pass the screening test. Otherwise, it is likely that the search process will go unstable.

2.1.3 Sequential Optimization

A technique for formulating the solution-finding problem was discussed in paragraph 2.1.1 of this volume. This technique has been extended to allow performance and design constraints to be included in the search for an optimum decoy configuration. The extended technique effectively transforms the constrained optimization problem onto a sequence of solution-finding problems which are solved using unconstrained optimization techniques. The technique is based on the Schmidt and Fox penalty function equation of Reference III-1 which will be considered in the following form:

$$F = k_1 \langle y_1 - UB_1 \rangle^E + \sum_{i=2}^{M} k_i \left\{ \langle LB_i - y_i \rangle^E + \langle y_i - UB_i \rangle^E \right\}$$

where:

- F is the penalty function which is searched for a zero or a minimum by the optimizer
- k_1 is the multiplier (scale factor) for the quantity being minimized
- y_1 is the quantity being minimized
- UB_1 is an upper bound on the quantity being minimized
- E is the exponent which is normally 2 but can be set to 1 for special problems
- M is the total number of terms in the penalty equation

TABLE III-1

SUMMARY OF SCREENING LIMITS

Item	Conditions	Lower Limit	Parameter	Upper Limit	Units
1		0.0	R_{N_1}	10000.0	inches
2	If ZTURN > 0.0	0.0	R_{N_2}	10000.0	inches
3		0.0	R_{N_1}/R_{B_1}	0.6	---
4	If ZTURN > 0.0	0.0	R_{N_2}/R_{B_2}	0.6	---
5		3.0	LA1	168.0	inches
6	If ZTURN > 0.0	3.0	LA2	168.0	inches
7		4.0	THETA1	40.0	degrees
8	If ZTURN > 0.0	4.0	THETA2	40.0	degrees
9		-10.0	ZTURN	Z0	feet
10	If ZTURN > 0.0	0.0	W2	W1	pounds
11	If NTHRUST ≠ 0	0.0	ISP	10000.0	seconds
12	If NTHRUST = 1	ZØFF	ZØN	ZO	feet
13	If NTHRUST = 2	TO	TØN	TØFF	seconds
14	If NTHRUST = 1	ZST	ZØFF	ZØN	feet
15	If NTHRUST = 2	TØN	TØFF	TST	seconds

k_i is the multiplier (scale factor) for each constraint

LB_i is the lower bound for each constraint

y_i is the value of each item being constrained

UB_i is the upper bound for each constraint

$\langle A \rangle$ is { A if A is positive
0.0 if A is zero or negative

Note that the user should input a lower bound for the quantity being minimized which is well below the expected minimum. This drops the first "lower bound" term from the equation and thus this term is not shown in the equation above.

There are two cases to be considered. The first is where the quantity being minimized is a calculated value or a design variable and the second is where the quantity is an input quantity which is not an active design variable.

For the cases where the quantity being minimized, y_1, is a calculated value or a design variable, the procedure is to input the exponents, the upper and lower bounds, and the multipliers. The first upper bound, UB_1, is selected to be reasonably large (based on experience and judgment). The multipliers, k_i, are allowed for numerical purposes and do not theoretically enter into the process at all. The first solution-finding operation is initiated from an input initial decoy configuration. The optimizer modifies the configuration until every constraint is satisfied. At this point every term of the penalty equation is zero and the value of the penalty function, F, is therefore zero. The parameters describing this acceptable decoy are carried over to describe the initial configuration for the next solution-finding step. The first upper bound, UB_1, is reduced for the second solution-finding operation. Each time that it is possible to find an acceptable decoy, the constraint is tightened by a factor, W_{RF}, and the process is repeated:

$$(UB_1)_{I+1} = W_{RF}\,(y_1)_I$$

After a series of solution-finding problems, the constraint will have become so tight that a solution is no longer possible. In this situation, the search procedure finds that F has a minimum and that it is not possible to find a decoy where F equals zero, thus it is not possible to find a decoy which satisfies all the imposed constraints. The next-to-the-last decoy then is declared the optimum (within the tolerance implied by the factor, W_{RF}). The process described here is the one mechanized in the program; however, it is recognized that it may be desirable in the future to incorporate more sophisticated methods for finding the smallest compatible value of the upper bound UB_1. Approaching the optimum from the "acceptable" side has been found to be a practical technique for design work.

A parallel procedure is used when the quantity being minimized, y_1, is an input which has not been identified as a design variable. After each successful solution-finding operation, the value of the input itself is changed:

$$(y_1)_{I+1} \quad W_{RF}\,(y_1)_I$$

Again, the solution-finding process is repeated until it is no longer possible to find a solution. The next-to-the-last decoy is then declared the optimum (within the implied tolerance).

When the general multivariable optimizers are used, the exponents in the penalty equation must have a value of two so that the first derivatives of the function with respect to the design variables will be continuous. However, since the Fibonacci techniques do not have any continuity restrictions, the exponents can be set to a value of one and the constrained optimum can be searched for directly. For one- and two-variable problems where Fibonacci techniques are applicable, setting the exponents to one and providing suitable k_i multipliers eliminates the need for the series of solution-finding operations discussed above.

2.2 GRADIENT OF THE PENALTY FUNCTION

The gradient of the penalty function is calculated using finite differences. The increments, ΔX_i, are inputs to the program. Each element of the gradient is calculated as:

$$G_i = \frac{F(X_i + \Delta X_i) - F(X_i)}{\Delta X_i}$$

2.3 SEARCH LOGIC

Four separate search techniques are mechanized for possible selection by the user. The first is the Davidon Variable Metric Method for Minimization which is a multivariable unconstrained technique which utilizes the gradient and an approximation of the matrix of second partial derivatives to locate the minimum. The second technique is the Rosenbrock Rotating Coordinate Method which locates the unconstrained minimum of a multivariable function without the direct calculation of the gradient. The third technique is the one-variable Fibonacci method which locates the minimum of an unimodel function within a specified interval. The fourth technique is the two-variable Fibonacci method which locates the minimum within a specified region by obtaining the minimum of a series of one-variable solutions. These four search techniques will be discussed in more detail in the following sections.

2.3.1 Davidon Method

The Variable Metric Method for Minimization is a multivariable technique which uses special gradient methods to locate unconstrained minimums or zeros of a function. The report written by William C. Davidon which describes this method (Ref. III-3) is reproduced as Appendix III-1 to this volume since the report is not now readily available (Ref. III-4, p. 20) and since the material contained in it is essential to the understanding of the method. Additional summary comments and notes regarding modifications are presented in the following paragraphs. A simplified flow chart of the Davidon Method is shown in Figure III-8.

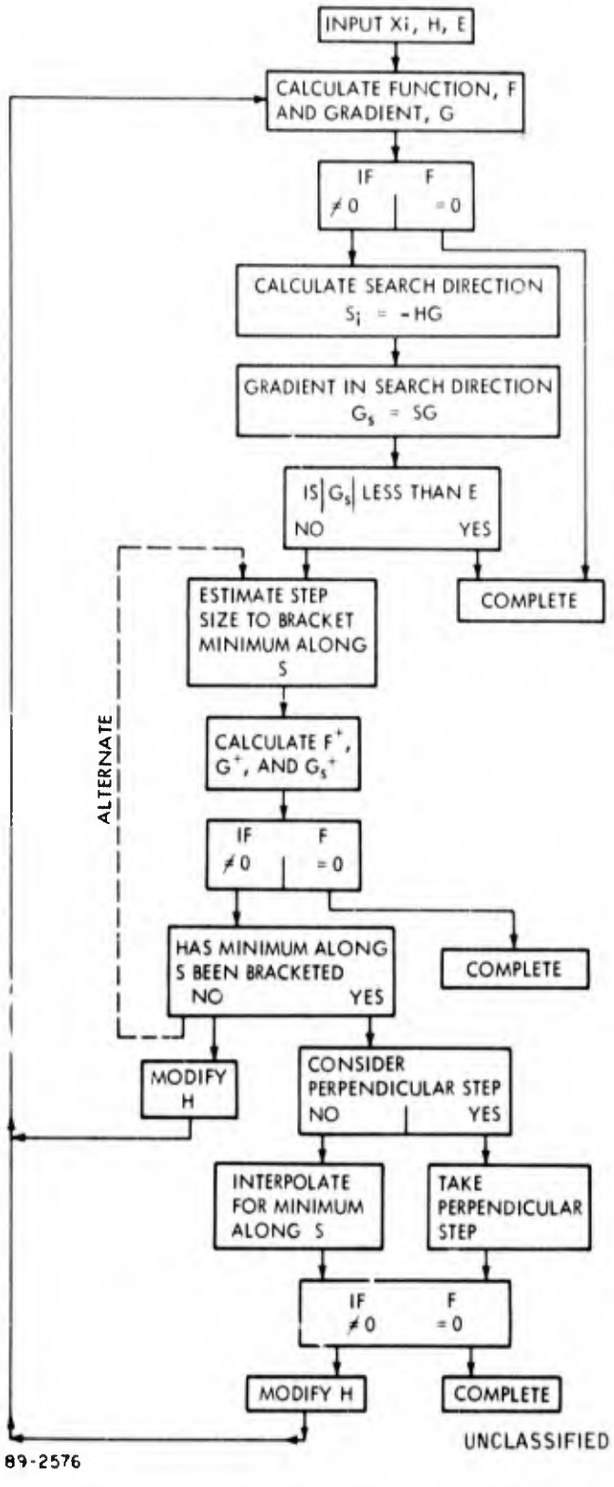

Figure III-8 SIMPLIFIED DAVIDON FLOW CHART

This method is a modified gradient technique having more sophistication than the first-order steepest-descent methods and far less computational requirements per step than the second-order gradient methods. The program requires an initial starting coordinate (initial design point), X^P, an estimate of the inverse of the matrix of second partial derivatives of the function with respect to the design variables, H, and a procedure for evaluating the function, F, and its gradient, G. The Davidon method selects a step size, λ, and a search direction based on the modified gradient, HG. The next decoy design to be evaluated, X, is determined from the matrix equation:

$$X = X^P - \lambda HG$$

The step size is estimated by the program (based on the value of the function, the gradient, and the estimate of H to overstep or bracket the minimum along the search direction. If the minimum has been bracketed, an interpolation is made for the approximate minimum. Based on the behavior of the function during the overstep and the interpolation, the metric H is modified and the process is repeated from the best point available. The identity matrix is typically used for the initial estimate of H unless other information is available.

It is the use of first-order calculations (gradient) to improve the estimate of the second-order parameter H which gives the Davidon technique its power and efficiency. If the penalty function becomes zero, an acceptable decoy design has been obtained and the problem is complete. If the transformer-gradient becomes less than a tolerance, ϵ, a nonzero minimum has been located. This implies that it is not possible to reduce the function further.

If the estimated step size does not bracket the minimum, the Davidon program modifies the H matrix and selects a new search direction. An alternate approach which is more consistent with the basic theory is to change the estimated step size until the new point does bracket the minimum. Although this approach is theoretically sound, actual experience in running both approaches has indicated that the original approach is faster for most problems.

Another variation away from the basic theory is included in the program at the point where the minimum in the search direction has been bracketed. Calculations are made to estimate whether the function is behaving in such a way that a "perpendicular" step would be more advantageous than back-tracking to interpolate for the minimum in the search direction. This possibility is attractive because of the characteristics of certain functions. Safeguards are included in the program so that the process is stable. For example, if the perpendicular step is worse than expected, the program returns to the normal logic and interpolates for the minimum in the search direction.

The program, as mechanized, differs from the description in the appendix with regard to the limits on the maximum size of the step length, λ. In the program the step length is:

$$\lambda = \text{smaller of} \begin{cases} 2.0 \\ -M\,(f/gs) \end{cases}$$

where M is an input which may be adjusted by the user.

The random step operations described for subroutine STUFF have not been mechanized since they would tend to interfere with the sequential constrained optimization process.

2.3.2 Rosenbrock Method

The Rosenbrock Rotating Coordinate Minimization Technique (Reference III-5) is an algorithm for selecting trial values for the input parameters of a given system model in such a way that a function of the performance of the system optimized.

The technique is referred to as "rotating coordinates" because of the fashion in which the variables are perturbed. Rather than varying the input parameters of the system model one-at-a-time, this method rotates the coordinate system in parameter space so that one axis points in the "best" direction of search. The remaining axes for exploration, which are mutually orthogonal, are obtained with a Gram-Schmidt orthogonalization procedure. A search is taken along each of these directions one at a time using the logic which is described below, and then a new set of axes are developed. A geometric interpretation of the axes systems is shown in Figure III-9 and flow charts for the technique are shown in Figures III-10 and III-11.

The search technique involved consists of taking trial steps along each of the coordinate axes. The trial is a "success" if the functional value is less than the value on the previous trial; otherwise it is a "failure." The step sizes are determined in the following manner. An initial step size (ΔX) is an input quantity. After a successful trial, the length of the previous step is multiplied by a constant α, ($\alpha > 1$) and this is added to the previous value used to locate the next trial. After a "failure," the previous step size is multiplied by $-\beta$, ($0 < \beta < 1$) and this is added to the previous value. If this stepping procedure produces a functional value within a specified tolerance level (TØL) of the previous functional value the step is called a "success." The trials in a given direction are complete when there has been a "success" followed by a "failure." The initial step in the new search (i.e., after the rotation of the coordinate axes) is dependent upon the total of the successful steps from the previous search. In particular, if d_n is the algebraic sum of all successful trials in the n^{th} direction, then the initial trial of the next search in the n^{th} direction will be γd_n, ($\gamma > 0$), where γ is a preset constant. Although all of the above constants, α, β, γ, TØL, are preset, they may be input as different values to suit the need of a particular problem.

After a set of trials has been completed in one direction, the program searches along the next orthogonal direction until all N directions have been treated. A new set of directions is then calculated. All of the trials along the N directions and the subsequent calculation of a new set of directions is called a "stage."

The rotating coordinate axes are related to the parameter axes by the direction cosine matrix $[C_{\ell n}]$, with which steps in a given direction can be resolved into parameter changes. For the first stage, $[C_{\ell n}]$ is a unit matrix so that each step, e_n, corresponds to a change in only one of the system parameters X_ℓ. For each subsequent stage, a new direction cosine matrix is computed using the Gram-Schmidt procedure as follows:

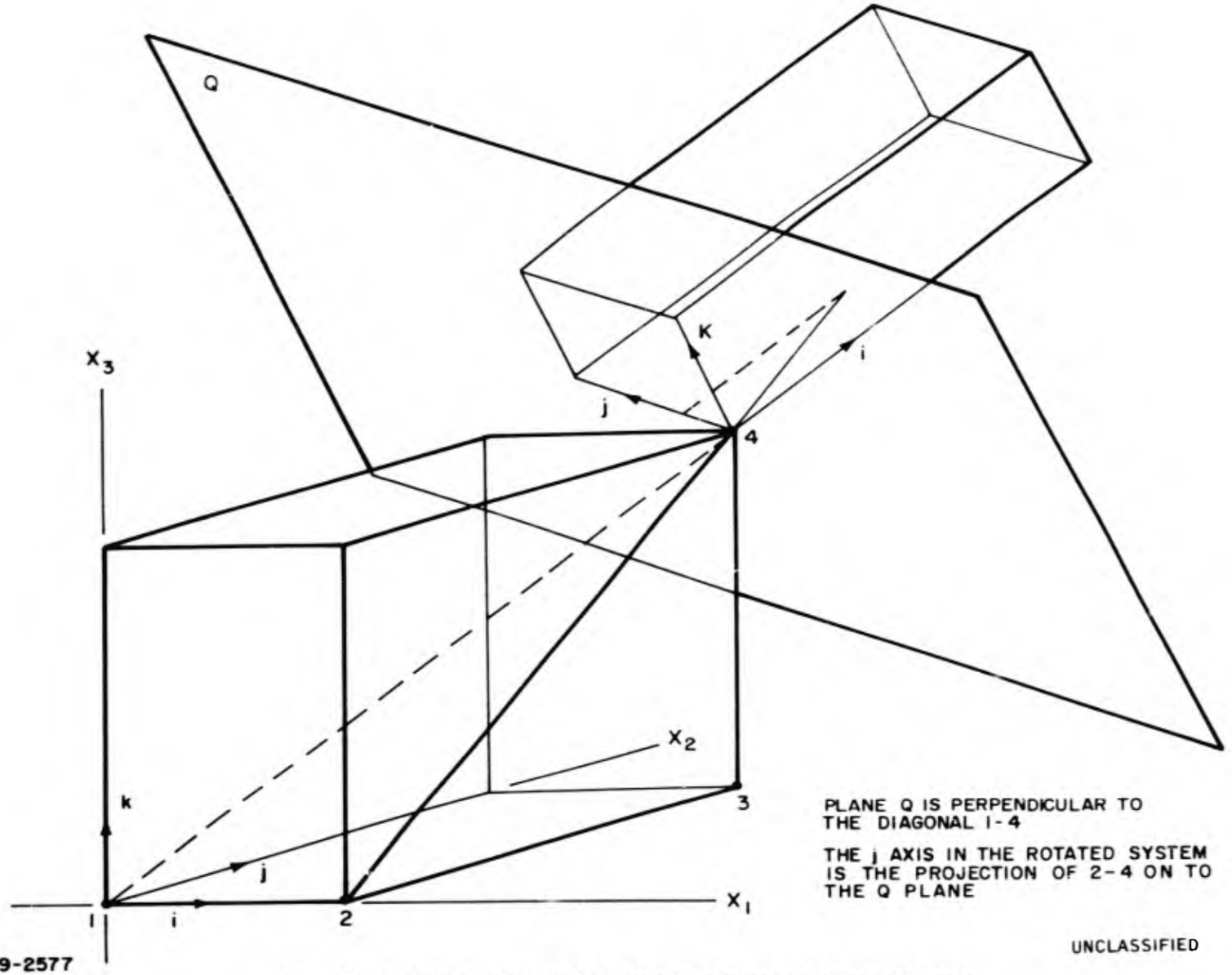

PLANE Q IS PERPENDICULAR TO THE DIAGONAL 1-4

THE j AXIS IN THE ROTATED SYSTEM IS THE PROJECTION OF 2-4 ON TO THE Q PLANE

UNCLASSIFIED

Figure III-9 GEOMETRICAL DESCRIPTION OF ROSENBROCK'S ROTATING COORDINATE TECHNIQUE

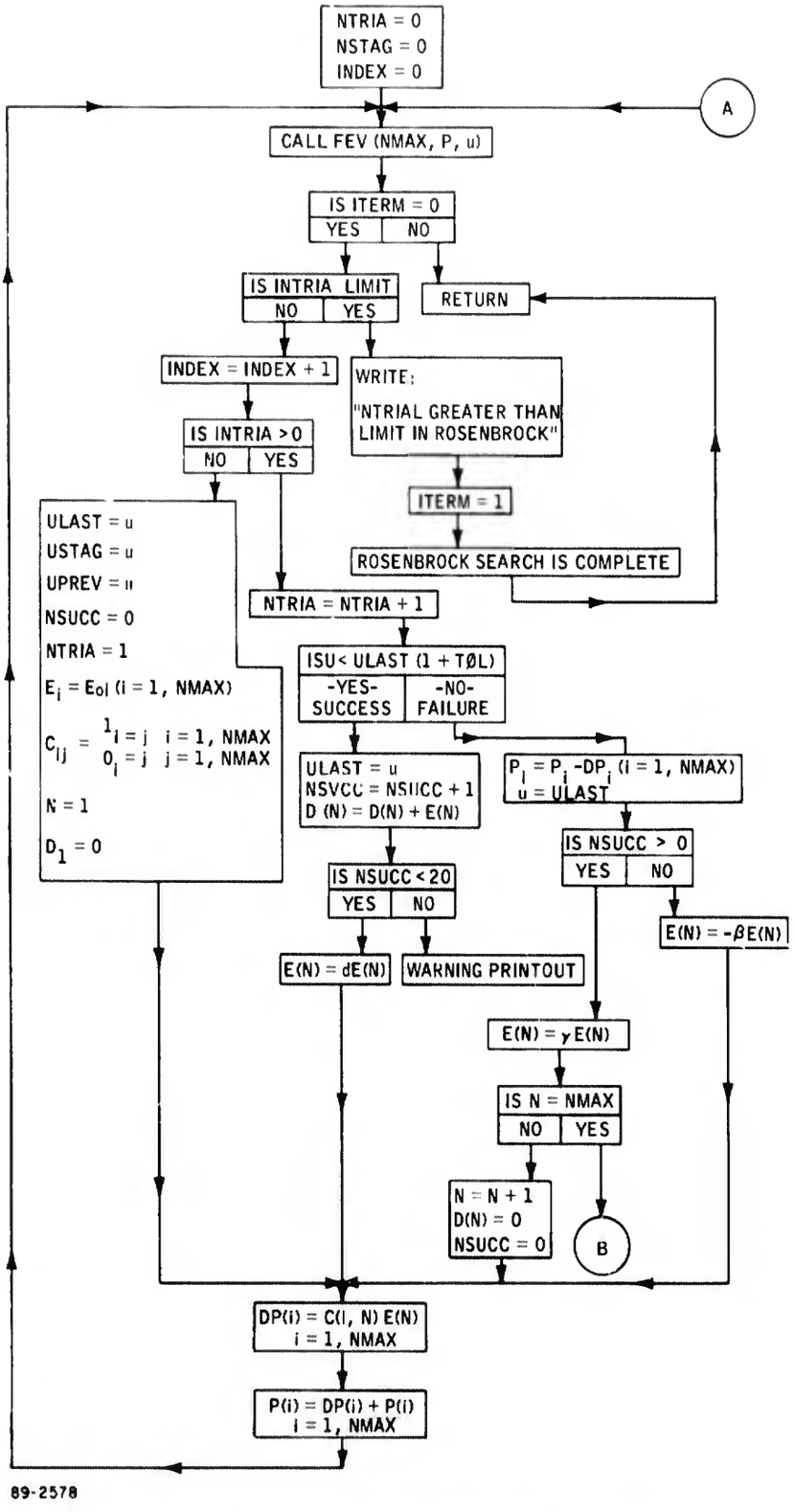

Figure III-10 ROSENBROCK FLOW CHART, PART 1

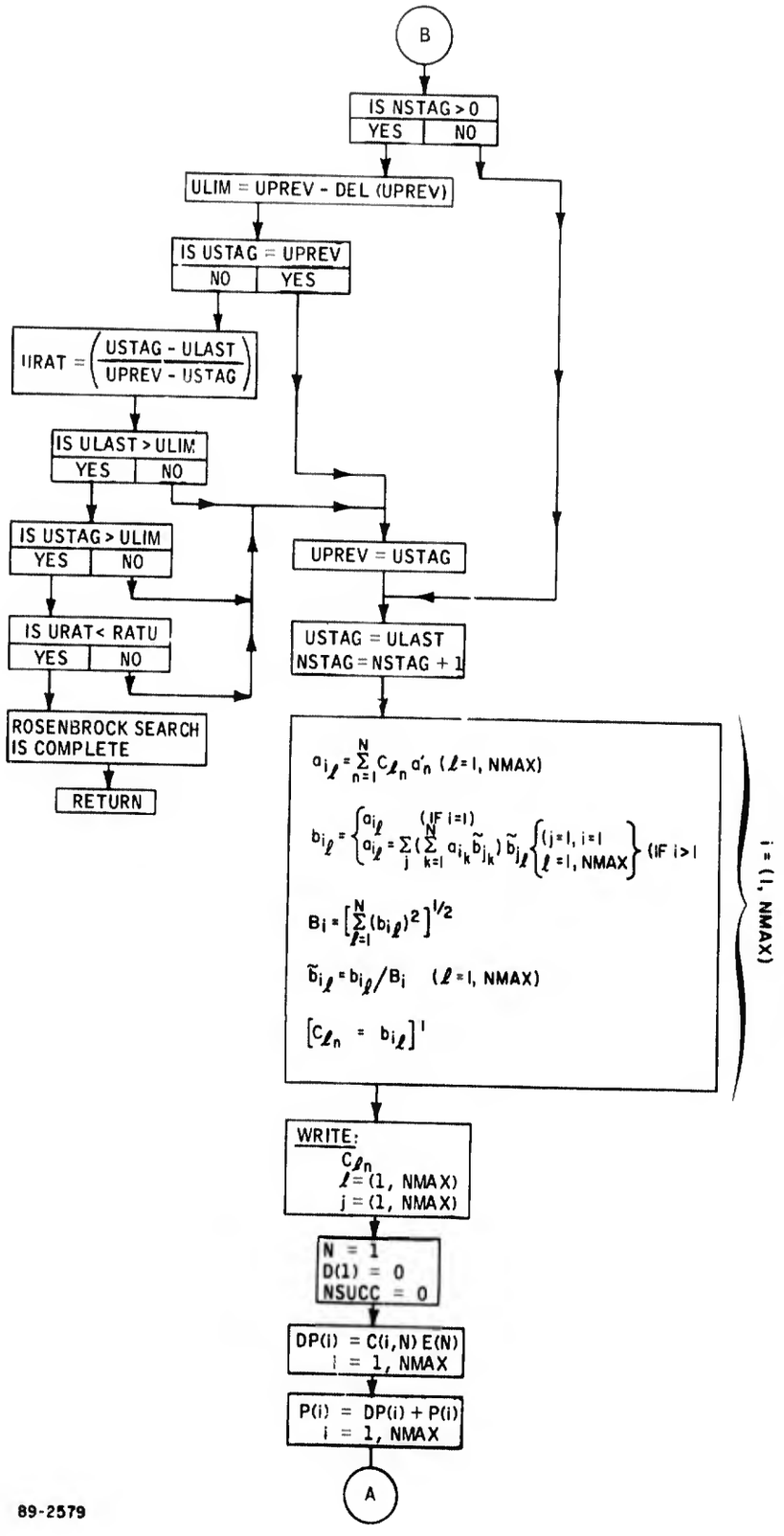

Figure III-11 ROSENBROCK FLOW CHART, PART 2

Let $\bar{\xi}_1^{\,o}, \bar{\xi}_2^{\,o}, \ldots, \bar{\xi}_N^{\,o}$ be the set of orthogonal unit vectors defining the directions in the original stage. Suppose that d_1 is the algebraic sum of all successful steps in the direction $\bar{\xi}_1^{\,o}$, etc. Then define the set of vectors:

$$\bar{A}_1 = d_1 \bar{\xi}_1^{\,o} + d_2 \bar{\xi}_2^{\,o} + \ldots + d_N \bar{\xi}_N^{\,o}$$

$$\bar{A}_2 = d_2 \bar{\xi}_2^{\,o} + \ldots + d_N \bar{\xi}_N^{\,o}$$

$$\vdots$$

$$\bar{A}_N = d_N \bar{\xi}_N^{\,o}$$

The orthogonal unit vectors $\bar{\xi}_1^{\,1}, \bar{\xi}_2^{\,1}, \ldots, \bar{\xi}_N^{\,1}$ for the next stage are now obtained using the following vector equations:

$$\bar{B}_1 = \bar{A}_1$$

$$\bar{\xi}_1^{\,1} = \bar{B}_1 / |\bar{B}_1|$$

$$\bar{B}_2 = \bar{A}_2 - (\bar{A}_2 \cdot \bar{\xi}_1^{\,1}) \bar{\xi}_1^{\,1}$$

$$\bar{\xi}_2^{\,1} = \bar{B}_2 / |\bar{B}_2|$$

$$\vdots$$

$$\bar{B}_N = \bar{A}_N - \sum_{j=1}^{N-1} (\bar{A}_N \cdot \bar{\xi}_j^{\,1}) \bar{\xi}_j^{\,1}$$

$$\bar{\xi}_N = \bar{B}_N / |\bar{B}_N|$$

The new direction cosine matrix is obtained by taking the transpose of the matrix comprised of the components of $\bar{\xi}_N^{\,1}$ along the parameter axes. With the new coordinate system defined, the search is repeated in each of the new directions in turn. The result of applying these equations several times is to ensure that ξ_1 lies along the direction of fastest advance, ξ_2 along the best direction which can be found normal to ξ_1 and so on.

The stopping logic is based on the value of the function. For a value of the function that is undefined, an error message is printed out and the search is stopped. The same thing happens if the total number of function evaluations for a given set of constraints equals an input limit. If the value of the function is zero or if three succeeding functional values are within a defined interval of each other, a solution is considered to have been found. Considering the diagram below, the intervals for successive functional values which define a solution are

$$(F_s - F_{s+2}) < \text{DEL} * F_s \quad \text{and} \quad \frac{F_{s+1} - F_{s+2}}{F_s - F_{s+1}} < \text{RATU}$$

where DEL and RATU are input limits.

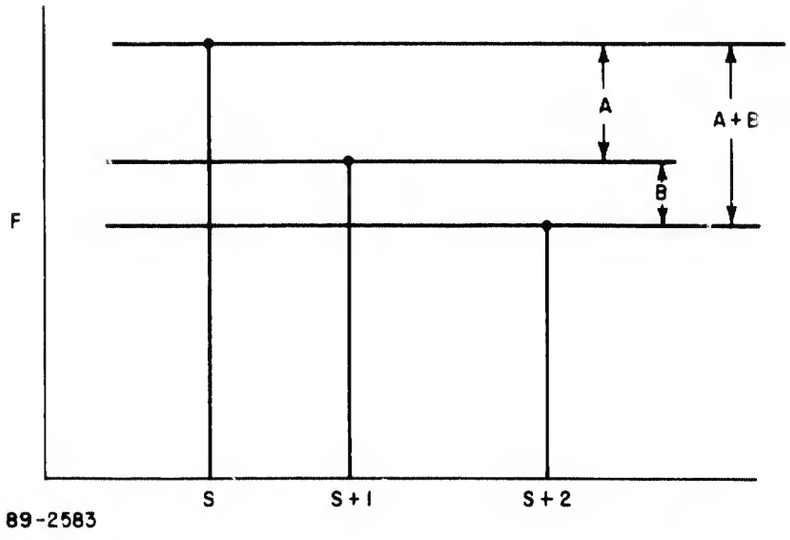

The functional values, F_s , F_{s+1} , F_{s+2}, are those obtained when the trial steps have been completed for all the system orientations.

2.3.3 One-Variable Fibonacci Method

The Fibonacci search technique is a search scheme for finding the maximum or minimum of a one-variable function within defined limits. The function has to be at least piecewise continuous, single valued, and also have only one optimum (i.e., maximum or minimum) within the interval. These restrictions define a unimodal function (pp. 10-13 of Reference III-6). The initial interval, L_1 , is defined by an upper bound, B , and a lower bound, A , where

$$L_1 = B - A$$

Either the number of function evaluations, F , to be made during the search or an end-of-search accuracy limit, A_c , defined in terms of a number of independent variable units away from the actual maximum or minimum within the interval also has to be given.

The technique is based on direct comparison of values of the function, which are used to exclude parts of the search interval (Figure III-12). The placement and comparison of the points is continued until the interval is sufficiently small or until the function is zero. The points are located so as to maximize the interval to be excluded at each step. The three cases shown in Figure III-12 illustrate the comparison and exclusion steps. The left end of the first case can be excluded since the minimum must be either in the center or right sections. The right end of the second case is excluded. The third case shows that both ends can be excluded if both values of the function are exactly the same. Flow charts of this technique are presented in Figures III-13 and III-14.

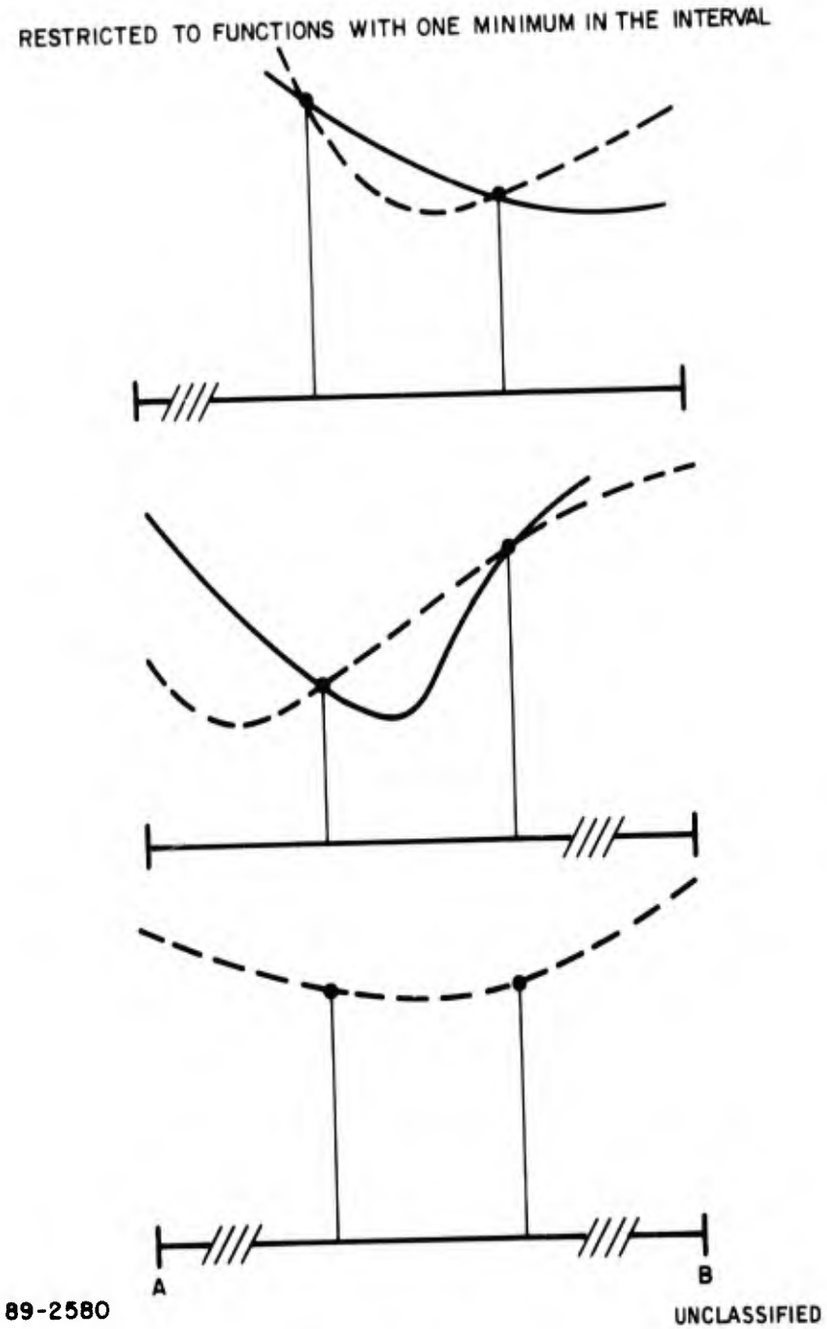

Figure III-12 ONE VARIABLE FIBONACCI SEARCH

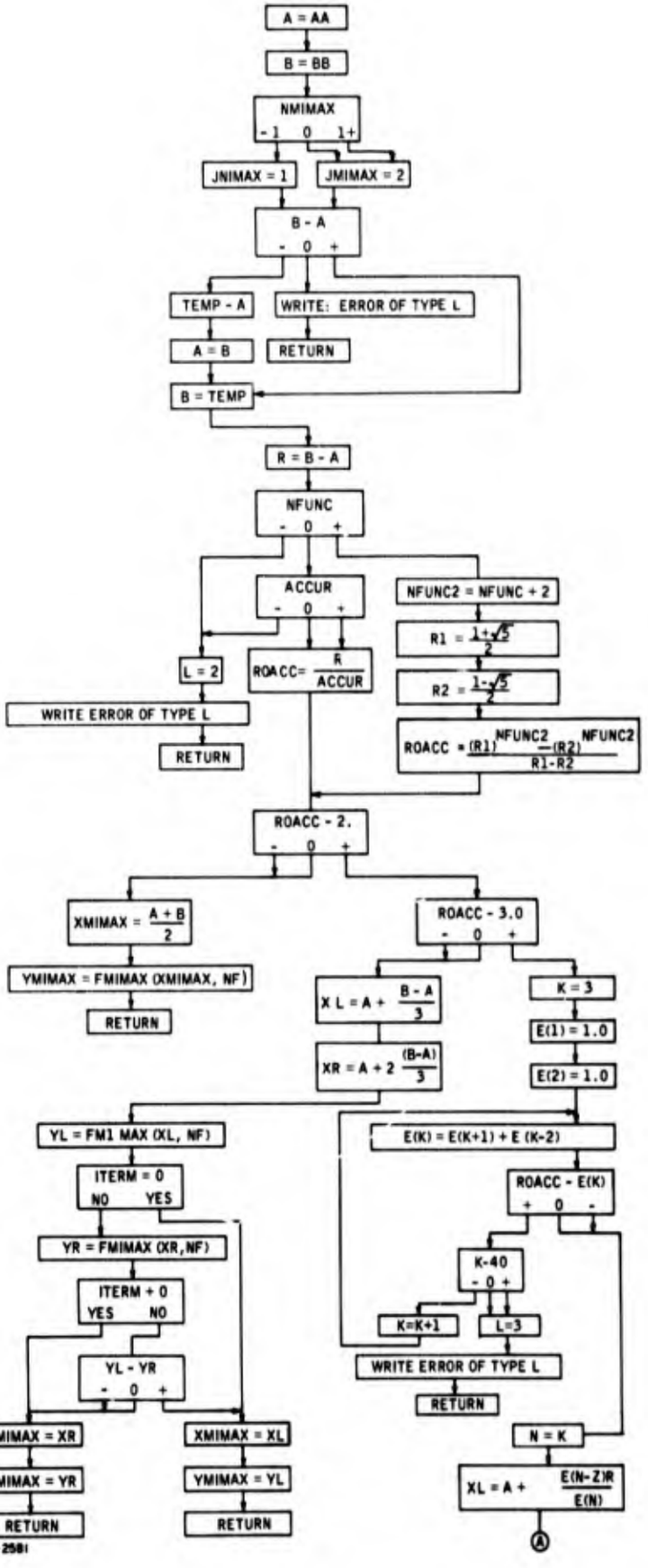

Figure III-13 FIBONACCI FLOW CHART, PART 1

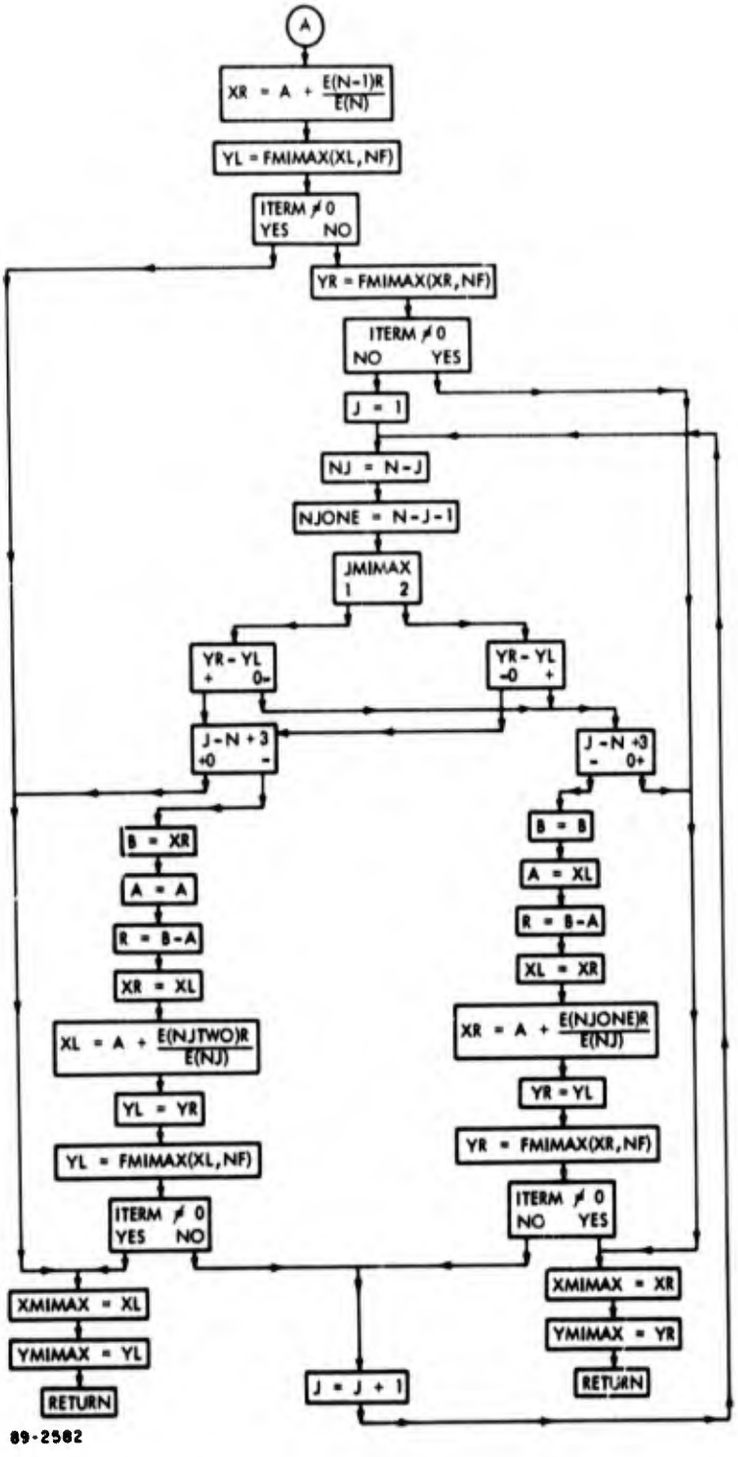

Figure III-14 FIBONACCI FLOW CHART, PART 2

The location of the first two points in the initial search interval is dependent upon the total number of function evaluations to be made during the search. If the accuracy is given, a trial Fibonacci number, F_{NT}, is defined

$$F_{NT} = \frac{L_1}{A_c}$$

The actual Fibonacci number is obtained through an iteration process where

$$F_1 = 1$$

$$F_2 = 2$$

$$F_n = F_{n-1} + F_{n-2} \qquad n = 3, 4, 5, \cdots$$

The iteration process is continued until the first value of n at which $F_n \geq F_{nT}$ is found. The number of function evaluations to be used within a given accuracy limit is then:

$$N_F = n - 2$$

Likewise, if the number of function evaluations is given the associated Fibonacci number is found by applying the above process in reverse order.

The two evaluation points in the first interval are located as follows:

$$X_1 = A + \left(\frac{F_{n-1}}{F_n}\right) L_1$$

$$X_2 = A + \left(\frac{F_{n-2}}{F_n}\right) L_1$$

and the corresponding functional values, Y_1 and Y_2 are computed. Comparing the two functional values and choosing one of the associated evaluation points to be a new end point yields a new interval for computing the next evaluation point. For instance, in the search for a maximum the evaluation point associated with the smallest functional value becomes an end point for the new interval containing the other evaluation point and the remaining end point. Then a new evaluation point is placed in the new interval a distance of ΔX units from the end point retained from the previous interval.

$$\Delta X = \left(\frac{F_{n-j}}{F_n}\right) L_1 \qquad j = 3, 4, \cdots, N_K$$

where the subscript j is the number of the particular evaluation point being found for that interval. The new functional value for the interval is computed and compared with the functional value retained from the previous interval so that a new interval can be determined. This process is repeated until the

appropriate number of function evaluations have been made. The maximum or minimum of the function is obtained by directly comparing the functional value of the final evaluation point, the evaluation point retained from the last interval, and the new end point for the last interval.

2.3.4 Two-Variable Fibonacci Method

The Fibonacci search technique for a two-variable function in a bounded region is the application of the one-variable Fibonacci search to each variable. Taking one of the variables to be the secondary independent variable and the other to be the primary independent variable, the method employed in this technique is the optimization of the primary independent variable during each step of the optimization of the secondary independent variable. That is, for each evaluation point selected during the optimization of the secondary independent variable, the primary independent variable is optimized. Then, the secondary value and the optimum primary value are stored in a table. This process is repeated until the desired number of evaluations have been made on the secondary independent variable. The table is then searched for the optimum secondary value, producing also the associated optimum primary value.

The restriction of unimodality (see description of one variable Fibonacci) applies in a stricter sense for the two variable Fibonacci technique. Not only does the two variable function have to be unimodal, but the associated one-variable functions for the one-variable Fibonacci searches must also be unimodal. For a unimodal two-variable function, whether or not the two one-variable functions are unimodal sometimes depends on which independent variable is chosen to be the secondary variable. Thus, the choice of which variable is to be the secondary independent variable is important. For the case of a unimodal two-variable function where both choices for the secondary independent variable lead to multimodal one-variable functions, the two-variable Fibonacci search technique may not be reliable.

3.0 BASIC ANALYSIS CALCULATIONS

The analysis calculations involve the basic calculations required for a single vehicle and the comparison and effectiveness calculations which are required to evaluate the degree of simulation of two vehicles. The basic calculations are discussed in Section 3.0 and include the trajectory, wake, and miscellaneous calculations. The comparisons are discussed in Section 4.0 and the effectiveness model operations are discussed in Section 5.0. The analysis calculations are performed in order to define the quantities, y_j, in the penalty function equation of Section 2.1.

3.1 TRAJECTORY CALCULATIONS

The trajectory calculations* are incorporated into the ADTECH Decoy Design program to provide the flight characteristics of the candidate decoy designs. Three methods of computing the trajectory are available (a) particle trajectory, (b) rotational three degree of freedom method, and (c) simplified angle of attack solution. The effects of ablation, thrust, and angle of attack oscillation can be included in the trajectory calculations. The program operates within the following geometric and flow constraints:

- Cone half-angle $4^{\circ} \leq \theta_c \leq 40^{\circ}$
- Body length $0.25' \leq L_A \leq 14'$
- Surface temperature $1000^{\circ}\ R \leq T_w \leq 6000^{\circ}\ R$
- Bluntness ratio $0.0 \leq \lambda \leq 0.6$
- Altitude $0.0' \leq Z \leq 400{,}000'$
- Free-stream Mach number $5.0 \leq M_{\infty} \leq 30.0$
- Angle of attack at 300 kft $0^{\circ} \leq \alpha \leq 20^{\circ}$
- Angle of attack below 150 kft $0^{\circ} \leq \alpha \leq \theta_c$

The mathematical description of the trajectory program is presented in this part of the report. The description is broken up into sections, each containing an individual area of analysis involved in the program. Since there is no direct correspondence between the sections in the mathematical description and the subroutines in the numerical description, the brief description of each section given below lists the subroutines that contain the area of analysis being described.

The preliminary calculations section (3.1.1) contains the flow field, geometry, and thrusting calculations. This includes the free-stream, edge, and wall flow field properties, geometry before and after shape change, and all of the thrusting parameters. The subroutine involved is PRELIM.

The heating section (3.1.2) contains the calculation of the aerodynamic heating rates at various stations along the body. The subroutine involved is AERODY.

* Developed for the U. S. Army Material Command, Redstone Arsenal, Alabama, under Contract DA-01-021-AMC-90034(Y).

The ablation effects (3.1.3) section contains the calculation of the sidewall and nose recession rates, mass loss rates at various stations along the body, and the total vehicle mass loss rate. The subroutines involved are MASSLO, EVIL, NOSEBL, and TØMALØ.

The angle of attack section (3.1.4) contains the calculation of the oscillatory angle of attack of the vehicle. The subroutine involved is a portion of ROTATE.

The drag section (3.1.5) contains the calculation of the flight drag coefficient. The effects of ablation and angle of attack are included in the calculations. The subroutine involved is DRAGCO.

The equations of motion section (3.1.6) contains the calculation of the derivatives of the flight trajectory parameters and the integration of the equations of motion to determine the flight trajectory. The subroutines involved are DEREQ, TEQUAT, ADM4RK, and a portion of ROTATE.

The values of the curve-fit coefficients called A_i and B_i in the equations of Section 3.0 are defined in the source listing of subroutine ZPRS in Appendix I.

3.1.1 Preliminary Calculations

The preliminary calculation of the geometric, flow field, and thrusting parameters is done in the subroutine PRELIM. The operations involved can be broken up into seven major areas of calculation: (a) body geometry definition, (b) aerodynamic coefficients, (c) atmospheric free-stream properties, (d) wind tunnel free-stream properties, (e) flow field properties, (f) thrusting quantities, and (g) weight increments. In the following analysis each of the seven areas will be presented separately, along with a listing of the inputs necessary to perform the calculations.

To define the geometric properties of the body, the following inputs are necessary: cone half-angle, θ_c (degrees), nose radius, R_N (feet), and base radius, R_B (feet). The sharp cone slant length is given by:

$$L = \frac{R_B}{\sin \theta_c} \quad \text{(ft)}$$

the axial length from the stagnation point by:

$$L_A = L \left[\cos \theta_c - \frac{R_N}{R_B} (1 - \sin \theta_c) \right] \quad \text{(ft)}$$

and the surface distance from the nose of a blunt cone by:

$$S = R_N \left(\frac{\pi}{2} - \theta_c \right) + \frac{R_B}{\sin \theta_c} - \frac{R_N}{\tan \theta_c} \quad \text{(ft)}$$

where θ_c has the units of radians. The bluntness ratio is defined as:

$$\lambda = \frac{R_N}{R_B}$$

The base diameter is $D = 2R_B$ (ft)

and the reference area is:

$$A_{ref} = \pi R_B^2 \quad (ft.^2)$$

The inputs necessary to compute the aerodynamic coefficients are the cone half-angle, θ_c (degrees), nose radius, R_N (feet), base radius, R_B (feet), bluntness ratio, λ, and the nondimensional center of gravity location from the nose, $X_{c.g.}/D$. The center of gravity location is input in tabular form, as a function of altitude, with the appropriate value being used for the altitude point under consideration. The partial derivative of the normal force coefficient with respect to angle of attack is given by:

$$C_{N_\alpha} = 1.92 \cos^2 \theta_c \left[1 - \frac{1}{2} (\lambda \cos \theta_c)^2\right]$$

The center of gravity location is determined by multiplying the base diameter by the appropriate value of the nondimensional center of gravity location from the input table:

$$X_{c.g.} = D \left(\frac{X_{c.g.}}{D}\right)$$

The partial derivative of the pitching moment coefficient with respect to angle of attack is given by:

$$C_{M_\alpha} = -0.96 \left(\frac{2[1 - (\lambda \cos \theta_c)^3] - 3\lambda \cos^3 \theta_c [1 - (\lambda \cos \theta_c)^2]}{3 \tan \theta_c} + \frac{(R_N - X_{c.g.}) \cos^2 \theta_c \left[1 - \frac{1}{2} (\lambda \cos \theta_c)^2\right]}{R_B} - \lambda \sin \theta_c \cos^2 \theta_c [1 - (\lambda \cos \theta_c)^2] \right)$$

Using the above results, the nondimensional center of pressure distance from the nose of the body becomes:

$$\frac{X_{CP}}{D} = -\frac{C_{M_\alpha}}{C_{N_\alpha}} + \frac{X_{c.g.}}{D}$$

where the appropriate value for $\frac{X_{c.g.}}{D}$ is taken from the input table.

The partial derivative of the pitching moment coefficient with respect to the pitching rate can either be input or calculated as follows:

$$C_{M_q} = -0.96 \left\{ \left(\frac{\lambda \cos^3 \theta_c}{\sin \theta_c} \right)^2 [1 - (\lambda \cos \theta_c)^2] - \frac{4 \lambda \cos^3 \theta_c}{3 \sin^2 \theta_c} [1 - (\lambda \cos \theta_c)^3] \right.$$

$$+ \frac{1 - (\lambda \cos \theta_c)^4}{2 \sin^2 \theta_c} + \frac{\cos^2 \theta_c}{2} \left[\lambda \cos \theta_c \left(\frac{R_N - X_{c.g.}}{R_B} \right) \right]^2$$

$$- \frac{2[X_{c.g.} - R_N(1 - \sin \theta_c)]}{3 R_B \tan \theta_c} \left\{ 2[1 - (\lambda \cos \theta_c)^3] - 3 \lambda \cos^3 \theta_c [1 - (\lambda \cos \theta_c)^2] \right\}$$

$$\left. + \left(\frac{\cos \theta_c}{R_B} \right)^2 [1 - (\lambda \cos \theta_c)^2] [X_{c.g.} - R_N(1 - \sin \theta_c)]^2 \right\}$$

To conduct a flight analysis on a body, the atmospheric free-stream properties must be computed. The necessary inputs are the altitude, Z (feet) and the free-stream velocity, U_∞ (ft/sec). For a nonstandard atmosphere, a table of free-stream density, ρ_∞ (slug/ft3) and speed of sound, a_∞ (ft/sec) as functions of altitude must be input to provide these two values at the altitude point being considered. For a standard atmosphere, the appropriate values of the free-stream density and the speed of sound are obtained from the 1962 standard atmosphere (subroutine ARFDT2). Changing units on the free-stream density to lbm/ft^3 gives:

$$\rho_{\infty_1} = 32.174 \, \rho_\infty$$

Free-Stream Temperature ($^\circ$ R):

$$T_\infty = 4.16 \times 10^{-4} \, a_\infty^2$$

Free-Stream Viscosity ($lb\text{-}sec/ft^2$):

$$\mu_\infty = \frac{(32.2)(2.27 \times 10^{-8})(T_\infty)^{1.5}}{T_\infty + 198.6}$$

Free-Stream Reynolds Number based on the Axial Length of the Body:

$$Re_{\infty L_A} = \frac{\rho_{\infty_1} U_\infty L_A}{\mu_\infty}$$

Free-Stream Pressure (lb/ft^2):

$$P_\infty = \rho_{\infty_1} R T_\infty$$

Free-Stream Mach Number:

$$M_\infty = \frac{U_\infty}{a_\infty}$$

To perform the drag calculations for wind tunnel conditions, the free-stream Mach number, M_∞, free-stream Reynolds number per inch, $Re_\infty(1/in)$, and the free-stream total pressure, P_o (lb/ft^2), are necessary inputs. Changing the units on the free-stream Reynolds number to (1/ft), one has:

$$Re_{\infty_f} = 12.0\ Re_\infty$$

The Free-Stream Pressure (lb/ft^2):

$$P_\infty = \frac{P_o}{\left[1 + \frac{\gamma - 1}{2} M_\infty^2\right]^{\gamma/\gamma - 1}}$$

The Free-Stream Temperature (^{o} R):

$$T_\infty = \frac{1}{2.0\ Re_{\infty_f}} \left\{ \frac{P_\infty M_\infty}{1.490825 \times 10^{-8} R} + \left[\left(\frac{P_\infty M_\infty}{1.490825 \times 10^{-8} R} \right)^2 + 4(198.6)\ Re_{\infty_f} \left(\frac{P_\infty M_\infty}{1.490825 \times 10^{-8} R} \right) \right]^{1/2} \right\}$$

The Free-Stream Density (lbm/ft^3):

$$\rho_{\infty_1} = \frac{P_\infty}{R\ T_\infty}$$

or changing Units on the Free-Stream Density to $slug/ft^3$:

$$\rho_\infty = \frac{\rho_{\infty_1}}{32.174}$$

The Free-Stream Speed of Sound (ft/sec):

$$a_\infty = \frac{\sqrt{T_\infty}}{0.020396}$$

The Free-Stream Viscosity ($lb\text{-}sec/ft^2$):

$$\mu_\infty = \frac{(32.2)(2.27 \times 10^{-8})(T_\infty)^{1.5}}{T_\infty + 198.6}$$

and the Free-Stream Velocity:

$$U_\infty = M_\infty\ a_\infty$$

The flow field properties at the edge of the boundary layer are determined with the aid of the free-stream and geometric properties calculated above. The calculations are as follows:

The Stagnation Enthalpy (Btu/lbm):

$$H_s = 0.24\, T_\infty + (2.0 \times 10^{-5})\, U_\infty^{\,2}$$

Stagnation Pressure (lb/ft^2):

$$P_S = P_\infty \left\{ \left[\left(\frac{2}{(\gamma+1)} \right) M_\infty^{\,2} \right]^{\frac{\gamma}{\gamma-1}} \left[\frac{(1-\gamma) + 2\gamma M_\infty^{\,2}}{\gamma+1} \right]^{\frac{1}{\gamma-1}} \right\}$$

Free-Stream Dynamic Pressure (lb/ft^2):

$$q_\infty = \frac{1}{2}\, \rho_\infty\, U_\infty^{\,2}$$

Free-Stream Reynolds Number based on the Sharp-Cone Slant Length:

$$Re_{\infty_L} = \frac{\rho_{\infty_1}\, U_\infty\, L}{\mu_\infty}$$

Edge Velocity (ft/sec):

$$U_e = U_\infty \left[1 - \frac{1.4}{M_\infty^{\,2}} (M_\infty \sin\theta_c)^{1.9} \right]^{1/2}$$

Edge Pressure (lb/ft^2):

$$P_e = P_\infty \left\{ 1 + 2.8\, (M_\infty \sin\theta_c)^2 \left[\frac{2.5 + 8.M_\infty \sin\theta_c}{1. + 16.M_\infty \sin\theta_c} \right] \right\}$$

Edge Temperature (^{o} R):

$$T_e = T_\infty \times \begin{cases} 1 + 0.0966\, M_\infty \sin\theta_c + 0.2267\, (M_\infty \sin\theta_c)^2 \\ \qquad \text{for } M_\infty \sin\theta_c < 5.7 \\ \displaystyle\sum_{i=o}^{4} \sum_{k=o}^{2} A(90 + i + 5k)[M_\infty \sin\theta_c]^i \left[\frac{P_\infty}{2116.} \right]^k \\ \qquad \text{for } M_\infty \sin\theta_c \geq 5.7 \end{cases}$$

Edge Density (lbm/ft^3):

$$\rho_e = \frac{P_e}{R\,T_e}$$

Edge Mach Number:

$$M_e = \frac{U_e}{U_\infty} \quad \frac{M_\infty}{\sqrt{T_e / T_\infty}}$$

Edge Viscosity ($lb\text{-}sec/ft^2$):

$$\mu_e = \frac{(32.2)(2.27 \times 10^{-8})(T_e)^{1.5}}{T_e + 198.6}$$

and Edge Reynolds Number based on the Surface Distance from the Nose of a Blunt Cone:

$$Re_{e_s} = \frac{\rho_e\, U_e\, S}{\mu_e}$$

If the transition altitude, Z_{TR} , is not input, it is calculated in the following manner:

$$Z_{TR} = \begin{cases} \displaystyle\sum_{i=o}^{1} \sum_{j=o}^{2} \sum_{k=o}^{1} A(300 + j + 3i + 6k)(\theta_c)^i (L)^j (\lambda)^k \\ \qquad \text{for } \theta_c \leq 15^o \text{ and } \lambda \leq 0.3 \\ \displaystyle\sum_{i=o}^{1} \sum_{j=o}^{2} \sum_{k=o}^{1} A(300 + j + 3i + 6k)(15.)^i (L)^j (0.3)^k \\ \qquad \text{for } \theta_c > 15^o \text{ and } \lambda > 0.3 \end{cases}$$

In the following calculations the appropriate value of wall temperature is used:

$T_w(2, 8)$ for $Z \geq Z_{TR}$

$T_w(3, 8)$ for $Z < Z_{TR}$

For the above wall temperatures, the notation is as follows:

$T_w(2, 8)$ = wall temperature at the maximum diameter point of a sharp cone in laminar flow.

$T_w(3, 8)$ = wall temperature at the maximum diameter point of a sharp cone in turbulent flow.

These two values are calculated in the ablation effects portion of this write up.

Constant Pressure Specific Heat at the Edge of the Boundary Layer (Btu/lbm^{o} R):

$$C_{P_e} = \begin{cases} 0.2398 \text{ for } T_e < 700^{o} \text{ R} \\ \sum_{i=o}^{5} A(105+i)(T_e)^{i} \text{ for } 700^{o} \text{ R} \leq T_e \leq 5000^{o} \text{ R} \\ A(111) + A(112)\, T_e \text{ for } T_e > 5000^{o} \text{ R} \end{cases}$$

Constant Pressure Specific Heat at the Wall (Btu/lbm^{o} R):

$$C_{P_\infty} = \begin{cases} 0.2398 \text{ for } T_w(j, 8) < 700^{o} \text{ R} \\ \sum_{i=o}^{5} A(105+i)[T_w(j, 8)]^{i} \text{ for } 700^{o} \text{ R} \leq T_w(j, 8) \leq 5000^{o} \text{ R} \\ A(111) + A(112)\, T_w(j, 8) \text{ for } T_w(j, 8) > 5000^{o} \text{ R} \end{cases}$$

Dimensionless Wall Enthalpy:

$$\bar{H}_w = \frac{C_{P_w}\, T_w(j, 8)}{33.86}$$

Wall Viscosity (lbf-sec/ft^2):

$$\mu_w = \frac{(32.2)(2.27 \times 10^{-8})[T_w(j, 8)]^{1.5}}{T_w(j, 8) + 198.6}$$

Chapman-Rubensin Constant for Edge Conditions:

$$C_e = \frac{\mu_w\, T_e}{\mu_e\, T_w(j, 8)}$$

Viscous Interaction Parameter:

$$\bar{\chi} = M_e^3 \sqrt{\frac{C_e}{Re_{e_s}}}$$

Free-Stream Chapman-Rubensin Constant:

$$C_\infty = \frac{\mu_w T_\infty}{\mu_\infty T_w(j, 8)}$$

Hypersonic Rarefaction Parameter:

$$\bar{\chi}_1 = M_\infty \sqrt{\frac{C_\infty L}{Re_{\infty_L} S}}$$

The calculation of the thrusting parameters is initiated by the input of a thrust history table. This table may take one of two forms: (a) thrust as a function of altitude, or (b) thrust as a function of time. For the convenience of running a number of cases with the same profile but at different thrust levels, the table is in terms of a nondimensional thrust, T_H/T_{H_0}. The dimensional thrust along the trajectory is then obtained by multiplying the nondimensional thrust table values by an input reference thrust level, T_{H_0}. Also required as input are the thrust offset angles and distances. These are the angular misalignment of the thrust vector in the yaw direction (ψ_a) and in the pitch direction (θ_p), measured in that order in the body-fixed coordinate system, and the distance the thrust vector is offset from the two coordinate axes that are normal to the body centerline (ΔZ and ΔY). The thrust at specified altitudes or times in the trajectory is given by:

$$T_{H_\infty} = T_{H_0} \left(\frac{T_H}{T_{H_0}} \right)_{\text{TABLE}} \qquad \text{(LBF)}$$

where linear interpolation is used to determine the proper value for altitudes or times that are between the tabulated nondimensional thrust values. The effective thrust acting on the vehicle is then:

$$T_H = T_{H_\infty} - A_e P_\infty \qquad \text{(LBF)}$$

The components of the effective thrust in the body coordinate system are:

$$T_{H_X} = T_H \cos \theta_a \cos \psi$$

$$T_{H_Y} = T_H \cos \theta_a \sin \psi$$

$$T_{H_Z} = T_H \sin \theta_a$$

The moments generated by thrust offset are given by:

$$M_X = -\Delta Y\ T_{H_Z} - \Delta Z\ T_{H_Y}$$

$$M_Y = \Delta Z\ T_{H_X} + (X_{c.g.} - L_A)\ T_{H_Z}$$

$$M_Z = (X_{c.g.} - L_A)\ T_{H_Y} - \Delta Y\ T_{H_X}$$

The instantaneous total weight of the vehicle is determined by subtracting the weight loss increments due to the altitude or time step along the trajectory from the total weight of the vehicle determined in the previous step. For the case of the first step along the trajectory, the total weight used is the initial weight of the vehicle. The necessary inputs are the total vehicle weight from the previous step (W_o), the weight loss due to thrusting for the present step (ΔW_{TH}), and the weight loss due to ablation for the present step (ΔW). The instantaneous vehicle weight at the end of any trajectory step is given by:

$$W = W_o - \Delta W_{TH} - \Delta W \qquad \text{(lb)}$$

and the associated vehicle mass is:

$$M = \frac{W}{32.174} \qquad \text{(slugs)}$$

3.1.2 Heating

The subroutine AERODY calculates the heating rates at different stations along the body surface in continuum flow. (See para. 3.1.5.) For a sharp cone the body stations are the stagnation point and the maximum diameter point. For a blunt cone the body stations are the stagnation point, tangent point, 20 percent station, 40 percent station, 60 percent station, 75 percent station, 90 percent station, the maximum diameter point for laminar and turbulent flow, and the sonic point for turbulent flow only. The percentage stations are located according to the initial axial length of the cone. The notation used to identify the different heating values is:

Q(1, 1) = Stagnation point heating

Q(2, j) = Laminar heating

Q(3, j) = Turbulent heating

Q(4, 1) = Sonic point heating in turbulent flow

where

j = 1 Implies tangent point on a blunt cone

j = 2-7 Implies the 20 percent, 40 percent, 60 percent, 75 percent, 90 percent stations and maximum diameter point on a blunt cone

j = 8 Implies the maximum diameter point of a sharp cone

All of the heating rates calculated in the section have the units Btu/ft^2-sec. The quantities needed to calculate the heating rates are the free-stream density, ρ_{∞_1} (lbm/ft^3), free-stream Mach number, M_∞, free-stream velocity, U_∞ (ft/sec), cone angle, θ_c (degrees), bluntness ratio, λ, nose radius, R_N (feet), cone axial length, L_A (feet), free-stream/stagnation pressure ratio, P_∞/P_s, dimensionless stagnation enthalpy, H_s/RT_o, stagnation pressure, P_s (lb/ft^2), sharp-cone slant length, L (feet), and transition altitude, Z_{TR} (feet). All the above quantities are calculated in the subroutine PRELIM.

The stagnation point heating for sharp and blunt cones is:

$$\dot{Q}(1,1) = \begin{cases} 1.76 \times 10^4 \left[\left(\dfrac{\rho_{\infty_1}}{0.002375}\right)\left(\dfrac{U_\infty}{2.6 \times 10^4}\right)^{3.15}\right]^{1/2} & \text{for } \lambda = 0.0 \\ 1.76 \times 10^4 \left[\left(\dfrac{\rho_{\infty_1}}{0.002375\, R_N}\right)\left(\dfrac{U_\infty}{2.6 \times 10^4}\right)^{3.15}\right]^{1/2} & \text{for } \lambda > 0.0 \end{cases}$$

For a sharp cone, the edge-stagnation pressure ratio at the maximum diameter is given by:

$$\left(\frac{P_e}{P_s}\right)_8 = 0.0331 \exp\left[0.0064\,\theta_c - 0.33(M_\infty - 5.0)^{0.85}\right] + 4.68 \times 10^{-4}\,(\theta_c)^{1.88032}$$

If $Z \geq Z_{TR}$, the laminar flow heating rate for a sharp cone at the maximum diameter point is calculated as:

$$\dot{Q}(2,8) = \frac{[10]^{0.5142\,[\mathrm{Log_e}(H_s/RT_o)]^{0.9736}}}{0.9664 + \theta_c[5.28 \times 10^{-3} + 2.88 \times 10^{-4}\,\theta_c]} \sqrt{\frac{\left(\frac{P_e}{P_s}\right)_8}{2116.\left(\frac{L_A}{P_s}\right)}}$$

For $Z < Z_{TR}$, the turbulent flow heating rate for a sharp cone at the maximum diameter point is calculated as:

$$K_{1_T} = 0.9 + 0.02\,\theta_c$$

$$K_{3_T} = 0.69 + L_A\left[3.18 \times 10^{-2} - 6.9 \times 10^{-4}\, L_A\right]$$

$$\dot{Q}(3,8) = \frac{0.745\left[\mathrm{Log}_e\left(H_s/RT_o\right)\right]^{0.8122}}{0.6\left(K_{1_T}\right)\left(K_{3_T}\right)}\,[10] \qquad \left[\left(\frac{P_e}{P_s}\right)_8 \quad \left(\frac{P_s}{2116.}\right)\right]^{0.8}$$

For calculating the appropriate heating rates on a blunt cone, the different surface stations must be located with respect to the initial axial length. The location of the blunt cone tangent point - axial location of the tangent point between the spherical nose and the conical body - is given by:

$$\left(\frac{X}{L_A}\right)_1 = \frac{R_N(1 - \sin\theta_c)}{L_A}$$

If the body is to have a discontinuous shape change at some point in the trajectory (determined by the shape change altitude, Z_{TURN}), the following is true for $Z > Z_{TURN}$:

$$\Delta L_A = \frac{L_{A_1}}{L_A}$$

For $Z \leq Z_{TURN}$:

$$\Delta L_A = \frac{L_{A_2}}{L_A}$$

where L_{A_1} is the axial length before shape change and L_{A_2} is the axial length after shape change. The body stations are located as follows:

20 percent station

$$\left(\frac{X}{L_A}\right)_2 = 1 - 0.8\,\Delta L_A$$

40 percent station

$$\left(\frac{X}{L_A}\right)_3 = 1 - 0.6\,\Delta L_A$$

60 percent station

$$\left(\frac{X}{L_A}\right)_4 = 1 - 0.4\,\Delta L_A$$

75 percent station

$$\left(\frac{X}{L_A}\right)_5 = 1 - 0.25\,\Delta L_A$$

90 percent station

$$\left(\frac{X}{L_A}\right)_6 = 1 - 0.1\,\Delta L_A$$

Maximum diameter station

$$\left(\frac{X}{L_A}\right)_7 = 1.0$$

The pressure distribution over a blunt cone is determined as follows:

$$\left(\frac{X}{L_A}\right)_j \geq \frac{1.13\,R_N}{L_A \tan^2\theta_c} ,$$

then the sharp cone maximum diameter pressure is used:

$$\left(\frac{P_e}{P_s}\right)_j = \left(\frac{P_e}{P_s}\right)_8$$

Or if

$$\left(\frac{X}{L_A}\right)_j < \frac{1.13\,R_N}{L_A \tan^2\theta_c} ,$$

then the pressure distribution is:

$$\frac{P_e}{P_s} = \left\{ \frac{P_\infty}{P_s} + \tan^2\theta_c \sum_{n=0}^{2} \sum_{i=0}^{2} \sum_{k=0}^{2} A(135 + n + 3i + 9k) \left[(0.174\,\theta_c)^n \left(\frac{10.}{M_\infty}\right)^i \right] 0.2\,\mathrm{Log}_e \left[\left(\frac{X}{L_A}\right)_j \frac{1.13}{L_A \tan^2\theta_c} \right] \right\}^k$$

for $\theta_c < 20^\circ$

$$\frac{P_e}{P_s} = \left\{ \frac{P_\infty}{P_s} + \tan^2\theta_c \sum_{n=0}^{1} \sum_{i=0}^{2} \sum_{k=0}^{2} A(41 + n + 2i + 6k) \right.$$

$$\left. (0.174\,\theta_c)^n \left(\frac{10.}{M_\infty}\right)^i \right\} 0.2\,\mathrm{Log}_e \left[\left(\frac{X}{L_A}\right)_j \frac{1.13\,R_N}{L_A \tan^2\theta_c} \right] \Bigg\}^k$$

for $\theta_c > 20^\circ$

If $Z > Z_{TR}$, the laminar heating rate is calculated for the blunt cone. At the tangent point, the blunt cone laminar heating rate is:

$$\dot{Q}(2,1) = 1.732\ \dot{Q}(1,1) \left\{ 0.007789 + 1.849 \left(\frac{P_e}{P_s}\right)_j \right.$$

$$\left. - 1.6832 \left[\left(\frac{P_e}{P_s}\right)_j\right]^2 + 0.841 \left[\left(\frac{P_e}{P_s}\right)_j\right]^3 \right\}$$

The heating rates at the various stations along the conical frustum of a blunt cone in laminar flow are:

$$\dot{Q}(2,j) = \frac{0.5142\,[\mathrm{Log}_e(H_s/RT_o)]^{0.9736}}{[10]\ [0.9664 + 5.28\times10^{-3}\,\theta_c + 2.88\times10^{-4}\,\theta_c^2] \left[1 + 1.782 \left(\frac{R_N}{R_B}\right) - 2.008 \left(\frac{R_N}{R_B}\right)^2\right]}$$

$$\sqrt{\frac{\left(\frac{P_e}{P_s}\right)_j}{2116 \left(\frac{L_A}{P_s}\right)\left(\frac{X}{L_A}\right)_j}}$$

For $Z < Z_{TR}$ the turbulent heating rate is calculated for the blunt cone. The turbulent flow heating rate at the sonic point on a blunt cone is:

$$\dot{Q}(4,1) = \begin{cases} \dfrac{3760.(\rho_{\infty_1})^{0.8}\ (U_\infty)^{3.45}}{(0.002375)^{0.8}\ (10)^{13.8}\ (R_N)^{0.2}} \\ \qquad \text{for } Z \leq 115{,}000 \text{ ft.} \\ \dfrac{3760(\rho_{\infty_1})^{0.8}\,[U_\infty]^{(2.254 + 2.246 \times 10^{-5} Z - 1.469 \times 10^{-10} Z^2 + 3.671 \times 10^{-15} Z^3)}}{(0.002375)^{0.8}\ (R_N)^{0.2}\ [10]^{4(2.254 + 2.246 \times 10^{-5} Z - 1.469 \times 10^{-10} Z^2 + 3.671 \times 10^{-15} Z^3)}} \\ \qquad \text{for } Z > 115{,}000 \text{ ft.} \end{cases}$$

The tangent point heating rate for a blunt cone in turbulent flow is given by:

$$\dot{Q}(3,1) = \begin{cases} \dfrac{13460}{\left[R_N\left(1 - \dfrac{\theta_c}{57.3}\right)\right]^{0.2}} \left(\dfrac{\rho_{\infty_1}}{2.375 \times 10^{-3}}\right)^{0.8} \left[\left(\dfrac{P_e}{P_s}\right)_1\right]^{\frac{4.1}{6.0}} \left\{1 - \left[\left(\dfrac{P_e}{P_s}\right)_1\right]^{\frac{1}{6}}\right\}^{0.4} \\ [0.0001\ U_\infty]^{3.45} \\ \qquad \text{for } Z \leq 115{,}000 \text{ ft.} \\ \dfrac{13460}{\left[R_N\left(1 - \dfrac{\theta_c}{57.3}\right)\right]^{0.2}} \left(\dfrac{\rho_{\infty_1}}{2.375 \times 10^{-3}}\right)^{0.8} \left[\left(\dfrac{P_e}{P_s}\right)_1\right]^{\frac{4.1}{6.0}} \left\{1 - \left[\left(\dfrac{P_e}{P_s}\right)_1\right]^{\frac{1}{6}}\right\}^{0.4} \\ [0.0001\ U_\infty]^{(2.254 + 2.246 \times 10^{-5} Z - 1.469 \times 10^{-10} Z^2 + 3.671 \times 10^{-15} Z^3)} \\ \qquad \text{for } Z > 115{,}000 \text{ ft.} \end{cases}$$

The heating rates at the various stations along the conical frustum of a blunt cone in turbulent flow are:

$$K_{1T} = 0.9 + 0.02\,\theta_c$$

$$K_{2T} = \begin{cases} 1.0 \text{ for } \dfrac{R_N}{R_B} > 0.2 \\ 0.6 + 2.0\left(\dfrac{R_N}{R_B}\right) \text{ for } \dfrac{R_N}{R_B} \leq 0.2 \end{cases}$$

$$K_{3T} = 0.69 + 0.0318L - 0.00069L^2$$

$$K_{4T} = 1.0$$

$$K_{5T} = 0.69 + 0.0318\,L_A - 0.00069\,L_A^2$$

$$K_{6T} = 0.6$$

$$K_{7T} = 1.0$$

$$K_{8T} = 0.69 + 0.0318\left[L_A - R_N + \frac{R_N}{\sin\theta_c}\right] - 0.00069\left[L_A - R_N + \frac{R_N}{\sin\theta_c}\right]^2$$

$$K_{9T} = 0.901 - 0.867\left[\left(\frac{X}{L_A}\right)_j - \frac{1.13\,R_N}{3L_A\tan^2\theta_c}\right] + 0.966\left[\left(\frac{X}{L_A}\right)_j - \frac{1.13\,R_N}{3L_A\tan^2\theta_c}\right]$$

$$Q(3,j) = \begin{cases} \dfrac{\left[\left(\dfrac{P_e}{P_s}\right)_j \left(\dfrac{P_s}{2116}\right)\right]^{0.8} [10]^{0.745\,[\mathrm{Log}_e(H_s/RT_o)]^{0.8122}}}{(K_{1T})\ (K_{2T})\ (K_{3T})\ (K_{4T})} \\ \qquad \text{for } \left(\dfrac{X}{L_A}\right)_j \leq \dfrac{1.13\,R_N}{3L_A \tan^2\theta_c} \\ \dfrac{\left[\left(\dfrac{P_e}{P_s}\right)_j \dfrac{P_s}{2116}\right]^{0.8} [10]^{0.745\,[\mathrm{Log}_e(H_s/RT_o)]^{0.8122}}}{(K_{1T})\ (K_{2T})\ (K_{5T})\ (K_{9T})} \\ \qquad \text{for } \left(\dfrac{X}{L_A}\right)_j \leq \dfrac{1.13\,R_N}{L_A \tan^2\theta_c} \\ \dfrac{\left[\left(\dfrac{P_e}{P_s}\right)_j \left(\dfrac{P_s}{2116}\right)\right]^{0.8} [10]^{0.745\,[\mathrm{Log}_e(H_s/RT_o)]^{0.8122}}}{(K_{1T})\ (K_{6T})\ (K_{7T})\ K_{8T})} \\ \qquad \text{for } \left(\dfrac{X}{L_A}\right)_j > \dfrac{1.13\,R_N}{L_A \tan^2\theta_c} \end{cases}$$

3.1.3 Ablation Effects

The ablation effects on body geometry and vehicle weight are accounted for in the subroutines MASSLO, EVIL, NOSEBL, and TOMALO. It is important to note that the ablation effects are computed only in the laminar and turbulent continuum regimes. For most normal heat shield materials, the mass loss rate is determined by using the steady state ablation method at the body stations utilized in the aerodynamic heating calculations. In cases where the heat shield material chars during the reentry process or has some other unusual ablation characteristics, the mass loss rate is determined from a curve fit of experimental data. The total mass loss rate is then obtained by integrating the individual mass loss rates over the surface of the vehicle. The steady state ablation method entails an iterative solution of simultaneous equations for the surface temperature and the wall recession rate. The iterative mass transfer rate solution includes the following energy considerations: convective energy, conduction flux, surface radiation losses, and sublimation energy. Nose blunting is also included in the category

of ablation effects. The equations involved in the mass loss rate calculations provide reasonable answers only for normal reentry conditions. The purpose of these mass transfer rate equations is to obtain a reasonable approximation to the effects of ablation on drag. Consequently, the results of the ablation effects equations should not be used in heat shield design.

The subroutine EVIL, in conjunction with the subroutine MASSLO, is used to calculate the mass loss rate, $\dot{m}(i, j)$ (lbm/ft^2-sec), surface recession rate $\dot{s}(i, j)$ (ft/sec), and the wall temperature $T_w(i, j)$ (^{o} R) at the appropriate body stations. The definitions of the different subscript combinations for the above quantities are given in the drag calculations section (3.1.5). As was mentioned above, the method employed to determine the mass transfer rate is heat shield-material dependent. For OTWR in turbulent flow, and LT_a, Teflon, or any other input material in laminar or turbulent flow the steady state ablation method is used. For OTWR in laminar flow, and Carbon Phenolic, or Phenolic Nylon in laminar or turbulent flow, curve fits for $\dot{m}(i, j)$ and $\dot{s}(i, j)$ as functions of the cold wall heating and $T_w(i, j)$ as a function of $\dot{s}(i, j)$ are utilized.

To perform the mass loss rate, wall recession rate, and wall temperature calculations the following material property constants are needed:

$$\beta_1,\ \beta_2,\ \beta_3,\ \beta_4,\ H_{ref},\ \epsilon,\ \rho_2,\ F,\ \Delta\rho,\ N_{SL},\ N_{GL},\ N_{ST},\ N_{GT},\ C_{P_2},\ C_{P_G},\ \text{and}\ \Delta H_c.$$

For the heat shield materials mentioned above, the material property constants are given in subroutine CHNTBL. Also needed is the stagnation pressure, P_s (lb/ft^2), an initial guess at the wall temperature, T_{w_o} (^{o} R), and the appropriate heating rates, $Q(i, j)$ (Btu/ft^2 sec).

The iterative steady state ablation method proceeds as follows. For the first pass through the equations, the wall temperature is set equal to the initial guess at the wall temperature: $T_w(i, j) = T_{w_o}$. Then, for each subsequent iteration, the wall temperature calculated at the end of the previous iteration is used

$$\Delta T = 0.005\, T_w(i, j) + \frac{25000.}{T_w(i, j)}$$

$$\dot{S}(i, j) = \beta_1\, T_w(i, j) + e^{\text{Log}_e\left|\beta_2\left[T_w(i, j)\right]^{\beta_3}\right| - \beta_4 / T_w(i, j)}$$

$$K_1 = e^{\text{Log}_e(1.11057 \times 10^7) - 1.1112 \times 10^5 / T_w(i, j)}$$

$$K_2 \qquad \frac{\sqrt{201.8340(K_1)^2 + 756.2732\left(\frac{P_s}{2117}\right) K_1} - 12.7657\, K_1}{2\left[K_1 + 4\left(\frac{P_s}{2117}\right)\right]}$$

$$\gamma_1 = 13.654 + 469.585\ K_2$$

$$\gamma_2 = 0.256012 + 0.005558\ K_2$$

$$\gamma_3 = 5.345 \times 10^{-6} - 4.27 \times 10^{-7}\ K_2$$

The nondimensional wall enthalpy is given by:

$$\bar{H}_w = \frac{\gamma_1 + \gamma_2\, T_w(i, j) + \gamma_3 [\, T_w(i, j)]^2}{33.86}$$

$$\bar{E}_1 = \frac{\bar{H}_w}{35.89}$$

$$\bar{E}_2 = \frac{0.349 \left(\dfrac{H_s}{RT_o} \right) + \dfrac{1}{2} (\bar{H}_w)}{0.349 \dfrac{H_s}{RT_o} + 17.945}$$

$$\bar{E}_3 = 0.95 - \left[\frac{\bar{H}_w - H_{ref}}{\dfrac{H_s}{RT_o}} \right]$$

$$e_1 = \begin{cases} -0.037 & \text{for laminar and turbulent flow at stagnation point} \\ 0.0 & \text{for laminar flow at all other body station} \\ 0.0 & \text{for turbulent flow at all other body stations or turbulent sonic point flow} \end{cases}$$

$$e_2 = \begin{cases} 0.0 & \text{for laminar and turbulent flow at stagnation point} \\ -0.185 & \text{for laminar flow at all other body stations} \\ -0.502 & \text{for turbulent flow at all other body stations or turbulent sonic point flow} \end{cases}$$

$$\dot{Q}_{OF} = \dot{Q}(i, j) (\bar{E}_1)^{e_1} (\bar{E}_2)^{e_2}$$

for the case where $Q_{OF} \leq 0.0$ in any iteration, the iterative process is stopped and

$$\dot{s}(i, j) = 0.0$$

$$\dot{m}(i, j) = 0.0$$

$$\bar{f} = \begin{cases} \dfrac{\dot{s}(i, j)\, H_s\, [\rho_2\, N_{SL} + \Delta\rho\, N_{GL}]}{\dot{Q}_{OF}} & \text{for } Z \geq Z_{TR} \\ \dfrac{\dot{s}(i, j)\, H_s\, [\rho_2\, N_{ST} + \Delta\rho\, N_{GT}]}{\dot{Q}_{OF}} & \text{for } Z < Z_{TR} \end{cases}$$

$$Q_B = e^{-(\bar{f} + 0.618\, \bar{f}^{\,2})}$$

$$\dot{Q}_T = 4.7853 \times 10^{-13}\, \epsilon\, [T_w(i, j)]^4$$

$$\dot{Q}_C = \phi_B\, \bar{E}_3\, \dot{Q}_{OF}$$

$$\bar{L} = \dot{s}(i, j)\, \{[T_w(i, j) - 500.]\, (\rho_2\, C_{P_2} + C_{P_G}\, \Delta\rho) + \Delta\rho\, \Delta H_c\}$$

$$\bar{R} = \dot{Q}_c \cdot\cdot (\dot{Q}_T + \dot{Q}_S)$$

The new wall temperature to be used in the next iteration is then:

$$T_w(i, j) = T_w(i, j) + \begin{cases} \Delta T & \text{for } \bar{L} - \bar{R} < 0 \text{ and } \Delta T > 0 \\ & \text{or } \bar{L} - \bar{R} > 0 \text{ and } \Delta T < 0 \\ -0.5\, \Delta T & \text{for } \bar{L} - \bar{R} < 0 \text{ and } \Delta T < 0 \\ & \text{or } \bar{L} - \bar{R} > 0 \text{ and } \Delta T > 0 \end{cases}$$

The iterative calculations end and a solution has been found once

$$|\bar{L} - \bar{R}| < \begin{cases} 1.0 \\ \text{or} \\ 0.01\, L \end{cases}$$

or if 100 iterations have been made. Then, appropriate wall temperature is the $T_w(i, j)$ used in the last iteration and:

$$\dot{m}(i, j) = \dot{s}(i, j)\, (\rho_2 + \Delta\rho)$$

The curve fit solution for phenolic nylon heat shield material in laminar or turbulent flow is as follows:

$$\dot{m}(i,j) = \begin{cases} 10^{\left[-2.5228 + 7.3759 \times 10^{-3}\ \dot{Q}(i,j)\right]} \\ \qquad \text{for } \dot{Q}(i,j) \leq 100. \\ -1.62367642 \times 10^{-3} + 1.78922793 \times 10^{-4}\ \dot{Q}(i,j) \\ \quad + 1.32113696 \times 10^{-8} \left[\dot{Q}(i,j)\right]^2 - 5.087475 \times 10^{-12} \left[\dot{Q}(i,j)\right]^3 \\ \qquad \text{for } 100. < \dot{Q}(i,j) \leq 3000. \\ \dot{Q}(i,j) \left[\dfrac{1.0 - \dfrac{1700}{H_s}}{1845. + 11.1 \left(\dfrac{H_s}{RT_o}\right)} \right] \\ \qquad \text{for } \dot{Q}(i,j) > 3000. \end{cases}$$

The wall recession rate for phenolic nylon is ratioed from the wall recession rate of OTWR in laminar flow.

$$\dot{s}(i,j) = \frac{\left[\dot{s}(i,j)_{OTWR}\right] \dot{m}(i,j)}{\dot{m}(i,j)_{OTWR}}$$

$$T_w(i,j) = \begin{cases} 6944.74035 + 645.367146 \left[\text{Log}_{10}\ \dot{s}(i,j)\right] \\ \quad - 148.589173 \left[\text{Log}_{10}\ \dot{s}(i,j)\right]^2 \\ \qquad \text{for } \dot{s}(i,j) \geq 10^{-4} \\ 9030. + 1756 \left[\text{Log}_{10}\ \dot{s}(i,j)\right] \\ \qquad \text{for } \dot{s}(i,j) < 10^{-4} \end{cases}$$

The curve fit solution for OTWR heat shield material in laminar flow only is:

$$\dot{m}(i,j) = \begin{cases} 0.0 \text{ for } \dot{Q}(i,j) < 13.0 \\ -0.01929 + 0.00015\,\dot{Q}(i,j) \\ \quad \text{for } 13.0 \le Q(i,j) \le 15.6 \\ -1.27424339 \times 10^{-3} + 1.3607167 \times 10^{-4}\,\dot{Q}(i,j) \\ -1.09091516 \times 10^{-6}\,[\dot{Q}(i,j)]^2 + 7.98275747 \times 10^{-9}\,[\dot{Q}(i,j)]^3 \\ -1.65210579 \times 10^{-11}\,[\dot{Q}(i,j)]^4 \\ \quad \text{for } 15.6 \le \dot{Q}(i,j) < 250. \\ -1.05650025 \times 10^{-3} + 7.61118699 \times 10^{-5}\,\dot{Q}(i,j) \\ +3.342517 \times 10^{-8}\,[Q(i,j)]^2 - 6.91682422 \times 10^{-12}\,[\dot{Q}(i,j)]^3 \\ \quad \text{for } 250 \le \dot{Q}(i,j) < 3000. \\ Q(i,j)\left[\dfrac{1.0 - \dfrac{1500}{H_s}}{3640 + 8.1\,\dfrac{H_s}{RT_o}}\right] \\ \quad \text{for } \dot{Q}(i,j) \ge 3000. \end{cases}$$

The wall recession rate is:

$$\dot{s}(i,j) = \begin{cases} -5.23741 \times 10^{-4} + 1.6115 \times 10^{-6}\ \dot{Q}(i,j) \\ \qquad \text{for } \dot{Q}(i,j) < 1000. \\ -1.1119676 \times 10^{-4} + 4.03376719 \times 10^{-7}\ \dot{Q}(i,j) \\ +9.70131261 \times 10^{-10} [\dot{Q}(i,j)]^2 - 2.45527504 \times 10^{-13} [\dot{Q}(i,j)]^3 \\ \qquad \text{for } 1000 \leq \dot{Q}(i,j) < 3000. \\ \dfrac{\dot{m}(i,j)}{\rho_2 + \Delta\rho} \\ \qquad \text{for } \dot{Q}(i,j) \geq 3000. \end{cases}$$

and the wall temperature is given by:

$$T_w(i,j) = 6346.34912 + 550.628796 [\text{Log}_{10}\ \dot{S}(i,j)] + 19.6585366 [\text{Log}_{10}\ \dot{S}(i,j)]^2$$

For carbon phenolic heat shield material in laminar flow, the ablation characteristics are given by:

$$\dot{m}(i,j) = \begin{cases} 0.0 \text{ for } \dot{Q}(i,j) < 8.0 \\ 6.5788 \times 10^{-4} - 1.59773 \times 10^{-4}\ \dot{Q}(i,j) + 9.8485 \times 10^{-6} [\dot{Q}(i,j)]^2 \\ \qquad \text{for } 8.0 \leq \dot{Q}(i,j) < 11.3 \\ -9.9516436 \times 10^{-4} + 9.78022 \times 10^{-5}\ \dot{Q}(i,j) \\ \qquad \text{for } 11.3 \leq \dot{Q}(i,j) < 23.1 \end{cases}$$

$$\dot{m}(i,j) = \begin{cases} -1.73043255 \times 10^{-3} + 1.25965766 \times 10^{-4}\,\dot{Q}(i,j) \\ \quad - 8.56939032 \times 10^{-8}\,[\dot{Q}(i,j)]^2 + 4.65548312 \times 10^{-12}\,[\dot{Q}(i,j)]^3 \\ \quad \text{for } 23.1 \le \dot{Q}(i,j) \le 1000. \\ 1.23284002 \times 10^{-2} + 3.30858843 \times 10^{-5}\,\dot{Q}(i,j) \\ \quad + 4.60267808 \times 10^{-9}\,[\dot{Q}(i,j)]^2 \\ \quad \text{for } \dot{Q}(i,j) > 1000. \end{cases}$$

$$\dot{s}(i,j) = \begin{cases} 1.0 \times 10^{-18} \quad \text{for } \dot{Q}(i,j) < 24.7 \\ -2.12296558 \times 10^{-6} + 1.18955951 \times 10^{-7}\,\dot{Q}(i,j) \\ \quad + 1.40098706 \times 10^{-10}\,[\dot{Q}(i,j)]^2 \\ \quad \text{for } 24.7 \le \dot{Q}(i,j) < 275. \\ 7.66757321 \times 10^{-5} - 4.95033115 \times 10^{-7}\,\dot{Q}(i,j) \\ \quad + 1.55581653 \times 10^{-9}\,[\dot{Q}(i,j)]^2 - 8.4923939 \times 10^{-13}\,[\dot{Q}(i,j)]^3 \\ \quad \text{for } 275 \le \dot{Q}(i,j) < 1000. \\ -3.186484 \times 10^{-4} + 3.869 \times 10^{-7}\,\dot{Q}(i,j) + 2.171792 \times 10^{-10}\,[\dot{Q}(i,j)]^2 \\ \quad \text{for } \dot{Q}(i,j) \ge 1000. \end{cases}$$

$$T_w(i,j) = 6687.41134 + 446.431845\,[\mathrm{Log}_{10}\,\dot{S}(i,j)] + 12.0991623\,[\mathrm{Log}_{10}\,\dot{S}(i,j)]^2$$

For carbon phenolic heat shield material in turbulent flow, the curve fit solution for the ablation characteristics incorporates a portion of the first iteration from the steady state ablation method. As in the iterative solution, an initial trial value is chosen for the wall temperature: $T_w(i,j) = T_{w_o}$ then, the solution proceeds as follows:

$$\Delta T = 0.005\, T_{w_o} + \frac{25000.}{T_{w_o}}$$

$$S_{PD} = \beta_1 T_{w_o} + e^{\mathrm{Log_e}[\beta_2 (T_{w_o})^{\beta_3}] - \beta_4 / T_{w_o}}$$

$$K_1 = e^{\mathrm{Log_e}(1.11057 \times 10^7) - 1.1112 \times 10^5 / T_{w_o}}$$

$$K_2 = \frac{\sqrt{201.8340 (K_1)^2 + 756.2732 \dfrac{P_s}{2117} K_1} - 12.7657\, K_1}{2\, K_1 + 4 \dfrac{P_s}{2117}}$$

$$\gamma_1 = 13.654 + 469.585\, K_2$$

$$\gamma_2 = 0.256012 + 0.005558\, K_2$$

$$\gamma_3 = 5.345 \times 10^{-6} - 4.27 \times 10^{-7}\, K_2$$

The nondimensional wall enthalpy is given by:

$$\bar{H}_w = \frac{\gamma_1 + \gamma_2 T_{w_o} + \gamma_3 (T_{w_o})^2}{33.86}$$

$$\bar{E}_1 = \frac{\bar{H}_w}{35.89}$$

$$E_2 = \frac{0.349 \left(\dfrac{H_s}{RT_o}\right) + \dfrac{1}{2} (\bar{H}_w)}{0.349 \left(\dfrac{H_s}{RT_o}\right) + 17.945}$$

$$\bar{E}_3 = 0.95 - \left[\frac{\bar{H}_w - H_{ref}}{\dfrac{H_s}{RT_o}}\right]$$

$$e_1 = \begin{cases} -0.037 & \text{for stagnation point in turbulent flow} \\ 0.0 & \text{for sonic point and all other body stations in turbulent flow} \end{cases}$$

$$e_2 = \begin{cases} 0.0 & \text{for turbulent flow at the stagnation point} \\ -0.502 & \text{for sonic point and all other body stations in turbulent flow} \end{cases}$$

$$\dot{Q}_{OF} = \dot{Q}(i, j) (\bar{E}_1)^{e_1} (\bar{E}_2)^{e_2}$$

$$f = \frac{S_{PD} H_s [\rho_2 N_{ST} + \Delta\rho N_{GT}]}{\dot{Q}_{OF}}$$

$$\phi_B = e^{-(\bar{f} + 0.618 \bar{f}^2)}$$

$$\dot{Q}_T = 4.7853 \times 10^{-13} \epsilon (T_{w_o})^4$$

$$\dot{Q}_C = \phi_B E_3 \dot{Q}_{OF}$$

$$\dot{Q}_{NET} = \dot{Q}_C - \dot{Q}_T$$

$$Q^* = C_{P_2} (6160 - T_{w_o}) + F + N_{ST} \left(\frac{H_s}{RT_o}\right)$$

$$\dot{m}(i, j) = \frac{\dot{Q}_{NET}}{Q^*}$$

$$\dot{s}(i, j) = \frac{0.8 \dot{m}(i, j)}{\rho_2}$$

$$T_w(i, j) = 6687.41134 + 446.431845 [\text{Log}_{10} \dot{S}(i, j)] + 12.0991623 [\text{Log}_{10} \dot{S}(i., j)]^2$$

The subroutine NOSEBL is used to calculate the derivatives with respect to time of the nose radius, base radius, and side walls in order to determine the shape change for a body in continuum flow with a constant cone half-angle. For cases where the bluntness ratio is less than or equal to 10^{-3}, the body is considered to be sharp. In the following calculations the appropriate wall recession rate, based upon the heat shield material being considered, must be employed. The only input necessary for these calculations is the wall recession rate, $\dot{S}(i, j)$ which was computed previously. For laminar or turbulent flow and sharp or blunt cones, the rate of change of the nose radius is given by:

$$\dot{R}_N = \frac{\dot{S}(1, 1) \sin \theta_c}{1 - \sin \theta_c}$$

For a sharp cone, the maximum diameter sidewall recession rate is:

$$\dot{S}_w = \begin{cases} 0.7071\ \dot{S}(2, 8) & \text{for } Z \geq Z_{TR} \\ 0.8706\ \dot{S}(3, 8) & \text{for } Z < Z_{TR} \end{cases}$$

For a blunt cone, the maximum diameter sidewall recession rate is:

$$\dot{S}_w = \begin{cases} \dot{S}(2, 7) & \text{for } Z \geq Z_{TR} \\ \dot{S}(3, 7) & \text{for } Z < Z_{TR} \end{cases}$$

Then, for both flow conditions and both body configurations, the base radius recession rate is given by:

$$\dot{R}_B = - \frac{\dot{S}_w}{\cos \theta_c}$$

The subroutine TOMALO is used to determine the rate of change in weight due to ablation. This is accomplished by integrating the mass loss rates for the different body stations over the surface of the body. The necessary inputs are the mass loss rates, $\dot{m}(i, j)$ at the various body stations, the axial locations of the body stations, $\left(\frac{X}{L_A}\right)_j$, and the axial length of the body, L_A. For a sharp cone, the total mass loss rate is:

$$\dot{w} = \begin{cases} -2.9618 \sqrt{2}\ (L_A)^2\ \dfrac{\tan \theta_c}{\cos \theta_c}\ \dot{m}(2, 8) \\ \qquad \text{for } Z \geq Z_{TR} \\ -3.04(2.0)^{0.2}\ \dfrac{\tan \theta_c}{\cos \theta_c}\ (L_A)^2\ \dot{m}(2, 8) \\ \qquad \text{for } Z < Z_{TR} \end{cases}$$

For a blunt cone, the total weight loss rate is composed of the mass loss rate from the spherical nose cap and the mass loss rate from the conical frustum. The total mass loss rate on the spherical nose is:

$$M_N = \begin{cases} \pi R_N^2 (1 - \sin\theta_c)[\dot{m}(1,1) + \dot{m}(2,1)] \\ \qquad \text{for } Z \geq Z_{TR} \\ 0.7351 R_N^2 \left\{ \dot{m}(1,1) + \dot{m}(4,1) + \left(\frac{0.766 - \sin\theta_c}{0.234}\right)[\dot{m}(4,1) + \dot{m}(3,1)] \right\} \\ \qquad \text{for } Z < Z_{TR} \end{cases}$$

The conical frustum contribution to the total mass loss rate is:

$$M_C = \begin{cases} \sum_{j=1}^{6} \pi \left(\frac{L_A}{\cos\theta_c}\right)^2 \left[\left(\frac{X}{L_A}\right)_{j+1} - \left(\frac{X}{L_A}\right)_j\right] \left\{ R_N \left(\frac{1 - \sin\theta_c}{L_A}\right) + 0.5 \sin\theta_c \left[\left(\frac{X}{L_A}\right)_{j+1} - \left(\frac{X}{L_A}\right)_j\right] \right\} [\dot{m}(2,j)] + \dot{m}(2,j+1) \\ \qquad \text{for } Z \geq Z_{TR} \\ \sum_{j=1}^{6} \pi \left(\frac{L_A}{\cos\theta_c}\right)^2 \left[\left(\frac{X}{L_A}\right)_{j+1} - \left(\frac{X}{L_A}\right)_j\right] \left\{ R_N \left(\frac{1 - \sin\theta_c}{L_A}\right) + 0.5 \sin\theta_c \left[\left(\frac{X}{L_A}\right)_{j+1} - \left(\frac{X}{L_A}\right)_j\right] \right\} [\dot{m}(3,j)] + \dot{m}(3,j+1) \\ \qquad \text{for } Z < Z_{TR} \end{cases}$$

Thus, the total weight loss rate is:

$$\dot{w} = -(M_N + M_C)$$

3.1.4 Angle of Attack

The angle of attack, which is incorporated into the drag calculations, is determined by the subroutine ROTATE. Two methods are available for calculating the angle of attack a. uncoupled rotational three-degree-of-freedom method and b. simplified angle of attack method. In both methods, the objective is to define an angle of attack value (α) from the oscillatory variations in angle of attack that occur from perturbing forces and moments. For the three-degree-of-freedom method the necessary inputs are the pitch and yaw Euler angles, θ_α and ψ, the rolling component of rotation, P, the maximum, $\approx{\alpha}'$, and minimum, $\sim{\alpha}'$, perturbed angle of attack values from the previous oscillation, the minimum, t_L, and maximum, t_H, time limits on the period of oscillation, the time of the first maximum in angle of attack, τ_1, the time of the second maximum in angle of attack, τ_2, the period of oscillation, t', the viscous interaction parameter, $\bar{\chi}$, cone half-angle, θ_c, and the bluntness ratio. The total angle of attack is given by:

$$\alpha' = \cos^{-1}[\cos\theta_\alpha \cos\psi]$$

The angle of attack, α, forwarded to the drag calculations is dependent upon the flow regime, cycle time, rolling rotation rate. For the strong interaction regime ($\bar{\chi} \geq \chi_{up}$):

$$\alpha = \alpha'$$

For laminar and turbulent continuum flow ($\bar{\chi} < \chi_{up}$):

$$\alpha = \begin{cases} \alpha' & \text{for } t' = 0 \\ \alpha' & \text{for } t' \geq t_H \\ \dfrac{2\approx{\alpha}'}{\pi} & \text{for } t' < t_L \text{ and } P = 0 \\ \dfrac{\approx{\alpha}' + \sim{\alpha}'}{2} & \text{for } t' < t_L \text{ and } P \neq 0 \end{cases}$$

For the case where the period of oscillation, t', is between the two limiting cycle times, an integrated angle of attack is calculated. As noted in the drag section, this angle of attack is used only to modify the forebody pressure drag. Thus, for $t_L \leq t' < t_H$, the angle of attack is calculated as follows:

$$\bar{A}_2 = [A_{12} + A_{15}\theta_c + A_{18}\theta_c^2] + [A_{21} + A_{24}\theta_c + A_{27}\theta_c^2]\lambda + [A_{30} + A_{33}\theta_c + A_{36}\theta_c^2]\lambda^2$$

$$\bar{A}_3 = [A_{13} + A_{16}\theta_c + A_{19}\theta_c^2] + [A_{22} + A_{25}\theta_c + A_{28}\theta_c^2]\lambda + [A_{31} + A_{34}\theta_c + A_{37}\theta_c^2]\lambda^2$$

then,

$$\bar{\alpha} = \int_{r_1}^{r_2} \frac{(\bar{A}_2\,\alpha + \bar{A}_3\,\alpha)}{t'}\,dr$$

The simplified angle of attack method is a straightforward approach requiring no integration. The angle of attack supplied to the drag calculations is dependent upon the period of oscillation, $\bar{t}$, of the vehicle. For this method the period is calculated below. The necessary inputs are the derivatives of the pitching moment coefficient with q and α, C_{M_q} and C_{M_α}, derivative of normal force coefficient with α, C_{N_α}, the minimum time limit on the period of oscillation, t_L, initial flight path angle, γf_o, initial Euler angle in the pitch direction, θ_α, drag coefficient, C_D, altitude variation of the axial moment of inertia, I, vehicle instantaneous weight, W, and the geometric and flow field properties. The calculations are as follows:

$$\beta_z = -\mathrm{Log_e}\left(\frac{\rho_{\infty_1}}{0.076474}\right)$$

If the initial altitude ($Z = Z_o$) is being considered then the drag coefficient is set to a constant value: $C_D = 0.8$. Otherwise the drag coefficient obtained from the drag calculation section is used.

$$A_{K1} = \frac{32.174\,\pi\,R_B^2\,Z}{4\,\beta_z\,W\,|\sin\gamma_{f_o}|}\left[2\,C_D - C_{N_\alpha} + \frac{4\,R_B^2\,C_{M_q}\,W}{32.174\,I}\right]$$

$$A_{K2} = \frac{32.174\,\pi\,R_B^2\,Z^2}{2W\,(\beta_z \sin\gamma_{f_o})^2}\left[\frac{(C_{N_\alpha} - C_D)\,\beta_z\,|\sin\gamma_{f_o}|}{Z} - \frac{2\,R_B\,W\,C_{M_\alpha}}{32.174\,I}\right]$$

The period of oscillation is given by:

$$\bar{t} = \frac{-2\pi Z}{\beta_z\,U_\infty \sin\gamma_{f_o}\,\sqrt{A_{K2}\,\rho_\infty}}$$

The total angle of attack equations necessitate the calculation of Bessel functions of the first and second kind of the zeroth and first orders. These Bessel functions are to be functions of S where:

$$\tilde{S} = 2\sqrt{\rho_\infty (A_{K1} + A_{K2})}$$

The Bessel functions calculated are:

$$Y_o(\tilde{S}),\ Y_1(\tilde{S}),\ J_o(\tilde{S}),\ J_i(\tilde{S})$$

For the initial altitude ($Z = Z_o$) only, the following calculations are made:

$$A_{C2} = \left\{ \left[\frac{2.3769 \times 10^{-3} \beta_z \theta_{a_o} A_{K1} J_o(\tilde{S})}{\beta_z + Z_o \exp(A_{K1} \rho_\infty)} \right] - \left[\frac{\tilde{S} \theta_{a_o} \beta_z J_1(\tilde{S}) \exp(-A_{K1} \rho_\infty)}{2 Z_o} \right] \right\}$$

$$\left\{ \frac{\tilde{S}\beta_z}{2Z_o} \left[Y_1(\tilde{S}) J_o(\tilde{S}) - J_1(\tilde{S}) Y_o(\tilde{S}) \right] \right\}^{-1}$$

$$A_{C1} = \frac{\theta_{a_o} e^{-\rho_\infty A_{K1}} - A_{C2} Y_o(\tilde{S})}{J_o(\tilde{S})}$$

The angle of attack ratio at the initial altitude is:

$$\frac{a}{a_i} = \frac{e^{\rho_\infty A_{K1}}}{\sqrt{\pi \sqrt{A_{K2} \rho_\infty}}}$$

For all other altitudes the angle of attack ratio is:

$$\frac{a}{a_o} = \frac{e^{\rho_\infty A_{K1}}}{\sqrt{\pi \sqrt{A_{K2} \rho_\infty}}}$$

The total angle of attack is then given by:

$$\alpha' = \begin{cases} \left[A_{C1} J_o(\tilde{S}) + A_{C2} Y_o(\tilde{S}) \right] e^{\rho_\infty A_{K1}} & \text{for } \bar{t} > t_L \\ 0.63661\, \theta_{a_o} & \text{for } \bar{t} \leq t_i \text{ and } Z = Z_o \\ 0.63661\, \theta_{a_o} \dfrac{(a/a_o)}{(a/a_i)} & \text{for } \bar{t} \leq t_L \text{ and } Z < Z_o \end{cases}$$

and

$$\alpha = \alpha'$$

3.1.5 Drag

The analytical expressions for the drag coefficients are ordered according to the flight regimes encountered during the reentry process: free molecular transition flow, strong interaction flow, laminar continuum flow, and turbulent continuum flow respectively. Since the theoretical developments in each regime are based on different analytical models, discontinuities exist at the regime interfaces. To provide a continuous drag history, fairing techniques are used between the flight regimes. The viscous interaction parameter, $\bar{\chi}$, the rarefaction parameter, $\bar{\chi}_j$, and the transition altitude, Z_{TR}, dictate which flow or fairing regime is to be used in the drag analysis. The range of applicability of the given body parameters and flight conditions for this drag model are:

- Cone Half-Angle $4^\circ \leq \theta_c \leq 27^\circ$
- Body Length $1' \leq L_A \leq 14'$
- Surface Temperature $1000^\circ R \leq T_w \leq 6000^\circ R$
- Bluntness Ratio $0.0 \leq \lambda \leq 0.6$
- Altitude $0.0' \leq Z \leq 400{,}000'$
- Free-Stream Mach Number $5.0 \leq M_\infty \leq 30.0$
- Angle of Attack at 300 kft $0^\circ \leq \alpha \leq 20^\circ$
- Angle of Attack < 150 kft $0^\circ \leq \alpha \leq \theta_c$

Several body and flow parameters are needed to initiate the drag calculations. They are cone half-angle, θ_c (degrees), angle of attack, α (degrees), free-stream velocity, U_∞ (ft/sec), altitude Z (ft.), and any two of the following: bluntness ratio λ, base radius R_B(ft.), or nose radius R_N (ft.). Also needed are the wall temperature, T_w (i,j) ($^\circ$R), mass loss rate, $\dot{m}$ (i,j) (lbm/ft^{2}sec), the wall enthalpy, H_w, and the total mass loss rate, $\dot{W}$ (lbm/sec). The wall temperature, wall enthalpy, and mass loss rate are calculated in the subroutine EVIL.

The subscripts i and j refer to specific flow regimes and body stations. The subscript combinations used in the drag calculations are as follows:

1,1 = stagnation point

2,1 = tangent point on a blunt cone in laminar flow

2,2 = 20 percent station of the initial length of the cone in laminar flow

2,3 = 40 percent station of the initial length of the cone in laminar flow

2,4 = 60 percent station of the initial length of the cone in laminar flow

2,5 = 75 percent station of the initial length of the cone in laminar flow

2,6 = 90 percent station of the initial length of the cone in laminar flow

2,7 = Maximum diameter point on a blunt cone in laminar flow

2,8 = Maximum diameter point of a sharp cone for the given cone half-angle in laminar flow

3,J where J = 1,2,...,8 = Turbulent flow for the same body stations used in laminar flow

4,1 = sonic point in turbulent flow

The total mass loss rate, $\dot{W}$, is calculated in the subroutine TØMALØ and is the integrated value of $\dot{m}(i,j)$ over the surface of the body.

In the laminar and turbulent flow regimes, the following notation will be used to identify the various skin friction drag terms. The skin friction drag coefficient will be denoted by $C_{D_f}(i,j,k)$ where:

i = 1: sharp cone

i = 2: blunt cone

j = 1: turbulent flow

j = 2: laminar flow

k = 1: ablation

k = 2: no ablation

Sharp cone inviscid pressure drag coefficient for the given cone angle:

$$C_{D_{P_{LEO}}} = \frac{P_e}{1/2\,\rho_\infty U_\infty^2}$$

The forebody pressure drag coefficient, as calculated below, is used in the strong interaction flow regime, laminar continuum regime, and turbulent continuum regime. For sharp and blunt cone configurations, the zero angle of attack forebody pressure drag coefficient is:

$$C_{D_{P_o}} = \begin{cases} \displaystyle\sum_{i=0}^{2}\sum_{j=0}^{2}\sum_{k=0}^{3} A(211+i+3j+9k)\left(\frac{1}{M_\infty}\right)^i (\lambda)^j \left(\frac{1}{\theta_c}\right)^k & \text{for } 4^\circ \leq \theta_c \leq 10^\circ \\ \displaystyle\sum_{i=0}^{2}\sum_{j=0}^{2}\sum_{k=0}^{3} A(247+i+3j+9k)\left(\frac{1}{M_\infty}\right)^i (\lambda)^j \left(\frac{1}{\theta_c}\right)^k & \text{for } 10^\circ < \theta_c \leq 20^\circ \\ \displaystyle\sum_{i=0}^{2}\sum_{j=0}^{2}\sum_{k=0}^{3} A(312+i+3j+9k)\left(\frac{1}{M_\infty}\right)^i (\lambda)^j \left(\frac{1}{\theta_c}\right)^k & \text{for } 20^\circ < \theta_c \leq 40^\circ \end{cases}$$

θ_c has the units of degrees in the above summations.

The corrections for angle of attack effects on forebody pressure drag are presented below.

$$K' = \sum_{i=0}^{3}\sum_{j=0}^{2}\sum_{k=0}^{2} A(348+i+4j+12k) \left[\text{Log}_{10}(\theta_c)\right]^i \left[\text{Log}_{10}(|\alpha|)\right]^j (\lambda)^k$$

If $K' < 0.0$, then set $K' = 0.0$.

$$\frac{C_{D_\alpha}}{C_{D_o}} = \begin{cases} \displaystyle\sum_{i=0}^{3}\sum_{j=0}^{2}\sum_{k=0}^{2} A(421 + i + 4j + 12k)(\theta_c)^i(|\alpha|)^j(\lambda)^k & \text{for } |\alpha| \leq 4^\circ \\ 10^{K'} & \text{for } 4^\circ < |\alpha| \leq 40^\circ \end{cases}$$

If $C_{D_\alpha}/C_{D_o} < 1.0$, then set $C_{D_\alpha}/C_{D_o} = 1.0$.

Thus, the forebody pressure drag coefficient for zero angle of attack is:

$$C_{D_P} = C_{D_{P_o}}$$

and for angle of attack cases:

$$C_{D_P} = C_{D_{P_o}} [C_{D_\alpha}/C_{D_o}]$$

> NOTE: If a rotational three-degree-of-freedom trajectory is being calculated and if the period of oscillation of the vehicle, t', is between the upper and lower cycle time limits that are input, the only angle of attack correction made is on the forebody pressure drag. The correction is:

$$C_{D_P} = C_{D_{P_o}} (1 + \bar{\alpha})$$

where $\bar{\alpha}$ is the integrated angle of attack calculated in the angle of attack section (SUBROUTINE ROTATE).

Necessary for the induced drag calculations in laminar and turbulent continuum flow are the induced pressure gradient parameter:

$$F_1(K) = 0.9 - 0.119\, M_\infty \sin\theta_c + 0.0108\,(M_\infty \sin\theta_c)^2$$

and the wall temperature parameter:

$$d_\infty = \frac{0.968}{M_\infty^2}\,\frac{T_w(2,8)}{T_\infty} + 0.058$$

To determine in which flow or fairing regime the drag calculations are made, a check is made on the values of $\bar{\chi}$ and $\bar{\chi}_1$. The endpoints of the fairing regime between free molecular transition flow and strong interaction flow are defined by $\chi 1_{up}$ and $\chi 1_{low}$. The values generally used are $\chi 1_{up} = 0.4$ and $\chi 1_{low} = 0.2$ but other values may be used in special cases to provide a smooth drag history. Likewise, the endpoints of the fairing regime between strong interaction drag and continuum drag are defined by χ_{up} and χ_{low}. The values generally used are $\chi_{up} = 6.0$ and $\chi_{low} = 4.0$ but, again, other values may be used.

1. If $\bar{\chi}_1 \geq \chi 1_{up}$, only the free-molecular drag is calculated.

2. If $\bar{\chi}_1 < \chi 1_{up}$ and $\bar{\chi}_1 \geq \chi 1_{low}$, the free-molecular drag and the strong interaction drag are both calculated and the fairing technique for values between those two regimes is utilized.

3. If $\bar{\chi}_1 < \chi 1_{low}$ and $\bar{\chi} > \chi_{up}$, only strong interaction drag is calculated.

4. If $\bar{\chi} \leq \chi_{up}$ and $\bar{\chi} \geq \chi_{low}$, the strong interaction drag and the laminar continuum drag are both calculated and the fairing technique for values between those two regimes is utilized.

5. If $\bar{\chi} \leq \chi_{low}$ and $Z \geq Z_{TR}$, the laminar continuum drag is calculated.

6. If $Z < Z_{TR}$ and $Z > (Z_{TR} - 20{,}547.8)$ both continuum laminar drag and continuum turbulent drag are calculated and the fairing technique for values between those two regimes is utilized.

7. If $Z \leq (Z_{TR} - 20{,}547.8)$ the continuum turbulent drag is calculated.

The free-molecular transition drag regime is described by the following system:

$$\text{(Transition System)} = P(c)\,\text{(Free Molecule Flow System)} + (1 - P(c))\,\text{(Continuum System)}$$

where $P(c)$ is the probability that a molecule will collide with the surface before colliding with another molecule.

A curve fit of $P(c)$ as a function of Knudsen number yields the following relationship:

$$\lambda_w = \frac{2.11053 \times 10^{-7}}{12.25\, \rho_{\infty_1} M_\infty} \sqrt{\frac{1305\, \pi}{\gamma T_\infty}}$$

$$D = 2 R_N$$

$$P(c) = \begin{cases} \displaystyle\sum_{i=0}^{20} B(i) \left[\text{Log}_{10} \left(\frac{\lambda_w}{D} \right)^i \right] & \text{for } \dfrac{\lambda_w}{D} \geq 0.04 \\ 0.506 - 0.147\, \text{Log}_{10} \left(\dfrac{0.04\, D}{\lambda_w} \right) & \text{for } \dfrac{\lambda_w}{D} < 0.04 \end{cases}$$

For a sharp cone the above system reduces to:

$$C_{D_C} = P(c)\, C_{D_{FM}} + (1 - P(c))\, C_{D_N}$$

The free-molecule drag coefficient is:

$$C_{D_{FM}} = f_x \left[\frac{1}{M_\infty \sin\theta_c \sqrt{\pi}} + \frac{1}{2 M_\infty^2} \left(\frac{T_w}{T_\infty} \right)^{1/2} \right] e^{-M_\infty^2 \sin^2\theta_c}$$

$$+ \left[1 + \frac{1}{2M_\infty^2} + \frac{\sin\theta_c \sqrt{\pi}}{2 M_\infty} \left(\frac{T_w}{T_\infty} \right)^{1/2} \right] \left[1 + \operatorname{erf}(M_\infty \sin\theta_c) \right]$$

where f_x is an axial accommodation coefficient taken to be 0.9. The continuum drag will be taken as the Newtonian value $C_{D_N} = 2 \sin^2\theta_c$.

For the blunt cone, we perform the analysis similar to a free-molecule or a Newtonian analysis. The drag on a blunt cone

$$C_{D_B} = C_{D_S} \left(\frac{R_N}{R_B} \right)^2 \cos^2\theta_c + C_{D_C} \left[1 - \left(\frac{R_N}{R_B} \right)^2 \right]$$

here C_{D_C} is the value of the drag obtained for a sharp cone as shown in the above equation. The quantity C_{D_S} is the free molecule drag coefficient on a spherical nose and a curve fit of experimental data yields

$$C_{D_S} = C_{D_{FM_S}} \sum_{n=1}^{20} A(174 + n) \left[\operatorname{Log}_{10} \left(\frac{Re_{\infty_L} D}{M_\infty L \sqrt{\gamma}} \right) \right]^{n-1}$$

where the free-molecular drag for a sphere is

$$C_{D_{FM_S}} \left[2 + \left(\frac{2}{M_\infty^2} \right) - \left(\frac{1}{2M_\infty^4} \right) \right] \operatorname{erf}(M_\infty) + \frac{e^{-M_\infty^2}}{\sqrt{\pi}} \left(\frac{1}{M_\infty^3} + \frac{2}{M_\infty} \right)$$

$$+ \frac{2}{3} \frac{\sqrt{\pi}}{M_\infty} \left(\frac{T_w}{T_\infty} \right)$$

Since the sphere drag is rather a small portion of the total blunt cone drag we will approximate the above result for hypersonic speeds

$$C_{D_{FM_S}} = 2.0$$

Thus, for a sharp cone in free-molecular transition flow

$$C_D = C_{D_{FM}} = C_{D_C}$$

and for a blunt cone in free-molecular transition flow

$$C_D = C_{D_{FM}} = C_{D_B}$$

The drag in the strong interaction regime is composed of interaction effects and pressure drag. The interaction drag is defined as follows:

$$C_{D_{ST}} = \begin{cases} \exp\left\{\sum_{i=0}^{1}\sum_{j=0}^{1}\sum_{k=0}^{1} A(200 + i + 2j + 4k)\right. \\ \left[\mathrm{Log}_e\left(\frac{\bar{X}_1}{\sin^2\theta_c}\right)\right]^i (\theta_c)^j \left[\frac{580.0}{T_\infty\left(1 + \frac{\gamma - 1}{2} M_\infty^2\right)}\right]^k \Bigg\} \\ \qquad \text{for } \theta_c < 15^\circ \\ \exp\left\{\sum_{i=0}^{1}\sum_{j=0}^{1}\sum_{k=0}^{1} A(384 + i + 2j + 8k)\right. \\ \left[\mathrm{Log}_e\left(\frac{\bar{X}_1}{\sin^2\theta_c}\right)\right]^i (\theta_c)^j \left[\frac{580.0}{T_\infty\left(1 + \frac{\gamma - 1}{2} M_\infty^2\right)}\right]^k \Bigg\} \\ \qquad \text{for } \theta_c \geq 15^\circ \end{cases}$$

The total drag in the strong interaction regime for sharp and blunt cones, including angle of attack effects, is:

$$C_D = C_{D_S} = (C_{D_{ST}} - C_{D_{P_{LEO}}}) \left[1 - \left(\frac{R_N}{R_B}\right)^2\right] \cos(\alpha') + C_{D_P}$$

The fairing between the free molecular and strong interaction regimes is a linear weighting based on the rarefaction parameter value between the drag coefficients of both regimes evaluated at the point of interest.

$$C_D = C_{D_{FM}} \left[\frac{\bar{X}_1 - X1_{low}}{X1_{up} - X1_{low}}\right] + C_{D_S} \left[1 - \frac{\bar{X}_1 - X1_{low}}{X1_{up} - X1_{low}}\right]$$

For laminar continuum flow, the drag is composed of forebody pressure drag, base pressure drag, skin friction drag, induced pressure drag, pressure gradient induced skin friction drag, and transverse-curvature induced skin friction drag. The forebody pressure drag is given in the preliminary calculations section. For the base pressure drag, a curve fit of test data gives

$$\frac{P_B}{P_\infty} = \begin{cases} \displaystyle\sum_{i=0}^{3}\sum_{j=0}^{2} A(487+i+4j)\left(\frac{1}{M_\infty}\right)^i \left(\frac{\dot{W}}{\rho_{\infty_1} U_\infty A_{Ref}}\right)^j & \text{for } 4.0 \leq M_\infty < 7.0 \\ \displaystyle\sum_{i=0}^{3}\sum_{j=0}^{2} A(499+i+4j)\left(\frac{1}{M_\infty}\right)^i \left(\frac{\dot{W}}{\rho_{\infty_1} U_\infty A_{Ref}}\right)^j & \text{for } M_\infty \geq 7.0 \end{cases}$$

$$C_{D_B} = \left[1 - \frac{P_B}{P_\infty}\right] \frac{1}{0.7\, M_\infty^2}$$

The sharp cone laminar skin friction drag for the no mass addition case was derived from the Blasius flat plate incompressible solution modified for conical flow and compressibility. The solution is

$$\frac{h^*}{h_e} = 0.5 + 0.5\,\frac{C_{P_w} T_w(2,8)}{C_{P_e} T_e} + 0.0935(\gamma - 1) M_e^2$$

$$C_{D_f}(1,2,2) = \frac{1.53}{\sqrt{Re_{\infty_L}}} \left(\frac{U_e}{U_\infty}\right)^{1.5} \left(\frac{P_e}{P_\infty}\right)^{0.5} \left(\frac{C_{P_e} T_e}{0.2398\, T_\infty}\right)^{-0.185} \left(\frac{h^*}{h_e}\right)^{-0.185} \cot\theta_c$$

The mass addition correction to skin friction drag and the boundary layer displacement effects in the induced drag components are dependent upon the laminar no blowing skin friction coefficient, which is:

$$C_{f_{o_L}} = \frac{1.15}{1.53} \tan\theta_c \frac{\rho_{\infty_1} U_\infty^2}{\rho_e U_e^2} C_{D_f}(1,2,2)$$

The blowing skin friction drag is then:

$$C_{D_f}(1,2,1) = \frac{C_{D_f}(1,2,2)}{1 + \frac{2\dot{m}(2,8)}{\rho_e U_e C_{f_{o_L}}}}$$

The effect of bluntness on the skin friction drag, for both blowing and no blowing cases, is as follows:

$$C_{D_f}(2,2,k) = C_{D_f}(1,2,k) \begin{cases} \sum_{i=0}^{4}\sum_{j=0}^{2} A(457+i+5j)\,[\mathrm{Log}_{10}(Re_{\infty_L})]^i \left(\frac{R_N}{R_B}\right)^j & \text{for } \frac{R_N}{R_B} < 0.2 \\ \sum_{i=0}^{4}\sum_{j=0}^{2} A(472+i+5j)\,[\mathrm{Log}_{10}(Re_{\infty_L})]^i \left(\frac{R_N}{R_B}\right)^j & \text{for } \frac{R_N}{R_B} \geq 0.2 \end{cases}$$

where the k in the skin friction drag coefficient subscript can be set for either mass transfer or no mass transfer.

If mass transfer and aerodynamic heating effects are being considered in the calculation of the induced drag components, the wall enthalpy is set equal to the wall enthalpy calculated in subroutine EVIL:

$$H_w = \overline{H_w}$$

If a nonablating case is being considered, the wall enthalpy is:

$$H_w = 0.24\, T_w(2,8)$$

The recovery enthalpy is:

$$H_R = 0.9\, H_s$$

For all three components of induced drag in laminar flow, the change in effective cone angle due to displacement effects is:

$$\theta_{eff} - \theta_c = \frac{C_{f_o}}{2\sqrt{3}} \left\{ \left[\frac{2\dot{m}(2,8)}{\rho_e U_e C_{f_{o_L}}} + \frac{1}{1 + \frac{1.25\,\dot{m}(2,8)}{\rho_e U_e C_{f_{o_L}}}} \right] * \sum_{i=0}^{1} \sum_{j=0}^{3} A(283 + i + 2j)(M_e^2)^i \left(\frac{H_w}{H_R} \right)^j \right\} + \frac{\dot{m}(2,8)}{3\rho_e U_e}$$

The induced pressure drag coefficient is therefore:

$$C_{D_{I_P}} = 1.33\sqrt{3} \left[1 - \left(\frac{R_N}{R_B} \cos\theta_c \right)^2 \right] C_{D_{P_{LEO}}}$$

$$(\theta_{eff} - \theta_c)\, F_1(K)\, M_e$$

The pressure induced skin friction drag is:

$$C_{D_{I_f}} = \frac{1.5}{M_e\sqrt{L}} \left[1 - \left(\frac{R_N}{R_B} \cos\theta_c \right)^2 \right] C_{D_f}(1,2,2)\, F_1(K)$$

$$(\theta_{eff} - \theta_c) \left[-0.823 + 0.524 \frac{T_w(2,8)}{T_e} + 0.483\, M_e^2 \right]$$

The transverse curvature induced drag is:

$$C_{D_{I_{tc}}} = \frac{1.5}{M_e^2\, d_\infty \tan\theta_c \sqrt{3L}} \left[1 - \left(\frac{R_N}{R_B} \cos\theta_c \right)^2 \right] C_{D_f}(1,2,2)$$

$$(\theta_{eff} - \theta_c) \left[0.517 + 0.913 \frac{T_w(2,8)}{T_e} + 0.0484\, M_e^2 \right]$$

The total induced drag for laminar flow is $C_{D_{I_{LAM}}} = C_{D_{I_P}} + C_{D_{I_f}} + C_{D_{I_{tc}}}$.
Thus, the total drag coefficient for laminar continuum flow is:

$$C_D = C_{D_{LAM}} = C_{D_P} + C_{D_B} + C_{D_f}(i,2,k) + C_{D_{I_{LAM}}}$$

where the appropriate skin friction drag is used depending upon the nose bluntness and ablation rate.

The fairing between the strong interaction regime and the laminar continuum regime is a linear weighting, based on the viscous interaction parameter value, of the drag coefficients of the two regimes evaluated at the point of interest.

$$C_D = C_{D_S}\left(\frac{\bar{X} - X_{low}}{X_{up} - X_{low}}\right) + C_{D_{LAM}}\left[1 - \left(\frac{\bar{X} - X_{low}}{X_{up} - X_{low}}\right)\right]$$

For turbulent continuum flow, the drag coefficient is composed of the forebody pressure drag, base pressure drag, skin friction drag, and induced pressure drag. The forebody pressure drag, along with angle of attack corrections, is given in the preliminary calculations section. The base drag equation for turbulent flow is the same as the equation for laminar flow and the appropriate equations can be found in the laminar flow section. The sharp cone turbulent flow skin friction drag for the no mass addition case was derived from the Shultz-Grunow flat plate incompressible solution, modified for compressibility and conical flow. The solution is as follows:

$$h^* = \left[0.5 + 0.5\,\frac{C_{P_w}\,T_w\,(3,8)}{C_{P_e}\,T_e} + 0.099\,(\gamma - 1)\,M_e^2\right] C_{P_e}\,T_e$$

$$T^* = \begin{cases} 3.5964\,h^* & \text{for } h^* \leq 1110 \text{ Btu/lbm} \\ \displaystyle\sum_{i=0}^{3}\sum_{j=0}^{2} A\,(162 + i + 4j)\,(h^*)^i \left(\frac{P_e}{2116.}\right)^j & \text{for } h^* > 1110 \text{ Btu/lbm} \end{cases}$$

$$r = \frac{T^*}{1.8}\left[1 - \frac{1}{8}\,\mathrm{Log}_{10}\left(\frac{P_e}{2116.}\right)\right]$$

$$ZZ = 2.5 + 0.1\tanh\left(\frac{r}{500} - 7\right) + 0.4\tanh\left(\frac{r}{1000} - 7\right) + \tanh\left(\frac{r}{2500} - 5.8\right)$$

$$\mu^* = \frac{(2.27 \times 10^{-8})(32.2)[T^*]^{1.5}}{T^* + 198.6}$$

$$\rho^* = \frac{\left(\frac{P_e}{2116.}\right)(39.65)}{(ZZ)(T^*)}$$

$$C_{D_f}(1,1,2) = \begin{cases} \left\{ 0.426 \cot \theta_c \left(\frac{\rho^*}{\rho_\infty}\right)\left(\frac{U_e}{U_\infty}\right)^2 \right\} A(118) \left[\text{Log}_{10} \left(\frac{\rho^* U_e}{\mu^*}\right)\right]^2 \\ + A(119) \left[\text{Log}_{10} \left(\frac{\rho^* U_e}{\mu^*}\right)\right] + A(120) \Bigg\}^{-1} \\ \qquad \text{for } L < 2.0 \text{ feet} \\ \left\{ 0.426 \cot \theta_c \left(\frac{\rho^*}{\rho_\infty}\right)\left(\frac{U_e}{U_\infty}\right)^2 \right\} \left[\text{Log}_{10} \left(\frac{\rho^* U_e}{\mu^*}\right)\right]^2 \\ \left[\text{Log}_{10} \frac{\rho^* U_e}{\mu^*} \right] \sum_{i=0}^{6} A(407+i)(L)^i + \sum_{i=0}^{6} A(400+i)(L)^i \\ + \sum_{i=0}^{6} A(414+i)(L)^i \Bigg\}^{-1} \\ \qquad \text{for } L \geq 2.0 \text{ feet} \end{cases}$$

The mass addition correction to the skin friction drag and the boundary layer displacement effects in the induced pressure drag is dependent upon the turbulent no blowing skin friction coefficient, which is:

$$C_{f_{o_T}} = (0.37)(1.15)\left(\frac{\rho^*}{\rho_e}\right) \frac{1}{\left[\text{Log}_{10}\left(\frac{\rho^* U_e L}{\mu^*}\right)\right]^{2.584}}$$

The turbulent flow, blowing skin friction drag is then:

$$C_{D_f}(1,1,1) = \frac{C_{D_f}(1,1,2)}{1.0 + \dfrac{1.2\,\dot{m}(3,8)}{\rho_e U_e C_{f_{o_T}}}}$$

The effect of bluntness on skin friction drag, for both the blowing and no blowing cases, is:

$$C_{D_f}(2,1,k) = C_{D_f}(1,1,k) \begin{cases} 1.0 - (0.8 + 0.052\,M_\infty)\dfrac{R_N}{R_B} & \text{for } \dfrac{R_N}{R_B} < 0.32 \\ 0.744 - 0.01664\,M_\infty & \text{for } \dfrac{R_N}{R_B} \geq 0.32 \end{cases}$$

In calculating the induced pressure drag if mass transfer and aerodynamic heating effects are being accounted for, the wall enthalpy is set equal to the wall enthalpy calculated in the subroutine EVIL:

$$H_w = \bar{H}_w$$

If a nonablating case is being considered, then the wall enthalpy is:

$$H_w = 0.24\,T_w(3,8)$$

The recovery enthalpy is:

$$H_R = 0.9\,H_s$$

The change in effective cone angle due to displacement effects is:

$$\theta_{eff} - \theta_c = \frac{C_{f_{o_T}}}{3.8} \left[\frac{2\dot{m}(3,8)}{\rho_e U_e C_{f_{o_T}}} + \frac{1}{1 + \frac{1.2\dot{m}(3,8)}{\rho_e U_e C_{f_{o_T}}}} \right]$$

$$\left[0.547 \frac{H_w}{H_R} + \left(0.53 + 0.68 \frac{H_w}{H_R} \right) M_e + \left(0.083 + 0.106 \frac{H_w}{H_R} \right) M_e^2 \right] + \frac{1.6\dot{m}(3,8)}{3.6 \rho_e U_e}$$

The induced pressure drag then becomes:

$$C_{D_{I_P}} = 1.11 \sqrt{3} \left[1 - \left(\frac{R_N}{R_B} \cos\theta_c \right)^2 \right] C_{D_{P_{LEO}}} (\theta_{eff} - \theta_c) F_1(K) M_e$$

and the total induced drag for turbulent flow is $C_{D_{I_{TURB}}} = C_{D_{I_P}}$. Thus the total drag coefficient for turbulent continuum flow is:

$$C_D = C_{D_{TURB}} = C_{D_P} + C_{D_B} + C_{D_f}(i, l, k) + C_{D_{I_{TURB}}}$$

where the appropriate skin friction drag is used, depending upon the bluntness ratio and ablation rate.

For the fairing region between the laminar and turbulent regimes, only the skin friction drag and total induced drag are modified because the forebody pressure drag and base drag equations are the same for laminar and turbulent flow. The fairing process is as follows:

$$\bar{P} = \left[\frac{(C_{f_{o_L}})(L_A)}{1.5} \right] \left[1.0 - \left(\frac{Z_{TR} - Z}{20{,}547.8} \right) \right]^{1.5} - \left[\frac{(C_{f_{o_T}})(L_A)^{1.6}}{1.8} \right]$$

$$\left[1 - \left(\frac{Z_{TR} - Z}{20{,}547.8} \right) \right]^{1.8} \Big/ \left[\frac{(C_{f_{o_L}})(L_A)}{1.5} - \frac{C_{f_{o_T}}(L_A)^{1.6}}{1.8} \right]$$

The faired induced drag is:

$$C_{D_I} = \bar{P} C_{D_{I_{LAM}}} + (1 - \bar{P}) C_{D_{I_{TURB}}}$$

and the faired skin friction drag is:

$$C_{D_f} = \bar{P}\, C_{D_f}(i, 2, k) + (1 - \bar{P})\, C_{D_f}(i, 1, k)$$

Thus, the total drag coefficient in the boundary layer transition regime is:

$$C_D = C_{D_P} + C_{D_B} + C_{D_f} + C_{D_I}$$

3.1.6 Equations of Motion

Flight trajectory points and the associated flight parameters are computed by an iterative process in subroutines DEREQ, TEQUAT, ADM4RK, and part of ROTATE. This involves the computation of the altitude derivatives of the thrusting and trajectory parameters at a given trajectory point and the integration of the derivatives over an altitude increment to determine the parameter values at the next trajectory point. The altitude increment over which the integration is performed is dependent upon the magnitude of the parameter derivatives and is controlled by the predictor-corrector in subroutine ADM4RK.

The computation of the altitude derivatives of the thrusting and trajectory parameters is done in subroutines DEREQ, TEQUAT, and ROTATE. The procedure used is a. compute the time derivatives of the parameters and b. change to altitude dependent derivatives by means of an appropriate multiplication factor. The necessary input quantities are the drag coefficient, C_D, total angle of attack, α', instantaneous mass of the vehicle, m, normal force coefficient, C_N, pitching moment coefficients, C_M, C_{M_q}, the Euler angles,(θ_a , ϕ, ψ,), the components of the rotation rate (p , q , r) , the moment of inertia about the body axis, I (in tabular form as a function of altitude), the moment of inertia along the body axis, I_{xx} (also in tabular form as a function of altitude), and the flow field, thrusting, and geometry parameters. The drag coefficient and angle of attack histories may either be calculated through the appropriate subroutines or be input as a function of altitude in tabular form. Any appendage on the vehicle may be accounted for by inputing an appendage drag, C_{D_W}, table as a function of altitude. This will be added to the vehicle drag to give the total vehicle drag history which is used in the trajectory calculations. In order to permit the input added drag tables to be used repeatedly for different sized vehicles, the input added drag is based on a constant input reference area, $A_{W_{Ref}}$, and then is scaled to the proper vehicle reference area. The total vehicle drag is then:

$$C_{D_T} = C_D + C_{D_W}\left(\frac{A_{W_{Ref}}}{\pi R_B^2}\right)$$

Changing the thrust vector from body coordinates to trajectory coordinates gives (lbf):

$$T_{H_{X_T}} = T_{H_X}(\cos\theta_a \cos\psi) + T_{H_Y}[\cos\psi \sin\theta_a \sin\phi - \sin\psi \cos\phi] + T_{H_Z}[\cos\psi \sin\theta_a \cos\phi + \sin\psi \sin\phi]$$

$$T_{H_{Y_T}} = T_{H_X}(\cos\theta_a \sin\psi) + T_{H_Y}[\sin\psi \sin\theta_a \sin\phi - \cos\psi \cos\phi]$$

$$+ T_{H_Z}[\sin\psi \sin\theta_a \cos\phi - \cos\psi \sin\phi]$$

$$T_{H_{Z_T}} = - T_{H_X} \sin\theta_a + T_{H_Y} \cos\theta_a \sin\phi + T_{H_Z} \cos\theta_a \cos\phi$$

The velocity vector in trajectory coordinates is given by (ft/sec)

$$\dot{X}_B = U_\infty \cos\theta_a \cos\psi$$

$$\dot{Y}_B = U_\infty [\cos\psi \sin\theta_a \sin\phi - \sin\psi \cos\phi]$$

$$\dot{Z}_B = U_\infty [\cos\psi \sin\theta_a \cos\phi + \sin\psi \sin\phi]$$

The normal and axial force coefficients are:

$$F_N = C_N \left(\frac{\rho_\infty U_\infty^2}{2}\right)(\pi R_B^2)$$

$$C_X = - C_{D_T} + C_N \tan(\alpha')$$

The body forces in the trajectory coordinate system are (lbf)

$$F_X = \frac{\rho_\infty U_\infty^2}{2} A_{Ref} C_X (\cos\theta_a \cos\psi)$$

$$- \frac{F_N \dot{Y}_B}{\sqrt{\dot{Y}_B^2 + \dot{Z}_B^2}} [\cos\psi \sin\theta_a \sin\phi - \sin\psi \cos\phi]$$

$$- \frac{F_N \dot{Z}_B}{\sqrt{\dot{Y}_B^2 + \dot{Z}_B^2}} [\cos\psi \sin\theta_a \cos\phi + \sin\psi \sin\phi]$$

$$F_Y = \frac{\rho_\infty U_\infty^2}{2} A_{Ref} C_X (\cos\theta_a \sin\psi)$$

$$- \frac{F_N \dot{Y}_B^2}{\sqrt{\dot{Y}_B^2 + \dot{Z}_B^2}} [\sin\psi \sin\theta_a \sin\phi - \cos\psi \cos\phi]$$

$$- \frac{F_N \dot{Z}_B}{\sqrt{\dot{Y}_B^2 + \dot{Z}_B^2}} [\sin\psi \sin\theta_a \cos\phi - \cos\psi \sin\phi]$$

$$F_Z = -\frac{\rho_\infty U_\infty^2}{2} A_{Ref} C_X \sin\theta_a - \frac{F_N \dot{Y}_B}{\sqrt{\dot{Y}_B^2 + \dot{Z}_B^2}} \cos\theta_a \sin\phi$$

$$- \frac{F_N \dot{Z}_B}{\sqrt{\dot{Y}_B^2 + \dot{Z}_B^2}} \cos\theta_a \cos\phi$$

The altitude derivatives of the thrusting and trajectory parameters are calculated by multiplying the thrusting and trajectory time derivatives by the derivative of time with respect to altitude (dt/dz). The derivatives calculated in TEQUAT are:

Velocity Derivative:

$$\frac{dU_\infty}{dz} = \frac{1}{U_\infty \sin\gamma_f} \left[\frac{T_{H_{X_T}}}{m} - \frac{\rho_\infty U_\infty^2}{2} \frac{C_D A_{Ref}}{m} - 32.21852 \left(\frac{R_e}{R_e + Z} \right)^2 \sin\gamma_f \right].$$

where R_e is the radius of the earth.

Flight Path Angle Derivative:

$$\frac{d\gamma_f}{dz} = \frac{1}{U_\infty \sin\gamma_f} \left\{ \frac{\cos\gamma_f}{U_\infty} \left[\frac{U_\infty^2}{R_e + Z} - 32.21852 \left(\frac{R_e}{R_e + Z} \right)^2 \right] - \left[\frac{F_Z + T_{H_{Z_T}}}{m U_\infty} \right] \right\}$$

Range Derivative:

$$\frac{dX_R}{dz} = \left[\cos(\psi_a) \cos\gamma_f \left(\frac{R_e}{R_e + Z} \right) U_\infty \right] \frac{1}{U_\infty \sin\gamma_f}$$

Cross Range Derivative:

$$\frac{dY_R}{dz} = \frac{1}{U_\infty \sin\gamma_f} \left[\sin(\psi_a) \cos\gamma_f \left(\frac{R_e}{R_e + Z} \right) U_\infty \right]$$

Thrust Misalignment Angle Derivative In The Yaw Direction:

$$\frac{d\psi_a}{dz} = -\frac{1}{U_\infty \sin\gamma_f} \left[\frac{F_Y + T_{H_{Y_T}}}{m U_\infty \cos\gamma_f} \right]$$

Thrusting Weight Derivative:

$$\frac{dW_{TH}}{dz} = -\frac{1}{U_\infty \sin \gamma_f}\left(\frac{T_{H_\infty}}{I_{SP}}\right)$$

The derivatives calculated in ROTATE are:

Euler Angle Derivative In The Yaw Direction:

$$\frac{d\psi}{dz} = \frac{1}{U_\infty \sin \gamma_f}\left[\frac{R\cos\phi + Q\sin\phi}{\cos\theta_a}\right]$$

Euler Angle Derivative In The Pitch Direction:

$$\frac{d\theta_a}{dz} = \frac{1}{U_\infty \sin \gamma_f}\left(Q\cos\phi - R\sin\phi\right)$$

Euler Angle Derivative In The Roll Direction:

$$\frac{d\phi}{dz} = \frac{1}{U_\infty \sin \gamma_f}\left[P + U_\infty \sin\gamma_f \frac{d\phi}{dz}\sin\theta_a\right]$$

Pitching Component of Rotation Derivative:

$$\frac{dQ}{dz} = \frac{1}{U_\infty \sin \gamma_f}\left\{\frac{\rho_\infty U_\infty^2 R_B A_{Ref}}{I}\left[C_M(\sin\theta_a\cos\psi\cos\phi\sin\psi\sin\phi) + \frac{R_B C_{M_q}}{U_\infty}Q\right] + \left(\frac{I - I_{xx}}{I}\right)PR + \frac{M_Y}{I}\right\}$$

Ablation Weight Derivative:

$$\frac{dW}{dz} = \frac{\dot{W}}{U_\infty \sin \gamma_f}$$

Yawing Component of Rotation Derivative:

$$\frac{dR}{dz} = \frac{1}{U_\infty \sin \gamma_f}\left\{\frac{\rho_\infty U_\infty^2 R_B A_{Ref}}{I}\left[C_M(\sin\phi\cos\phi - \sin\theta_a\cos\psi\sin\phi) + \frac{R_B C_{M_q}}{U_\infty}R\right] - \left(\frac{I - I_{xx}}{I}\right)PQ + \frac{M_Z}{I}\right\}$$

Rolling Component of Rotation Derivative:

$$\frac{dP}{dz} = \frac{1}{U_\infty \sin \gamma_f} \left(\frac{M_X}{I_{xx}} \right)$$

The next trajectory point is determined by integrating the above derivatives by means of the predictor-corrector method which alters the range (ΔZ) over which the integration is performed so that input accuracy levels are maintained. Since the predictor-corrector method is a numerical technique, it will not be explained here, but can be found in the numerical description of the program under the ADM4RK subroutine. Then, simply, the velocity at the next trajectory point is:

$$U_\infty = \int_Z^{Z - \Delta Z} \left(\frac{dU_\infty}{dz} \right) dz$$

The remaining derivatives are integrated in the same manner to obtain all the values of the parameters at the next trajectory point. Note that the integration of the weight derivatives provides the weight losses from thrusting and ablation over the integration altitude interval.

That is:

$$\Delta W_{TH} = \int_Z^{Z - \Delta Z} \left(\frac{d W_{TH}}{dz} \right) dz$$

$$\Delta W = \int_Z^{Z - \Delta Z} \left(\frac{dW}{dz} \right) dz$$

These, then, are used to calculate the instantaneous weight of the vehicle, as stated in the preliminary calculation section

$$W = W_o \Delta W - \Delta W_{TH}$$

3.2 WAKE CALCULATIONS

The decoy design program requires calculation of the radar cross-section (RCS) and the wake length as a function of the decoy configuration. This involves wake configuration calculations to define the wake flow field properties, and the RCS and wake length calculations. The input quantities necessary for the wake configuration calculations are the flow field and body geometry properties, transition altitude, Z_{TR}, drag coefficient, C_D, and the flight path angle γ_e. Also needed, and available through input tables, are the heat shield conductivity, K_W (Btu/ft^o-R-Hr), heat shield specific heat, C_{P_W} (Btu/ft^o-R-Hr), chemical enthalpy of the heat shield Δh_{CHEM}(ft^2/sec^2), heat shield density, ρ_w (lb/ft^3), heat shield thickness, δ_{wh} (in), ablation temperature of the heat shield, T_{ABL} (^{o}K), sea level density, ρ_{S_L} (lb/ft^3), scale height, β_Z (kft), and scaling constants, b_{15}, b_{21}, b_{22}, b_{23}, b_{25}.

3.2.1 Preliminary Wake Calculations

The calculations are as follows:

Altitudes are used in terms of thousands of feet.

$$Z_{BLT} = \frac{Z_{TR}}{1000.}$$

$$Z = \frac{Z}{1000.}$$

The total drag area is given by:

$$C_{D_T} A = C_D (\pi R_B^2)$$

The viscous drag area by:

$$C_{D_V} A = [C_D - (C_{D_P} + C_{D_B} + C_{D_I})] \pi R_B^2$$

The velocities have units of thousands of feet per second.

$$U_\infty = \frac{U_\infty}{1000.}$$

$$U_e = \frac{U_e}{1000.}$$

The mass ablation rate is:

$$\dot{m}'_{ABL} = -\dot{W}$$

The mass swallowed by the boundary layer is:

$$\dot{m}^{*}_{BLS} = \begin{cases} 2010\sqrt{2}\left(\frac{h_e}{h_\infty}\right)^{0.25}\left(\frac{P_e}{P_\infty}\right)^{0.5}\left(\frac{M_e}{M_\infty}\right)^{0.5}(R_B)^{1.5}\left(\frac{\rho_\infty\ U_\infty\ M_\infty}{\rho_{\mathfrak{L}}\ \sin\theta_c}\right)^{0.5} \\ \qquad \text{for } 1.98\ R_B > 2\ R_N \\ C_{76}\ \rho_\infty\ U_\infty\ \pi\ R_B{}^2\left(\frac{2000\ \rho_\infty\ U_\infty\ R_B}{M_\infty}\right)^{C_{77}} \\ \qquad \text{for } 2\ R_N \geq 1.98\ R_B \end{cases}$$

The length of the conical frustum along the cone is:

$$S_c = \begin{cases} 0.0 \\ \qquad \text{for } 2\ R_N \geq 1.98\ R_B \\ R_B - R_N \tan\theta_c \\ \qquad \text{for } 1.98\ R_B > 2\ R_N \end{cases}$$

Base diameter is:

$$D_B = 2\ R_B$$

3.2.2 Flow Field Calculations

The wake flow field calculations are:

Free-Stream Reynolds Number Based on the Body Diameter

$$Re_{UD} = \frac{10^3\ \rho_\infty\ U_\infty\ D_B}{\mu_\infty}$$

$$K_v = \frac{K_w\ U_\infty\ \sin\gamma_e}{\rho_w\ C_{Pw}\ \delta^2{}_{wH}}$$

Conical Wall Temperature

$$T_{WC} = \begin{cases} 278. + \dfrac{C_{60}\ (K_v\ Z)^{C_{59}}}{\left(\dfrac{S_c\ e^{z/\beta_z}}{\sin^2\theta_c}\right)^{1/2}\left(\dfrac{K_w}{\delta_{wH}\ U_\infty^{\ 3}}\right)} ; & Z > Z_{BLT} \\ T_{WC_{Z=Z_{BLT}}} + \dfrac{C_{160}\ [K_v\ (Z_{BLT} - Z)]^{C_{159}}}{\left(\dfrac{S_c\ e^{z/\beta_z}}{\sin^2\theta_c}\right)^{0.8}\left(\dfrac{K_w}{\delta_{wH}\ U_\infty^{\ 3}}\right)} ; & Z \le Z_{BLT} \end{cases}$$

Spherical Wall Temperature

$$T_{WSP} = 278. + C_{60}\ (K_v\ Z)^{C_{59}} \left(\frac{K_w\ D_B^{\ 1/2}\ \exp\ (Z/4\beta_z)}{U_\infty^{\ 3/2}\ \delta_{wH}} \right)$$

Total Mass Rate in the Boundary Layer

$$\dot{m}^*_{BL} = \dot{m}^*_{BLS} + \dot{m}^*_{ABL}$$

Wall Temperature

$$T_W = \begin{cases} T_{ABL} : (T_{ABL} \le T_{WC} \text{ and } 2R_N \le 0.99\ D_B) \text{ or } (T_{ABL} \le T_{WSP} \text{ and } 2R_N \ge 0.99\ D_B) \\ T_{WC} ; 2R_N < 0.99\ D_B \text{ and } T_{WC} < T_{ABL} \\ T_{WSP} ; 2R_N \ge 0.99\ D_B \text{ and } T_{WSP} < T_{ABL} \end{cases}$$

Wall Enthalpy

$$h_w = 1.087\ (10^4)\ T_W$$

Drag Area of the Second Entropy Layer

$$C_{D_{\Sigma S2}}\ A = C_{DT}\ A - C_{DV}\ A$$

$$M_{RAT} = \frac{\dot{m}^*_{ABL}}{\dot{m}^*_{BL}}$$

Universal Shock Angle

$$\theta_{S_\infty} = \begin{cases} 57.3\ \sin^{-1}\left\{\dfrac{1}{M_\infty}\left[\dfrac{6}{7}\left(\dfrac{P_e}{P_\infty}\right) - \dfrac{13}{7}\right]^{\frac{1}{2}}\right\} ; & \dfrac{P_e}{P_\infty} > \dfrac{19}{6} \\ 57.3\ \sin^{-1}\left(\dfrac{1}{M_\infty}\right) ; & \dfrac{P_e}{P_\infty} \le \dfrac{19}{6} \end{cases}$$

$$\theta_{S_\infty} = \max\ (\theta_{S_\infty}, \theta_c)$$

$$\theta_{S_\infty} = \min\ (\theta_{S_\infty}, 90.)$$

Mass Flow Rate in Second Entropy Layer

$$\dot{m}_{\Sigma S2} = 2000.0\ \rho_\infty\ U_\infty\ R_N^{\,2}\ \cot^2\ \theta_{S_\infty}$$

Velocity Along the Cone in the Second Entropy Layer

$$U_{2c} = U_\infty - \frac{500\ \rho_\infty\ U_\infty^{\,2}\ C_{D\Sigma S2}\ A}{\dot{m}^*_{\Sigma S2}}$$

$$U_{2c} = \max\,(U_{2c}, 1.0)$$

$$A_1 = 0.286 + 1.029\ M_\infty^{\,2} \left[1 - \left(\frac{U_{2c}}{U_\infty} \right)^2 \right]$$

Maximum Shock Angle

$$\theta_{S2} = 57.3\ \sin^{-1} \left\{ \frac{1}{M_\infty} \left[\frac{A_1 + (2.86 + A_1)^{1/2}}{2} \right]^{1/2} \right\}$$

$$\theta_{S2} = \max\ (\theta_{S2}, \theta_c)$$

Average Shock Angle

$$\bar{\theta}_{S2} = 0.5\ (\theta_{S2} + \theta_{S_\infty})$$

$$b_{35} = C_{119}\ U_\infty^{\,C_{120}}$$

Mass Flow Rate at the Nose

$$\dot{m}^*_N = 1000.0\ R_N^{\,2}\ C_{116}\ \rho_\infty\ U_\infty$$

$$S_{RAT} = \begin{cases} 1\ ; & \dot{m}^*_{BLS} \geq \dot{m}_N^* \\ \dfrac{\dot{m}^*_{BLS}}{\dot{m}_N^*}\ ; & \dot{m}^*_{BLS} < \dot{m}_N^* \end{cases}$$

Electron Density at the Nose (Table III-2)

$$n_{ern} = f_1\ (\rho_\infty, U_\infty)$$

TABLE III-2

EQUILIBRIUM NORMAL SHOCK ELECTRON DENSITY

ρ lb/ft^3	Velocity 10 kft/sec	14 kft/sec	18 kft/sec	22 kft/sec	26 kft/sec	30 kft/sec
0.0804	1.4×15^{12}	5×10^{15}	9.1×10^{16}	3.6×10^{17}	1×10^{18}	2×10^{18}
0.01171	2.3×10^{12}	8.1×10^{14}	1.4×10^{16}	5.4×10^{16}	1.5×10^{17}	2.2×10^{17}
0.001068	6×10^{11}	1.1×10^{14}	1.9×10^{15}	7×10^{15}	1.8×10^{16}	2.8×10^{16}
0.00033	1.2×10^{10}	9.2×10^{12}	1.7×10^{14}	7.4×10^{14}	1.8×10^{15}	3×10^{15}
1.112×10^{-4}	6.7×10^{8}	7.7×10^{11}	2×10^{13}	8.8×10^{13}	2.1×10^{14}	3.5×10^{14}
4.261×10^{-5}	4.3×10^{7}	1×10^{11}	3.5×10^{12}	1.5×10^{13}	4×10^{13}	7×10^{13}
1.7×10^{-5}	2×10^{10}	2×10^{10}	7.2×10^{11}	3.1×10^{12}	7.2×10^{12}	1×10^{13}
2.26×10^{-6}	1.15×10^{6}	4×10^{9}	2.1×10^{11}	7×10^{11}	1.3×10^{12}	2×10^{12}

For: $\rho \leq 2.26 \times 10^{-6}$ use value for $\rho = 2.26 \times 10^{-6}$

$\rho \geq 0.0804$ use value for $\rho = 0.0804$

$V < 10$ use linear interpolation to $n_e = 10^2$

$V \geq 30$ use value for $V = 30$ kft/sec

Number of Electrons Produced by the Nose Cap

$$N_{R_N} = \frac{(30.48)^3 \quad \dot{m}_N^{\bullet} \quad S_{RAT}}{\rho_\infty} \quad n_{ern}$$

Cone Pressure with Respect to Second Entropy Layer

$$P_{2c} = \frac{(7 M_\infty^2 \sin^2 \theta_{S2} - 1) P_\infty}{6}$$

Cone Enthalpy with Respect to Second Entropy Layer

$$h_{2c} = \frac{h_\infty \; P_{2c} \; (P_{2c} + 6 \; P_\infty)}{P_\infty \; (6 \; P_{2c} + P_\infty)}$$

Cone Density with Respect to Entropy Layer

$$\rho_{2c} = \rho_\infty \left[\frac{P_{2c} + 6 \; P_\infty}{6 \; P_{2c} + P_\infty} \right]^{-1}$$

Definition of the Flow Properties at the Cone

If $\dot{m}^{\bullet}_{BLS} \geq \dot{m}^{\bullet}_{\Sigma S2}$

$$\rho_c = \rho_e$$

$$h_c = h_e$$

$$P_c = (P_e / P_\infty) P_\infty$$

$$U_c = U_e$$

If $\dot{m}^{\bullet}_{BLS} < \dot{m}^{\bullet}_{\Sigma S2}$

$$\rho_c = \rho_{2c}$$

$$h_c = h_{2c}$$

$$P_c = P_{2c}$$

$$U_c = U_{2c}$$

Chemical Length

$$S_{CHEM} = \begin{cases} \dfrac{\rho_{2c}}{U_{2c}} \dfrac{C_{117}\ S_c\ \dot{m}^{\bullet}_{\Sigma S2}}{\dot{m}^{\bullet}_{BLS}} + \dfrac{\rho_e}{U_e} \dfrac{C_{117}\ S_c\ (\dot{m}^{\bullet}_{BLS} - \dot{m}^{\bullet}_{\Sigma S2})}{\dot{m}^{\bullet}_{BLS}} & ; \ \dot{m}^{\bullet}_{BLS} > \dot{m}_{\Sigma S2} \\ \dfrac{\rho_{2c}}{U_{2c}} \dfrac{C_{117}\ S_c\ \dot{m}^{\bullet}_{BLS}}{\dot{m}^{\bullet}_{\Sigma S2}} & ; \ \dot{m}^{\bullet}_{BLS} < \dot{m}^{\bullet}_{\Sigma S2} \end{cases}$$

Number of Electrons at Shoulder of Nose Cap

$$N_{SRN} = \frac{C_{112}\ N_{RN}\ \dot{m}^{\bullet}_N \left[1 - C_{121} + (1 + N_{RN}\ S_{CHEM})\ C_{121}\ \exp(-b_{35}\ S_{CHEM})\right]}{\dot{m}^{\bullet}_N + C_{123}\ S_{CHEM}\ N_{RN}\ T_w^{C_{124}}}$$

$$N_{e\phi H} = f_2 \left\{ \frac{\rho_c}{\rho_{\ell}}, \frac{h_c}{RT_o}, M_{RAT} \right\} \quad \text{(TABLES III-3 THRU-7)}$$

$$n_{eBL} = n_{e\phi H} \left[1 - \exp\left(-b_{22}\ S_{CHEM}^{C_{118}}\right)\right] \left[b_{21} + b_{23} \left(\frac{U_c - 22}{22}\right)\right]$$

Number of Electrons Leaving Boundary Layer

$$N_{BL} = \frac{(30.48)^3\ n_{eBL}\ \dot{m}^{\bullet}_{BL}}{P_c}$$

Number of Electrons Entering Wake Neck

$$N_S = N_{BL} + N_{SRN}$$

Cone Mach Number with Respect to Second Entropy Layer

$$M_{2c} = \frac{U_{2c}\ M_{\infty}}{U_{\infty}} \left(\frac{h_{\infty}}{h_{2c}}\right)^{1/2}$$

$$M_{2c} = \max\ (M_{2c}, 1)$$

Second Entropy Layer Mach Number

$$M_2 = f_3\ (M_{2c}, \theta_c) \quad \text{(Table III-8)}$$

Wake Mach Number

$$M_{e_w} = f_3\ (M_e, \theta_c) \quad \text{(Table III-8)}$$

TABLE III-3

η_e AS A FUNCTION OF NORMALIZED DENSITY AND ENTHALPY

h/RT_o \ ρ/ρ_o	10^2	1.0	10^{-1}	10^{-2}	10^{-3}	10^{-4}	10^{-5}	10^{-6}	0
0	0	0	0	0	0	0	0	0	0
30	0.72×10^{9}	0.72×10^{7}	0.45×10^{7}	0.19×10^{7}	0.58×10^{6}	0.92×10^{5}	0.52×10^{4}	0.80×10^{3}	↑
50	0.25×10^{14}	0.25×10^{12}	0.48×10^{11}	0.43×10^{10}	0.15×10^{8}	0.16×10^{8}	0.94×10^{6}	0.42×10^{5}	
70	0.20×10^{15}	0.20×10^{13}	0.91×10^{12}	0.60×10^{11}	0.28×10^{10}	0.16×10^{9}	0.60×10^{7}	0.32×10^{6}	
90	0.78×10^{16}	0.78×10^{14}	0.56×10^{13}	0.37×10^{12}	0.23×10^{11}	0.14×10^{10}	0.12×10^{9}	0.25×10^{7}	
110	0.35×10^{17}	0.35×10^{15}	0.29×10^{14}	0.27×10^{13}	0.26×10^{12}	0.32×10^{11}	0.31×10^{10}	0.32×10^{9}	
130	0.13×10^{18}	0.13×10^{16}	0.14×10^{15}	0.13×10^{14}	0.13×10^{13}	0.10×10^{12}	0.82×10^{10}	0.71×10^{9}	
150	0.34×10^{18}	0.34×10^{16}	0.34×10^{15}	0.30×10^{14}	0.24	0.18	0.14×10^{11}	0.11×10^{10}	
170	0.62×10^{18}	0.62×10^{16}	0.54×10^{15}	0.46×10^{14}	0.35	0.27	0.19	0.15	
190	0.90×10^{18}	0.90×10^{16}	0.80×10^{15}	0.68×10^{14}	0.50	0.36	0.27	0.18	
210	0.14×10^{19}	0.14×10^{17}	0.12×10^{16}	0.86×10^{14}	0.62	0.44	0.31	0.23	
230	0.17×10^{19}	0.17	0.14	0.10×10^{15}	0.76	0.53	0.40	0.27	
250	0.21	0.21	0.17	0.13	0.94×10^{13}	0.65	0.44	0.31	
270	0.25	0.25	0.21	0.15	0.10×10^{14}	0.74	0.51	0.42	
290	0.36	0.36	0.24	0.17	0.12	0.89	0.59	0.52	
310	0.38	0.38	0.28	0.20	0.14	0.97×10^{12}	0.68	0.60	
330	0.47	0.47	0.33	0.26	0.16	0.11×10^{13}	0.88	0.78	
350	0.56	0.56	0.42	0.28	0.19	0.13	0.95×10^{11}	0.90×10^{10}	
370	0.63	0.63	0.46	0.34	0.24	0.15	0.12×10^{12}	0.12×10^{11}	
390	0.70	0.70	0.57	0.38	0.28	0.23	0.16	0.14	
410	0.86	0.86	0.72	0.52	0.33	0.26	0.20	0.17	
430	0.20×10^{19}	0.20×10^{17}	0.83	0.62	0.45	0.35	0.25	0.24	
450	0.12×10^{20}	0.12×10^{18}	0.94×10^{16}	0.72×10^{15}	0.60	0.39	0.28	0.29	
470	0.14×10^{20}	0.14×10^{18}	0.14×10^{17}	0.10×10^{16}	0.74×10^{14}	0.45×10^{13}	0.42×10^{12}	0.33×10^{11}	0

K/TE: This table used when n_{Equil} is to be computed.

TABLE III-4

ELECTRON DENSITY AS A FUNCTION OF

NORMALIZED ENTHALPY AND AIR DENSITY

FOR 1000 ppm SODIUM SEED, $M_{RAT} = 0.0$

$$n_e = n_e \left\{ \frac{h}{RT_o} , \rho/\rho_o \right\} \text{ [electrons/cc]}$$

$\frac{h}{RT_o}$ / ρ/ρ_o [ATM]		Greater than 0.1	0.1	0.03	0.01	Less than 0.01
Less than	15	0.0	0.0	0.0	0.0	0.0
	15	0.70×10^{1}	0.50×10^{1}	0.32×10^{2}	0.95×10^{2}	0.90×10^{2}
	20	0.38×10^{3}	0.38×10^{3}	0.12×10^{4}	0.30×10^{4}	0.30×10^{4}
	40	0.32×10^{10}	0.32×10^{10}	0.11×10^{10}	0.20×10^{9}	0.20×10^{9}
	60	0.25×10^{12}	0.25×10^{12}	0.78×10^{11}	0.05×10^{11}	0.05×10^{11}
	80	0.32×10^{13}	0.32×10^{13}	0.10×10^{13}	0.14×10^{12}	0.14×10^{12}
	100	0.17×10^{14}	0.17×10^{14}	0.65×10^{13}	0.20×10^{13}	0.20×10^{13}
	120	0.84×10^{14}	0.84×10^{14}	0.31×10^{14}	0.78×10^{13}	0.78×10^{13}
	140	0.24×10^{15}	0.24×10^{15}	0.87×10^{14}	0.22×10^{14}	0.22×10^{14}
	160	0.44×10^{15}	0.44×10^{15}	0.16×10^{15}	0.38×10^{14}	0.38×10^{14}
Greater than	160	0.44×10^{15}	0.44×10^{15}	0.16×10^{15}	0.38×10^{14}	0.38×10^{14}

TABLE III–5

ELECTRON DENSITY AS A FUNCTION OF

NORMALIZED ENTHALPY AND AIR DENSITY

FOR 1000 ppm SODIUM SEED, $M_{RAT} = 0.01$

$$n_e = n_e \left\{ \frac{h}{RT_o} , \rho/\rho_o \right\} \text{ [electrons/cc]}$$

$\frac{h}{RT_o}$ \ ρ/ρ_o [ATM]		Greater than 0.1	0.1	0.03	0.01	Less than 0.01
Less than	15	0.0	0.0	0.0	0.0	0.0
	15	1.0×10^{5}	1.0×10^{5}	5.5×10^{4}	2.0×10^{4}	2.0×10^{4}
	20	3.5×10^{7}	3.5×10^{7}	1.9×10^{7}	7.0×10^{6}	7.0×10^{6}
	40	2.0×10^{11}	2.0×10^{11}	1.1×10^{11}	4.0×10^{10}	4.0×10^{10}
	60	1.3×10^{12}	1.3×10^{12}	2.3×10^{11}	1.6×10^{11}	1.6×10^{11}
	80	2.0×10^{12}	2.0×10^{12}	4.5×10^{11}	2.0×10^{11}	2.0×10^{11}
	100	4.5×10^{12}	4.5×10^{12}	2.0×10^{12}	6.0×10^{11}	6.0×10^{11}
	120	1.4×10^{13}	1.4×10^{13}	5.0×10^{12}	1.4×10^{12}	1.4×10^{12}
	140	2.4 ↑	2.4 ↑	9.0×10^{12}	2.0 ↑	2.0 ↑
	160	3.0 ↓	3.0 ↓	1.5×10^{13}	3.0 ↓	3.0 ↓
greater than	160	4.0×10^{13}	4.0×10^{13}	2.5×10^{13}	4.0×10^{12}	4.0×10^{12}

TABLE III-6

ELECTRON DENSITY AS A FUNCTION OF

NORMALIZED ENTHALPY AND AIR DENSITY

FOR 1000 ppm SODIUM SEED, $M_{RAT} = 0.1$

$$n_e = n_e \left\{ \frac{h}{RT_o} , \rho/\rho_o \right\} \text{ [electrons/cc]}$$

$\frac{h}{RT_o}$ \ ρ/ρ_o [ATM]	Greater than 0.1	0.1	0.03	0.01	Less than 0.01
Less than 15	0.0	0.0	0.0	0.0	0.0
15	2.4×10^{5}	2.4×10^{5}	1.2×10^{5}	4.5×10^{4}	4.5×10^{4}
20	1.5×10^{8}	1.5×10^{8}	7.1×10^{7}	2.7×10^{7}	2.7×10^{7}
40	7.6×10^{11}	7.6×10^{11}	3.7×10^{11}	1.4×10^{11}	1.0×10^{11}
60	5.6×10^{11}	5.6×10^{12}	2.4×10^{12}	7.1×10^{11}	7.1×10^{11}
80	1.3×10^{13}	1.3×10^{13}	5.8 ↕	1.7×10^{12}	1.7×10^{12}
100	1.6 ↕	1.6 ↕	6.2 ↕	1.7 ↕	1.7 ↕
120	2.1	2.1	7.7×10^{12}	2.0	2.0
140	3.0	3.0	1.1×10^{13}	2.7	2.7
160	4.0 ↕	4.0 ↕	1.5×10^{13}	3.5 ↕	3.5 ↕
Greater than 160	4.5×10^{13}	4.5×10^{13}	2.0×10^{13}	4.0×10^{12}	4.0×10^{12}

TABLE III-7

ELECTRON DENSITY AS A FUNCTION OF

NORMALIZED ENTHALPY AND AIR DENSITY

FOR 1000 ppm SODIUM SEED, $M_{RAT} = 1.0$

$$n_e = n_e \left\{ \frac{h}{RT_o}, \rho/\rho_o \right\} \text{ [electrons/cc]}$$

$\frac{h}{RT_o}$ \ ρ/ρ_o [ATM]		Greater than 0.1	0.1	0.3	0.01	Less than 0.01
Less than	15	0.0	0.0	0.0	0.0	0.0
	15	7.9×10^{5}	7.9×10^{5}	5.2×10^{5}	1.7×10^{5}	1.7×10^{5}
	20	2.3×10^{8}	2.3×10^{8}	1.5×10^{8}	5.0×10^{7}	5.0×10^{7}
	40	2.0×10^{12}	2.0×10^{12}	1.3×10^{12}	4.3×10^{11}	4.3×10^{11}
	60	1.8×10^{13}	1.8×10^{13}	8.0×10^{12}	2.5×10^{12}	2.5×10^{12}
	80	6.0×10^{13}	6.0×10^{13}	3.0×10^{13}	1.1×10^{13}	1.1×10^{13}
	100	1.4×10^{14}	1.4×10^{14}	5.7 ↑	1.5 ↑	1.5 ↑
	120	1.3 ↑	1.3 ↑	5.2	1.3	1.3
	140	1.2	1.2	4.7	1.2	1.2
	160	1.5 ↓	1.5 ↓	5.0 ↓	1.3 ↓	1.3 ↓
greater than	160	2.0×10^{14}	2.0×10^{14}	6.0×10^{13}	2.0×10^{13}	2.0×10^{13}

TABLE III-8

TABLE OF M VERSUS M_C AND θ_C

MC \ θC	0	2	6	10	14	18	22	26	30	45	> 45
1.0	1.0	1.13	1.29	1.43	1.57	1.70	1.84	2.00	2.13	2.76	100
3.0	3.0	3.11	3.33	3.58	3.85	4.15	4.49	4.88	5.32	7.79	100
6.0	6.0	6.30	7.00	7.84	8.89	10.2	12.0	14.6	18.4	100	100
9.0	9.0	9.64	11.2	13.4	16.7	21.8	31.6	53.0	100	100	100
12.0	12.0	13.1	16.2	21.0	29.8	51.0	100	100	100	100	100
15.0	15.0	16.8	22.0	33.4	58.0	100	100	100	100	100	100
18.0	18.0	20.6	29.0	49.2	100	100	100	100	100	100	100
21.0	21.0	24.6	37.7	80.0	100	100	100	100	100	100	100
24.0	24.0	28.8	48.6	100	100	100	100	100	100	100	100
27.0	27.0	33.4	63.0	100	100	100	100	100	100	100	100
30.0	30.0	38.0	81.0	100	100	100	100	100	100	100	100
> 30.0	100	100	100	100	100	100	100	100	100	100	100

Wake Density

$$\rho_{e_W} = \rho_e \left(\frac{1.0 + 0.2\ M_e^2}{1.0 + 0.2\ M_{e_W}^2} \right)^{2.5}$$

Wake Enthalpy

$$h_{e_W} = h_e \left(\frac{1.0 + 0.2\ M_e^2}{1.0 + 0.2\ M_{e_W}^2} \right)$$

Wake Velocity

$$U_{e_W} = \frac{U_e\ M_{e_W}}{M_e} \left(\frac{h_{e_W}}{h_e} \right)^{1/2}$$

Second Entropy Layer Density

$$\rho_2 = \rho_{2c} \left(\frac{1.0 + 0.2\ M_{2c}^2}{1.0 + 0.2\ M_2^2} \right)^{2.5}$$

Second Entropy Layer Enthalpy

$$h_2 = h_{2c} \left(\frac{1.0 + 0.2\ M_{2c}^2}{1.0 + 0.2\ M_2^2} \right)$$

Second Entropy Layer Velocity

$$U_2 = \frac{U_{2c}\ M_2}{M_{2c}} \left(\frac{h_2}{h_{2c}} \right)^{1/2}$$

Definition of Shoulder Flow Properties

If $\dot{m}^*_{BLS} > \dot{m}^*_{\Sigma S2}$

$M_s = M_{e_W}$

$\rho_s = \rho_{e_W}$

$h_s = h_{e_W}$

$U_s = U_{e_W}$

If $\dot{m}^*_{BLS} < \dot{m}^*_{\Sigma S2}$

$M_s = M_2$

$\rho_s = \rho_2$

$$h_s = h_2$$

$$U_s = U_2$$

Shoulder Reynolds Number

$$Re_s = \frac{\rho_s \, M_s \, Re_{UD} \, C_{169}}{\rho_\infty \, M_\infty} \left(\frac{h_s}{h_\infty} \right)^{C_{67}}$$

$$C_s = C_{164} + C_{165} \, \sin^{1/4} \theta_c \, Re_s^{-3/8} \, M_s^{-1/2}$$

Neck Enthalpy

$$h_N = h_w + C_s \left[h_s - h_w + 0.5 \, (10^6) \, U_s^2 \right] - \Delta h_{CHEM}$$

$$H_N/H_s = \frac{2 \, h_N}{2 \, h_s + 10^6 \, U_s^2}$$

Electron Density at the Neck

$$n_{e_N} = \frac{\rho_s \, N_s \, h_s}{(30.48)^3 \, \dot{m}^*_{BL} \, h_N}$$

$$\theta_{BLS} = \left(\frac{C_{D_T} A \, \rho_\infty}{2\pi \, \rho_s} \right)^{1/2} \frac{U_\infty}{U_s}$$

Shoulder Wake Momentum Thickness

$$\theta_s^* = \begin{cases} \theta_{BLS} \; ; \; \dot{m}^*_{BLS} \geq \dot{m}_{\Sigma S2} \\ \left[\frac{\rho_\infty}{2\pi\rho_s} \left(C_{D_V} A + \frac{\dot{m}^*_{\Sigma S2} \, C_{D\Sigma S2} \, A}{\dot{m}^*_{BLS}} \right) \right]^{1/2} \frac{U_\infty}{U_s} \; ; \; \dot{m}^*_{BLS} < \dot{m}^*_{\Sigma S2} \end{cases}$$

Shoulder Reynolds Number Base on Wake Momentum Thickness

$$Re_{\theta s} = \frac{\theta^*_s \, Re_s}{D_B}$$

$$G_T \begin{cases} \left[1 - \frac{h_N \left(1 - \frac{h_N}{h_s} \right)}{2 \, (10^6) \, C_{90} \, \rho_s \, \theta^*_s \, U_s^2 \, Re_{\theta s} \, (1 + H_N/H_S)} \right]^{-1} \; ; \; Z > Z_{BLS} \\ 0.0 \; ; \; Z \leq Z_{BLT} \end{cases}$$

Transition Electron Density Scaling Factor

$$b_5 = C_{83}\left[1 + C_{84}\, M_{RAT}^{\,C_{85}} + C_{86}\, M_{RAT}^{\,C_{87}} + C_{88}\left(\frac{\rho_S}{\rho_{SL}}\right)^{C_{84}}\right]$$

$$b_{11} = C_{91} + C_{92}\, M_{RAT}^{\,C_{93}}$$

Electron Decay Rate

$$b_1 = \left\{\frac{C_{69}\left[C_{115} + b_{11}\left(\frac{\rho_S}{\rho_{SL}}\right)^{C_{125}}\right]}{10^6\, U_s^{\,2}\, \theta_{BLS}}\right\} C_{CON}^{\,B_{CON}}$$

$$K_e = (\theta_s^*)^{-2} - \frac{7.5\,(10^{28})\,\rho_S\, C_{100}}{n_{eN}}$$

$$G_{t_{CHEM}} = \begin{cases}\left[1.0 + \dfrac{h_N}{4.0\, C_{90}\, h_s\, K_e\, \rho_s\, \theta^*_s\, Re_{\theta_s}}\right]^{-1} & ;\ Z > Z_{BLT} \\ 1.0 & ;\ Z \le Z_{BLT}\end{cases}$$

Transition Electron Density

$$n_{e_t} = \left\{\left(\frac{10^{-3}\, C_{124}\, C_{69}\, b_5\, \rho_s^{\,C_{133}}\, G_T}{\theta^*_s\, U_s^{\,C_{134}}}\right)\left[1.0 - \exp\left\{-|h_N|\left(C_{135} + C_{136}\,|h_N|^{C_{130}} + C_{131}\,|h_N|^{C_{132}}\right)\right\}\right] + 1.11\,(10^{27})\,\rho_s\, C_{100} + n_{eN}\, G_{T_{CHEM}}\right\} C_{CON}^{\,A_{CON}}$$

3.2.3 Radar Cross Section and Length Calculations

The necessary inputs for the radar cross section (RCS) and wake length calculations are the radar frequency, f (Hz), pulse length, τ (μsec), sea level collision frequency, ν_s (CPS), radar noise level to which the wake length is measured, σ_{NL} (m^2), altitude, Z (kft), free-stream Mach number, M_∞, scale height, β_Z (kft), look angle as a function of altitude, ϕ_l (degrees), electron decay rate, b_1, and transition electron density, n_{et} (e/cc). The wake diameter is taken as the vehicle base diameter

$$D_w = D$$

$$K = 2\pi f^2 \times 10^9$$

Surface Scattering Correction for Base Diameter

$$D_w^* = \frac{(K\, b_{24}\, D_w)^3}{2 \sin^2 \phi + (K\, b_{24}\, D_w)^3}$$

Atmospheric Density as a Function of Altitude

$$\rho_\infty = e^{-\frac{Z}{\beta_Z}}$$

Electron Density at which the Plasma Becomes Overdense

$$n_{e_{CR}} = \left(\frac{f^2}{10^8}\right)\left[1.0 + \rho_\infty^2 \left(\frac{\nu_s^2}{f^2}\right)\right]^{C_5}$$

Transition Point Onset of Overdense Region

$$X_t = \frac{C_1}{\rho_\infty}\left(1.0 - \frac{C_2}{M_\infty^{C_3}}\right) + C_4$$

Onset of Constant Multiple Scattering Region

$$X_{OD} = \begin{cases} \frac{1}{b_1}\left\{ f_n \left(\frac{n_{e_t}}{n_{e_{CR}}}\right)^2 \right\} & ; \; X_{2\,BOD} \geq X_{3B} \\ X_{2\,BOD} & ; \; X_{2\,BOD} < X_{3B} \end{cases}$$

$$X_{ODP} = \begin{cases} X_{OD} & ; \; X_{OD} \geq 0. \\ 0.0 & ; \; X_{OD} < 0. \end{cases}$$

$$\phi = \begin{cases} \phi_1 & ; \; \phi_1 \leq 90.^\circ \\ 180 - \phi_1 & ; \; \phi_1 > 90.^\circ \end{cases}$$

$$L_{OU} = \text{smaller of } \left(\frac{3.r \times 10^2}{2.\cos\phi}\right), \; X_{ODP}$$

Point of Onset of Single Multiple Scattering Region

$$X_{SS} = \frac{1}{b_1} \left\{ f_n \left[\frac{n_{e_t}}{n_{e_{CR}} \sin^2 \phi} \right]^2 \right\}$$

$$X_{SSP} = \begin{cases} X_{SS} & ; \; X_{SS} \geq 0. \\ 0.0 & ; \; X_{SS} < 0. \end{cases}$$

$$L_{SS} = \text{smaller of} \left(\frac{3.r \times 10^2}{2. \cos \phi} \; , \; X_{SSP} \right)$$

Point of Onset of Variable Multiple Scattering Region

$$X_{MS} \begin{cases} \frac{2}{b_1 \, b_{20}} f_n \left\{ 2 \left[\frac{b_o \left(\frac{f^2}{10^8} \right)^2 D_w^4}{\left\{ 1 + b_2 \left(\frac{f^2}{10^8} \right) D_w^2 \right\}^{b_3}} \right] \left(\frac{n_{e_t}}{n_{e_{CR}}} \right)^{b_{20}} \sin \phi^{(4 - 2 \, b_{20})} \right\} & ; \; b_{20} \neq 0 \\ X_{OD} & ; \; b_{20} = 0.0 \end{cases}$$

$$X_{MSP} = \begin{cases} X_{MS} & ; \; X_{MS} \geq X_{ODP} \\ X_{ODP} & ; \; X_{MS} < X_{ODP} \end{cases}$$

$$L_{MS} = \frac{X_{MSP} - X_{ODP}}{2.0}$$

$$L_{MSD} = \text{smaller of} \left(X_{MSP} \; , \; \frac{150 \, r}{\cos \phi} \right)$$

$$A_1 = L_{OD} \, D_w^* \sin^2 \phi + \frac{D_w^*}{b_1} \left(\frac{n_{e_t}}{n_{e_{CR}}} \right)^2 \left[\left(\frac{e^{-b_1 L_{OD}} - e^{-\frac{150 b_1 r}{\cos \phi}}}{16} \right) \sin^2 \phi \right.$$

$$\left. + \frac{b_o \left(\frac{f^2}{10^8} \right)^2 D_w^4}{\left[1.0 + b_2 \left(\frac{f^2}{10^8} \right) D_w^2 \right]^{b_3}} \left(e^{-b_1 L_{SS}} - e^{-\frac{150 \, b_1 \, r}{\cos \phi}} \right) \right]$$

Peak Radar Cross Section

If $b_{20} \neq 0.0$

$$\sigma_p = A_1 \cdot L_{MS} D_w^* \sin^2\phi \cdot \frac{D_w^* \sin^2\phi}{4 b_1} \left(\frac{n_{e_t}}{n_{e_{CR}}}\right)^8 \left(e^{-4 b_1 L_{OD}} - e^{-\frac{600 b_1'}{\cos\phi}}\right)$$

$$\cdot \left\{ 2 D_w^* \left[\frac{b_0 \left(\frac{f^2}{10^8}\right)^2 D_w^4}{\left(1.0 + b_2 \left(\frac{f^2}{10^8}\right) D_w^2\right)^{b_3}} \right] \frac{(\sin^2\phi)^{(2 - b_{20})}}{b_1 b_{20}} \left(\frac{n_{e_t}}{n_{e_{CR}}}\right)^{b_{20}} \right.$$

$$\left. \left(e^{\frac{-b_1 b_{20}}{2} L_{MSD}} - e^{\frac{-b_1 b_{20} L_{SS}}{2}}\right) \right\}$$

If $b_{20} = 0.0$

$$\sigma_p = A_1 \cdot L_{MSD} D_w^* \sin^2\phi \cdot \frac{D_w^* \sin^2\phi}{4 b_1} \left(\frac{n_{e_t}}{n_{e_{CR}}}\right)^8 \left(e^{-4 b_1 L_{OD}} - e^{\frac{-600 b_1'}{\cos\phi}}\right)$$

$$\cdot D_w \left[\frac{b_0 \left(\frac{f^2}{10^8}\right)^2 D_w^4}{\left(1.0 + b_2 \left(\frac{f^2}{10^8}\right) D_w^2\right)^{b_3}} \right] (L_{SS} - L_{MSD}) \sin^4\phi$$

The wake length is based on a unimodal function of the axial distance in the wake, $\sigma(x)$, and an input radar noise level, $\sigma_{N.L.}$. The wake length is the distance from the maximum value of $\sigma(x)$ to the point where the function is equal to the noise level. The procedure employed is based on a course marching procedure to define the limits for the maximum of the function, followed by a fine resolution search for X_{max}, using a Fibonacci search technique. If the maximum of the function is above the noise level, the course marching procedure is again initiated from the peak and the limits for the point X_{root}, where the function is equal to the noise level, are established. The square of the difference between the function and the noise level is then minimized using the Fibonacci technique to define the root more accurately. The wake length is then calculated by:

$$L_w = X_{root} - X_{max}$$

The function, $\sigma(x)$, is defined by the following equations:

$$\sigma_T = \begin{cases} \sigma_P \ ; \ X_{ODP} > 0.0 \\ \sigma_P + \left[\left(\frac{NET}{n_{e_{CR}}}\right)^2 \left(\frac{\sin^2\phi}{16}\right) + \left(\frac{NET}{n_{e_{CR}}}\right)^8 \sin^2\phi\right] \Delta\sigma_{2B} \ ; \ X_{ODP} \le 0.0 \text{ and } X_{SSP} \ge 0.0 \\ \sigma_P + \left(\frac{NET}{n_{e_{CR}}}\right)^2 \left[D_w^* \frac{\sin^2\phi}{16} + \frac{b_0 \left(\frac{f^2}{10^8}\right)^2 D_w^4}{\left[1.0 + b_2 \left(\frac{f^2}{10^8}\right)^2 D_w^2\right]^{b_3}}\right] D_w \ ; \ X_{ODP} \le 0.0 \text{ and } X_{SSP} < 0.0 \end{cases}$$

$$Y_1 = \text{smallest of} \left(\frac{150\,r}{\cos\phi} \ , \ X_{ODP} \ , \ X - X_t \ , \ X_t + X_{ODP} + \frac{150\,r}{\cos\phi} - X\right)$$

$$\sigma_1 = \begin{cases} 0.0 \ ; \ X - X_t \le 0.0 \text{ or if } X - X_t > \frac{150\,r}{\cos\phi} + X_{ODP} \\ Y_1 D_w^* \sin^2\phi \ ; \text{ otherwise} \end{cases}$$

$$Y_2 = \text{smallest of} \left(\frac{150\,r}{\cos\phi} \ , \ 2L_{MS} \ , \ X - X_t - X_{ODP} \ , \ X_t + X_{MSP} + \frac{150\,r}{\cos\phi} - X\right)$$

$$\sigma_2 = \begin{cases} 0.0 \ ; \ X - X_t < X_{ODP} \text{ or if } X - X_t > \frac{150\,r}{\cos\phi} + X_{MSD} \\ \frac{1}{2} Y_2 D_w^* \sin^2\phi \ ; \text{ otherwise} \end{cases}$$

$$Y_{31} = \begin{cases} X_{MSP} \ ; \ \frac{150\,r}{\cos\phi} \ge (X - X_t - X_{MSP}) \\ X - \frac{150\,r}{\cos\phi} - X_t \ ; \text{ otherwise} \end{cases}$$

$$Y_{32} = \begin{cases} X - X_t \ ; \ X \le X_t + X_{SSP} \\ X_{SSP} \ ; \ X > X_t + X_{SSP} \end{cases}$$

If $X - X_t < X_{MSP}$ or if $X - X_t > \frac{150\,r}{\cos\phi} + X_{SSP}$

$\sigma_3 = 0.0$

If $X - X_t \geq X_{MSP}$ and $X - X_t \leq \frac{150\,r}{\cos\phi} + X_{SSP}$ and $b_{20} \neq 0.0$

$$\sigma_3 = \frac{D_w^*}{b_1} \sin^2\phi \left[\frac{1}{16} \left(\frac{n_{e_t}}{n_{e_{CR}}} \right)^2 \left(e^{-b_1 Y_{31}} - e^{-b_1 Y_{32}} \right) + \frac{1}{4} \left(\frac{n_{e_t}}{n_{e_{CR}}} \right)^8 \left(e^{-4b_1 Y_{31}} - e^{-4b_1 Y_{32}} \right) \right]$$

$$+ \left\{ 2 \left(\frac{n_{e_t}}{n_{e_{CR}}} \right)^{b_{20}} \left(e^{-\frac{b_1 b_{20}}{2} Y_{31}} - e^{-\frac{b_1 b_{20}}{2} Y_{32}} \right) \right.$$

$$\left[\frac{b_o \left(\frac{f^2}{10^8} \right)^2 D_w^4}{\left[1.0 + b_2 \left(\frac{f^2}{10^8} \right) D_w^2 \right]^{b_3}} \right] \left(\frac{\sin^2\phi^{(2 - b_{20})}}{b_1 b_{20}} \right) D_w^* \left(\right.$$

If $X - X_t \geq X_{MSP}$ and $X - X_t \leq \frac{150\,r}{\cos\phi} + X_{SSP}$ and $b_{20} = 0.0$

$$\sigma_3 = \frac{D_w^*}{b_1} \sin^2\phi \left[\frac{1}{16} \left(\frac{n_{e_t}}{n_{e_{CR}}} \right)^2 \left(e^{-b_1 Y_{31}} - e^{-b_1 Y_{32}} \right) \right.$$

$$\left. + \frac{1}{4} \left(\frac{n_{e_t}}{n_{e_{CR}}} \right)^8 \left(e^{-4b_1 Y_{31}} - e^{-4b_1 Y_{32}} \right) \right]$$

$$+ (Y_{32} - Y_{31}) (\sin^4\phi) \left[\frac{b_o \left(\frac{f^2}{10^8} \right)^2 D_w^4}{\left\{ 1.0 + b_2 \left(\frac{f^2}{10^8} \right) D_w^2 \right\}^{b_3}} \right] D_w$$

$$Y_{41} = \begin{cases} X_{SSP}\,; & \frac{150\,r}{\cos\phi} \geq (X - X_t - X_{SSP}) \\ X - \frac{150\,r}{\cos\phi} - X_t\,; & \text{otherwise} \end{cases}$$

$Y_{42} = X - X_t$

If $X - X_t \leq X_{SSP}$

$\sigma_4 = 0.0$

If $X - X_t > X_{SSP}$:

$$\sigma_4 = \frac{D_w^* \sin^2\phi}{4 b_1} \left(\frac{n_{e_t}}{n_{e_{CR}}}\right)^8 \left(e^{-4 b_1 Y_{41}} - e^{-4 b_1 Y_{42}}\right)$$

$$+ \left\{\frac{D_w}{b_1}\left[\frac{\sin^2\phi}{16} \frac{D_w^*}{D_w} + \left(\frac{b_o \left(\frac{f^2}{10^8}\right)^2 D_w^4}{\left[1 + b_2\left(\frac{f^2}{10^8}\right) D_w^2\right]^{b_3}}\right)\right]\right.$$

$$\left.\left(\frac{n_{e_t}}{n_{e_{CR}}}\right)^2 \left(e^{-b_1 Y_{41}} - e^{-b_1 Y_{42}}\right)\right\}$$

$$\sigma(x) = \sigma_1 + \sigma_2 + \sigma_3 + \sigma_4$$

3.3 MISCELLANEOUS CALCULATIONS

Four miscellaneous operations are performed near the end of the analysis calculations. These are: a. the evaluation of a polynomial, b. the calculation of a vector of generalized differences, c. the calculation of the average densities of the decoys, and d. the calculation of a series of terms comparing the characteristics of the decoys immediately before and after the discontinuous shape change.

The polynomial evaluation was originally intended for comparison of the nominal free space radar cross section of a reentry vehicle, X_{C_7}, with a curve-fit of the nominal radar cross section of various decoys. The user supplies curve fit coefficients for the cross-section data applicable to the class of electromagnetic devices being used. The difference between the reentry vehicle and decoy could be calculated for use in the penalty function equation as:

$$\Delta_{RCS} = X_{C_7} - \sum_{K=1}^{N_3} \sum_{J=1}^{N_2} \sum_{I=1}^{N_1} {}^{a}COE_{((K-1)N_1N_2 + (J-1)N_1 + I)} \, R_{B_1}^{I-1} \, R_{N_1}^{J-1} \, \theta_1^{K-1}$$

This calculation was generalized to allow the polynomial to be a function of any three quantities in the ØCCUR vector, Q_i, and is now coded in the following form:

$$\Delta_{RCS} = X_{C_7} - X_{C_8} \sum_{K=1}^{N_3} \sum_{J=1}^{N_2} \sum_{I=1}^{N_1} {}^{a}COE_{((K-1)N_1N_2 + (J-1)N_1 + I)} Q_1^{I-1} Q_2^{J-1} Q_s^{K-1}$$

This equation allows the radar calculation described above to be performed ($X_{C_8} = 1.0$) and also allows direct use of the polynomial as a constraint if X_{C_7} is 0.0 and X_{C_8} is -1.0.

As many as twenty differences between pairs of quantities in the ØCCUR vector can be calculated:

$$G_j = Q_{H_j} - Q_{L_j} \qquad j = 1, 20 \text{ max}$$

where H_j and L_j are subscripts identifying the desired quantities in the ØCCUR vector.

The average density of the initial decoy is calculated from:

$$r = R_{N_1} \cos \theta_1$$

$$h = R_{N_1} (1 - \sin \theta_1)$$

$$V_1 = \pi h^2 (R_{N_1} - h/3) + (\pi/3)(L_{A_1} - h)(R_{B_1}^2 + R_{B_1} r + r^2)$$

$$D_1 = V_1 / W_1$$

If the vehicle undergoes a discontinuous shape change, then the average density of the decoy immediately after the shape change is:

$$r = R_{N_2} \cos \theta_2$$

$$h = R_{N_2} (1 - \sin \theta_2)$$

$$V_2 = \pi h^2 (R_{N_2} - h/3) + (\pi/3)(L_{A_2} - h)(R_{B_2}^2 + R_{B_2} r + r^2)$$

$$D_2 = V_2 / \Psi_2$$

The comparisons of the vehicles before and after discontinuous shape change are calculated:

$$D_1 = \Psi_{1_{FINAL}} - \Psi_2$$

$$D_2 = \theta_{1_{FINAL}} - \theta_2$$

$$D_3 = R_{N_{1_{FINAL}}} - R_{N_2}$$

$$D_4 = R_{B_{1_{FINAL}}} - R_{B_2}$$

$$D_5 = \lambda_{1_{FINAL}} - \lambda_2$$

$$D_6 = L_{A_{1_{FINAL}}} - L_{A_2}$$

$$R_1 = \Psi_2 / \Psi_{1_{FINAL}}$$

$$R_2 = \theta_2 / \theta_{1_{FINAL}}$$

$$R_3 = \begin{cases} R_{N_2} / R_{N_{1_{FINAL}}} \\ 0.0 \text{ if } R_{N_{1_{FINAL}}} = 0.0 \end{cases}$$

$$R_4 = R_{B_2} / R_{B_{1_{FINAL}}}$$

$$R_5 = \begin{cases} \lambda_2 / \lambda_{1_{FINAL}} \\ 0.0 \text{ if } \lambda_{1_{FINAL}} = 0.0 \end{cases}$$

$$R_6 = L_{A_2} / L_{A_{1_{FINAL}}}$$

These quantities are available for use as constraints (see Table 4 of Appendix II, the User's Manual).

4.0 COMPARISON OF DECOY WITH REENTRY VEHICLE

The basic analysis calculations described in Section 3.0 primarily involve the determination of data for a single vehicle. In this section the techniques used to compare a reentry vehicle and decoy will be discussed along with the definition of the corridor and effectiveness integrals. These integrals are calculated for use in the penalty function equation and in the effectiveness operations, respectively.

4.1 DIFFERENCE EVALUATIONS

As many as nine performance functions are stored for the reentry vehicle and the decoy. The differences between the reentry vehicle (R/V) performances and decoy (D) performance at the M altitudes are:

$$\Delta V_i = V_{R/V_i} - V_{D_i} \qquad i = 1, M$$

$$\Delta D_i = \dot{V}/g_{R/V_i} - \dot{V}/g_{D_i}$$

$$\Delta\beta_i = \beta_{R/V_i} - \beta_{D_i}$$

$$\Delta W_{L_{1_i}} = W_{L_{1_{R/V_i}}} - W_{L_{1_{D_i}}}$$

$$\Delta W_{L_{2_i}} = W_{L_{2_{R/V_i}}} - W_{L_{1_{D_i}}}$$

$$\Delta W_{L_{3_i}} = W_{L_{3_{R/V_i}}} - W_{L_{3_{D_i}}}$$

$$\Delta W_{R_{1_i}} = W_{R_{1_{R/V_i}}} - W_{R_{1_{D_i}}}$$

$$\Delta W_{R_{2_i}} = W_{R_{2_{R/V_i}}} - W_{R_{2_{D_i}}}$$

$$\Delta W_{R_{3_i}} = W_{R_{3_{R/V_i}}} - W_{R_{3_{D_i}}}$$

These nine vectors of differences will be referred to as ΔP_j in the following discussions.

In the influence calculations associated with MØDE = 2 in the program, the partial derivatives of the differences listed above with respect to the design variables, X, can be evaluated using finite differences. The first derivative is based on a basic decoy (1) and a comparison decoy (2):

$$\left(\frac{\partial \Delta P_j}{\partial x}\right)_i = \frac{\Delta P_{j_{i_2}} - \Delta P_{j_{i_1}}}{X_2 - X_1} \qquad \begin{matrix} i = 1, M \\ j = 1, 9 \end{matrix}$$

The second derivative is based on three decoys which are used to define two first derivatives. The second derivative is:

$$\left(\frac{\partial^2 \Delta P_j}{\Delta X^2}\right)_i = \frac{(\partial \Delta P_j/\partial X)_i\Big|_1 - (\partial \Delta P_j/\partial X)_i\Big|_2}{\left(\frac{X_3 + X_1}{2}\right) - \left(\frac{X_2 + X_1}{2}\right)} \qquad \begin{matrix} i = 1, M \\ j = 1, 9 \end{matrix}$$

4.2 INTEGRALS OF SPECIAL FUNCTIONS

The corridor integrals are defined in terms of the performance differences, ΔP; the corridors, T and B; and an arbitrary multiplier which can be a function of altitude, Z, if desired. The quantities ΔP, T, and B are all functions of altitude. For each of the nine performance functions there is a corridor integral of the form:

$$I_j = (AA_j Z^2 + AA_{j+1} Z + AA_{j+2}) \int_{Z_o}^{Z_f} \left[<B - \Delta P_j>^2 + <\Delta P_j - T>^2 \right] dZ \qquad j = 1, 9$$

where the square brackets mean that negative numbers are set to zero.

The effectiveness integrals are calculated using the performance differences, ΔP; and the standard deviation of the perceived error (uncertainty) in the defense measurement, σ_j . Both of these quantities are functions of altitude. For each of the nine performance functions there is an effectiveness integral of the form:

$$E_j = \int_{Z_o}^{Z_f} \left(\frac{\Delta P_j}{\sigma_j}\right)^2 dZ$$

5.0 EFFECTIVENESS MODEL OPERATIONS

A discussion of the effectiveness model operations is included in the main portion of the ADTECH IV Final Report. The effectiveness integrals, E_j, are discussed in Section 4.2 of this volume. For example:

$$\frac{S_v}{Z_o - Z_f} F_v = \frac{S_v}{Z_o - Z_f} \int_{Z_o}^{Z_f} \left(\frac{\Delta V}{\sigma_v}\right)^2 dz \approx \sum_{i=1}^{S_v} \left(\frac{\Delta V}{\sigma_v}\right)_i^2$$

The difference in the means of the logarithm of the likelihood ratio, μ, is calculated using only the terms which have been specified by the user:

$$\mu = \left\{ \frac{1}{Z_o - Z_f} \left(S_v E_v + S_D E_D + S_\beta E_\beta + S_{R_1} E_{R_2} + S_{R_2} E_{R_2} + S_{R_3} E_{R_3} + S_{W_1} E_{W_1} + S_{W_2} E_{W_2} + S_{W_2} E_{W_3} \right) \right\}^{1/2}$$

With the input probability of false dismissal, P_{FD}, the upper limit of integration, t_o, is calculated from the equation:

$$P_{FD} = \frac{1}{\sqrt{2\pi}} \int_{-\infty}^{t_o} \exp\left(-\frac{t^2}{2}\right) dt$$

Then with t_o and μ calculated the probability of discrimination of the decoy is:

$$P.D. = \frac{1}{\sqrt{2\pi}} \int_{-\infty}^{t_o + \mu} \exp\left(-\frac{t^2}{2}\right) dt$$

6.0 CLASSIC FUNCTIONS FOR TESTING THE OPTIMIZATION TECHNIQUES

Five functions or set of functions are provided for use in checking the search and optimization techniques. The substitution of analytic functions in place of the complete trajectory calculations significantly conserves machine time and also provides positive control for the checkout since the characteristics of the functions are explicitly defined.

The subscripts of the quantity X in the following equations refer to the locations in the vector called ØCCUR in the program. The vector of coefficients called A in the equations is the same as the vector of coefficients called A in the drag calculations, thus it is recommended that these calssic check cases and actual trajectory calculations not be utilized in the same job unless careful attention is given to the A coefficient vector and the ØCCUR vector for each case.

The first function is based on the one used by Rosenbrock (Refs. III-5 and III-6).

$$X_{100} = 100\ [X_2 - X_1^2]^2 + (1 - X_1)^2 + a_1$$

The second set of functions provides two additional equations which can be used to generate nonlinear constraints for use with the Rosenbrock function:

$$X_{100} = 100\,(X_2 - X_1^2)^2 + (1 - X_1)^2 + a_1$$

$$X_{101} = a_2 \left\{ X_2 - (a_8\,(X_1 - a_7)^3 + a_9\,(X_1 - a_7)^2 + a_{10}\,(X_1 - a_7) + a_{11}) \right\}$$

$$X_{102} = a_3 \left\{ X_2 - (a_{13}\,(X_1 - a_{12})^3 + a_{14}\,(X_1 - a_{12})^2 + a_{15}\,(X_1 - a_{12}) + a_{16}) \right\}$$

The third set of functions is based on the four-variable function with constraint functions which was developed by Rosen (Reference III-7).

$$X_{200} = X_1^2 + X_2^2 + 2X_3^2 + X_4^2 - 5X_1 - 5X_2 - 21\,X_3 + 7\,X_4 + a_{17}$$

$$X_{201} = -X_1^2 - X_2^2 - X_3^2 - X_4^2 - X_1 + X_2 - X_3 + X_4 + 8$$

$$X_{202} = -X_1^2 - 2X_2^2 - X_3^2 - 2X_4^2 + X_1 + X_4 + 10$$

$$X_{203} = -2X_1^2 - X_2^2 - X_3^2 - 2X_1 + X_2 + X_4 + 5$$

The fourth function is based on a two variable function which was Fiacco and McCormick (Reference III-8).

$$X_{300} = 4X_1 + X_2 + a_{25}\left(\frac{1}{X_1} + \frac{1}{X_2}\right) + a_{26}$$

The fifth function is a general quadratic function:

$$X_{400} = a_1 X_1^2 + a_2 X_1 X_2 + a_3 X_2^3 + a_4 X_1 + a_5 X_2 + a_6$$

This function was used to generate the optimizer check cases which were presented in Section 6.3 of the Users Manual (App. II).

7.0 REFERENCES

III-1. Avco Corporation, "Advanced Decoy Technology Program, ADTECH III, Final Report," AVMSD-0835-67-RR, or SAMSO-TR-68-13, (February 1968).

III-2. Schmit, L. A., Jr., and R. L. Fox, Integrated Synthesis-Analysis Concept for Optimum Structural Design, AIAA Annual Structural and Materials Conference, Fifth, Palm Springs, California (1-3 April 1964).

III-3. Davidon, William C., Variable Metric Method for Minimization, Argonne National Laboratory Report, ANL-5990 Rev., Univ. of Chicago, (November 1959).

III-4. Recent Advances in Optimization Techniques, A. Lavi and T. P. Vogl (New York, John Wiley & Sons, 1966).

III-5. Rosenbrock, H. H., An Automatic Method for Finding the Greatest or Least Value of a Function," The Computer Journal, 3, (1960) pp. 175-184.

III-6. Wilde, Douglass J., Optimum Seeking Methods, (Prentice-Hall, Inc., 1964)

III-7. Rosen, J. B., and S. Suzuki, Construction of Nonlinear Programming Test Problems, NASA CR-57188 (12 August 1964).

III-8. Fiacco, A. V. and G. P. McCormick, Programming Under Nonlinear Constraints by Unconstrained Minimization - A Primal-Dual Method, Research Analysis Corp., RAC-TP-96 (N64-13244, AD423903) (September 1963).

APPENDIX III-1

REPRODUCTION OF VARIABLE METRIC METHOD FOR MINIMIZATION

A report written by William C. Davidon
Argonne National Laboratory, ANL-5990 Rev.
University of Chicago, November 1959

VARIABLE METRIC METHOD FOR MINIMIZATION

William C. Davidon

This is a method for determining numerically local minima of differentiable functions of several variables. In the process of locating each minimum, a matrix which characterizes the behavior of the function about the minimum is determined. For a region in which the function depends quadratically on the variables, no more than N iterations are required, where N is the number of variables. By suitable choice of starting values and without modification of the procedure, linear constraints can be imposed upon the variables.

1. INTRODUCTION

The solution to many different types of physical and mathematical problems can be obtained by minimizing a function of a finite number of variables. Among these problems are least-squares fitting of experimental data, determination of scattering amplitudes and energy eigenvalues by variational methods, the solution of differential equations, etc. With the use of high-speed digital computers, numerical methods for finding the minima of functions have received increased attention. Some of the procedures which have been used are those of optimum gradient,[1] conjugate gradients,[2] the Newton-Raphson iteration,[3] and one by Garwin and Reich.[4] In many instances, however, all of these methods require a large number of iterations to achieve a given accuracy in locating the minimum. Also, for some behaviors of the function being minimized, the procedures do not converge.

The method presented in this paper has been developed to improve the speed and accuracy with which the minima of functions can be evaluated numerically. In addition, a matrix characterizing the behavior of the function in the neighborhood of the minimum is determined in the process. Linear constraints can be imposed upon the variables by suitable choice of initial conditions, without alteration of the procedure.

2. NOTATION

We will employ the summation convention:

$$a^{\mu}\, b_{\mu} \equiv \sum_{\mu=1}^{N} a^{\mu}\, b_{\mu}$$

In describing the iterative procedure, we will use symbols for memory locations rather than successive values of a number; e.g., we would write $x + 3 \longrightarrow x$ instead of $x_i + 3 = x_{i+1}$. In this notation, the sequence of operations is generally relevant. The following symbols will be used.

x^μ: $\mu = 1, \ldots, N$: the set of N independent variables

$f(\underline{x})$: the value of the function to be minimized evaluated at the point $\underline{x}$.

$g_\mu(\underline{x})$: the derivatives of $f(\underline{x})$ with respect to x^μ evaluated at x:

$$g_\mu(\underline{x}) = \frac{\partial f(\underline{x})}{\partial x^\mu}$$

$h^{\mu\nu}$: a non-negative symmetric matrix which will be used as a metric in the space of the variables.

Δ: The determinant of $h^{\mu\nu}$

c: 2 times fractional accuracy to which the function $f(\underline{x})$ is to be minimized

d: a limiting value for what is to be considered as a "reasonable" minimum value of the function. For least squares problems d can be set equal to zero.

K: an integer which specifies the number of times the variables are to be changed in a random manner to test the reliability of the determination of the minimum.

3. GEOMETRICAL INTERPRETATION

It is convenient to use geometrical concepts to describe the minimization procedure. We do so by considering the variables x^μ to be the coordinates of a point in an N-dimensional linear space. As shown in Fig. 1a, the set of $\underline{x}$ for which $f(\underline{x})$ is constant forms an N-1 dimensional surface in this space. One of this family of surfaces passes through each $\underline{x}$, and the surface about a point is characterized by the gradient of the function at that point:

$$g_\mu(\underline{x}) = \frac{\partial f(\underline{x})}{\partial x^\mu} .$$

These N components of the gradient can in turn be considered as the coordinates of a point in a different space, as shown in Fig. 1b. As long as $f(\underline{x})$ is differentiable at all points, there is a unique point $\underline{g}$ in the gradient space associated with each point $\underline{x}$ in the position space, though there may be more than one $\underline{x}$ with the same $\underline{g}$.

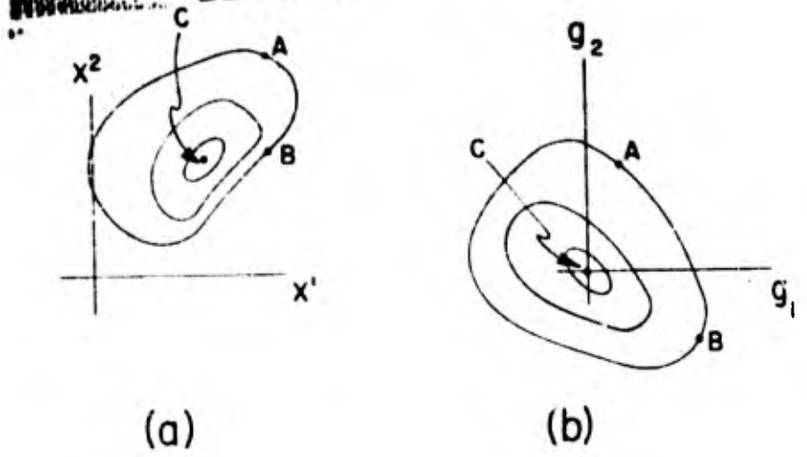

Fig. 1. Geometrical interpretation of x^μ and $g_\mu(\underline{x})$

In the neighborhood of any one point A the second derivatives of $f(\underline{x})$ specify a linear mapping of changes in position, $\underline{dx}$, onto changes in gradient $\underline{dg}$, in accordance with the equation

$$dg_\mu = \frac{\partial^2 f}{\partial x^\mu \partial x^\nu} \, dx^\nu . \tag{3.1}$$

The vectors $\underline{dx}$ and $\underline{dg}$ will be in the same direction only if $\underline{dx}$ is an eigenvector of the Hessian matrix:

$$\left\| \frac{\partial^2 f}{\partial x^\mu \partial x^\nu} \right\|$$

If the ratios among the corresponding eigenvalues are large, then for most $\underline{dx}$ there will be considerable difference in the directions of these two vectors.

All iterative gradient methods, of which this is one, for locating the minima of functions consist of calculating $\underline{g}$ for various $\underline{x}$ in an effort to locate those values of $\underline{x}$ for which $\underline{g} = 0$, and for which the Hessian matrix is positive definite. If this matrix were constant and explicitly known, then the value of the gradient at one point would suffice to determine the minimum. In that case the change desired in $\underline{g}$ would be $-\underline{g}$, so we would have

$$-g_\mu = \frac{\partial^2 f}{\partial x^\mu \partial x^\nu} \, \Delta x^\nu \quad , \tag{3.2}$$

from which we could obtain Δx^ν by multiplying Eq. (3.2) by the inverse of

the matrix $\left\| \frac{\partial^2 f}{\partial x^\mu \partial x^\nu} \right\|$ However, in most situations of interest, $\left\| \frac{\partial^2 f}{\partial x^\mu \partial x^\nu} \right\|$ is not constant, nor would explicit evaluation at points that might be far from a minimum represent the best expenditure of time.

Instead, an initial trial value is assumed for the matrix $\left\| \frac{\partial^2 f}{\partial x^\mu \partial x^\nu} \right\|^{-1}$ This matrix, denoted by $h^{\mu\nu}$, specifies a linear mapping of all changes in the gradient onto changes in position. It is to be symmetric and non-negative (positive definite if there are no constraints on the variables). After making a change in the variable $\underline{x}$, this trial value is improved on the basis of the actual relation between the changes in $\underline{g}$ and $\underline{x}$. If $\left\| \frac{\partial^2 f}{\partial x^\mu \partial x^\nu} \right\|$ is constant, then, after N iterations, not only will the minimum of the function be determined, but also the final value of $h^{\mu\nu}$ will equal $\left\| \frac{\partial^2 f}{\partial x^\mu \partial x^\nu} \right\|^{-1}$ We shall subsequently discuss the significance of this matrix in specifying the accuracy to which the variables have been determined

The matrix $h^{\mu\nu}$ can be used to associate a squared length to any gradient, defined by $h^{\mu\nu} g_\mu g_\nu$ If the Hessian matrix were constant and $h^{\mu\nu}$ were its inverse, then $\frac{1}{2} h^{\mu\nu} g_\mu g_\nu$ would be the amount by which $f(\underline{x})$ would exceed its minimum value. We therefore consider $h^{\mu\nu}$ as specifying a metric, and when we refer to the lengths of vectors, we will imply their lengths using $h^{\mu\nu}$ as the metric We have called the method a "variable metric" method to reflect the fact that $h^{\mu\nu}$ is changed after each iteration

We have divided the procedure into five parts which to a large extent are logically distinct. This not only facilitates the presentation and analysis of the method, but it is convenient in programming the method for machine computation.

4 READY: CHART I

The function of this section is to establish a direction along which to search for a relative minimum, and to box off an interval in this direction within which a relative minimum is located. In addition, the criterion for terminating the iterative procedure is evaluated.

Those operations which are only performed at the beginning of the calculation and not repeated on successive iterations have been included in Chart 1 (page 7). These include the loading of input data, initial print-outs, and the initial calculation of the function and its gradient. This latter calculation is treated as an independent subroutine, which may on its initial and final calculations include some operations not part of the usual iteration, such as loading operations, calculation of quantities for repeated use, special print-outs, etc. A counter recording the number of iterations has been found to be a convenience, and is labeled I.

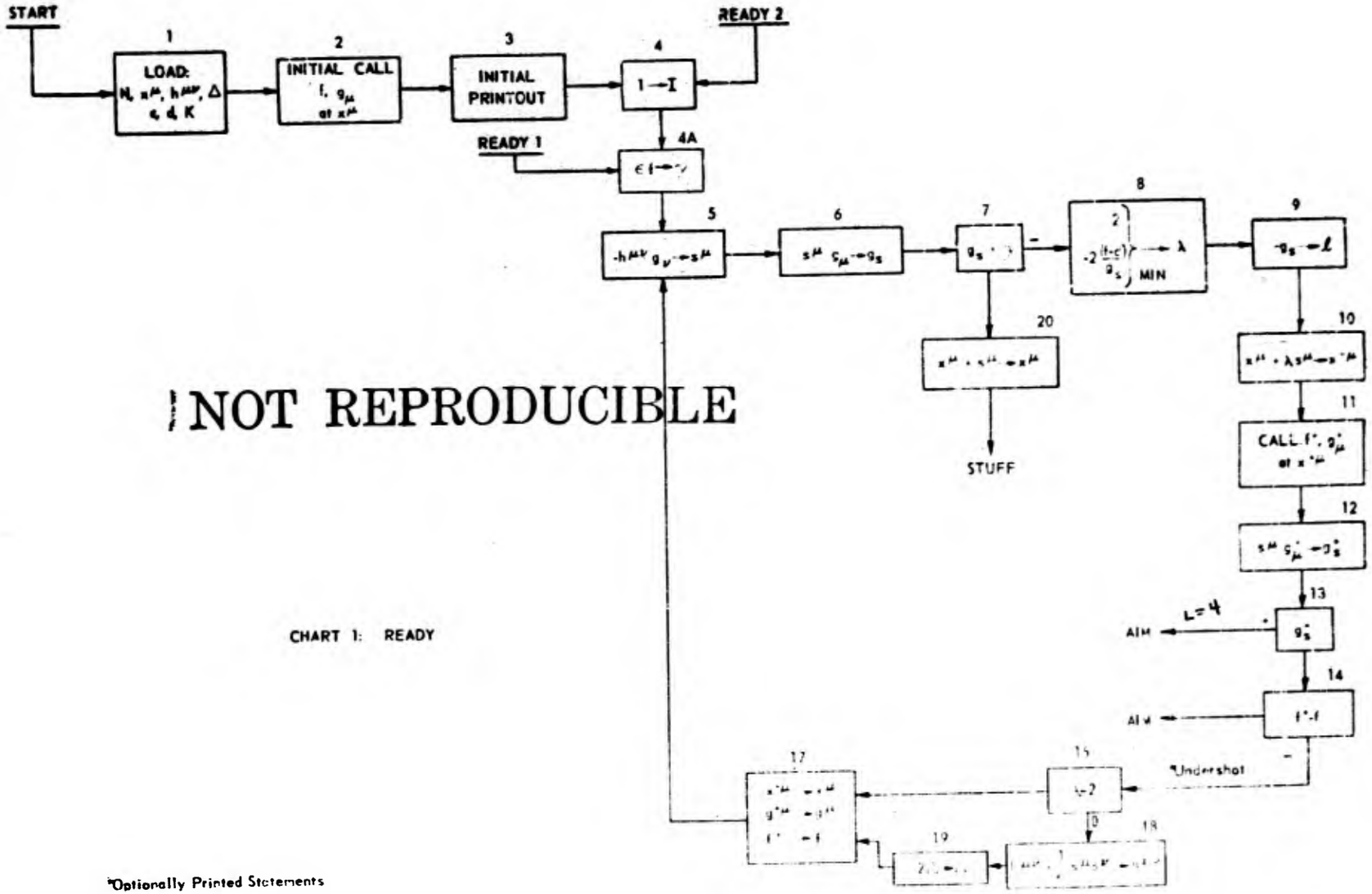

CHART 1: READY

*Optionally Printed Statements

The iterative part of the computation begins with "READY 1." The direction of the first step is chosen by using the metric $h^{\mu\nu}$ in the relation

$$-h^{\mu\nu}\, g_\nu \longrightarrow s^\mu . \tag{4.1}$$

The component of the gradient in this direction is evaluated through the relation

$$s^\mu\, g_\mu \longrightarrow g_s \tag{4.2}$$

From Eqs. (4.1) and (4.2) we see that $-g_s$ is the squared length of $\underline{g}$, and hence the improvement to be expected in the function is $-\frac{1}{2} g_s$. The positive definiteness of $h^{\mu\nu}$ insures that g_s is negative, so that the step is in a direction which (at least initially) decreases the function. If its decrease is within the accuracy desired, i.e., if $g_s + \epsilon > 0$, then the minimum has been determined. If not, we continue with the procedure.

In a first effort to box in the minimum, we take a step which is twice the size that would locate the minimum if the trial $h^{\mu\nu}$ were $\left\| \frac{\partial^2 f}{\partial x^\mu \partial x^\nu} \right\|^{-1}$. However, in order to prevent this step from being unreasonably large when the trial $h^{\mu\nu}$ is a poor estimate, we restrict the step to a length such that $(\lambda s^\mu) g_\mu$, the decrease in the function if it continued to decrease linearly, is not greater than some preassigned maximum, $\frac{1}{2}(f-\phi)$. We then change x^μ by

$$x^\mu + \lambda s^\mu \longrightarrow x^{+\mu} \quad , \tag{4.3}$$

and calculate the new value of the function and its gradient at $x^{+\mu}$. If the projection $s^\mu g_\mu^+ = g_s^+$ of the new gradient in the direction of the step is positive, or if the new value of the function f^+ is greater than the original f, then there is a relative minimum along the direction s between $\underline{x}$ and $\underline{x}^+$, and we proceed to "Aim" where we will interpolate its position. However, if neither of these conditions is fulfilled, the function has decreased and is decreasing at the point $\underline{x}^+$, and we infer that the step taken was too small. If the step had been limited by the preassigned change in the function d, we double d. If the step had been taken on the basis of $h^{\mu\nu}$, we modify $h^{\mu\nu}$ so as to double the squared length of s^μ, leaving the length of all perpendicular vectors unchanged. This is accomplished by

$$h^{\mu\nu} + \frac{1}{\ell}\, s^\mu\, s^\nu \longrightarrow h^{\mu\nu} \quad , \tag{4.4}$$

where ℓ is the squared length of s^μ. This doubles the determinant of $h^{\mu\nu}$. The process is then repeated, starting from the new position.

5. AIM: CHART 2

The function of this section is to estimate the location of the relative minimum within the interval selected by "Ready." Also a comparison is made of the improvement expected by going to this minimum with that from a step perpendicular to this direction.

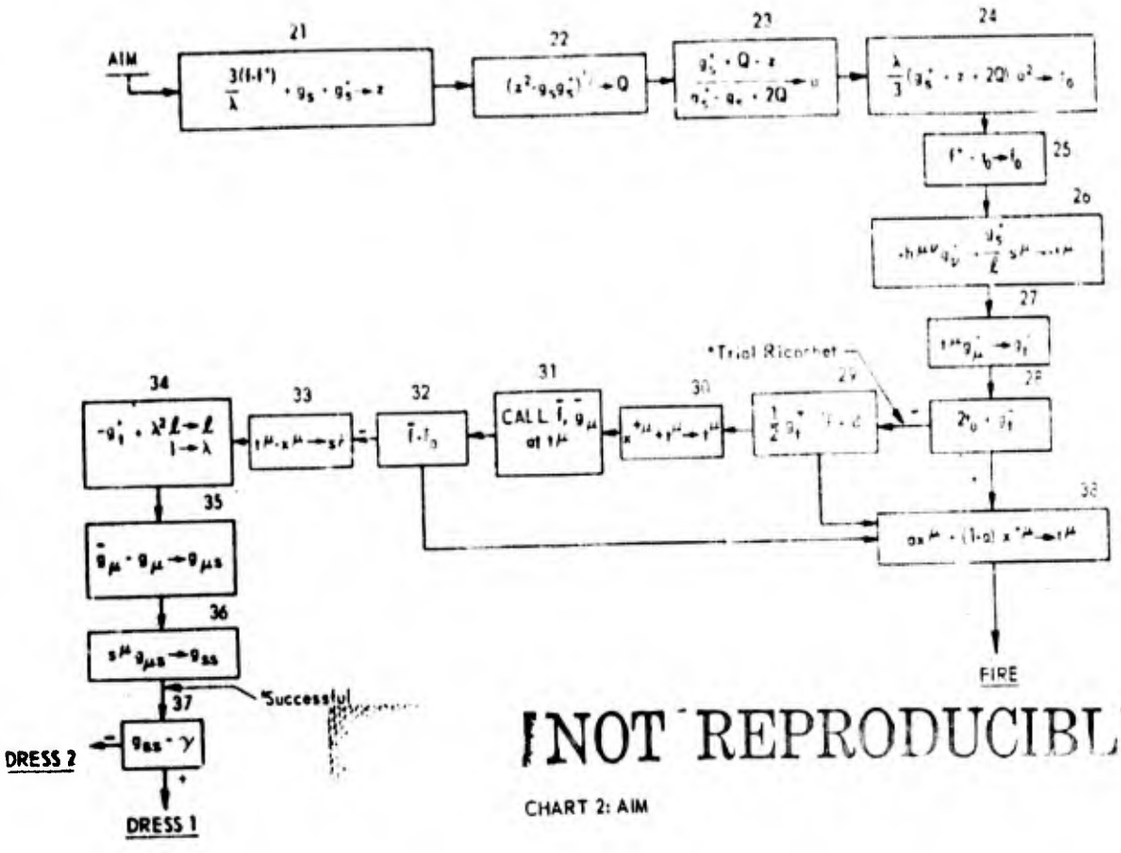

CHART 2: AIM

Inasmuch as the interpolation is along a one-dimensional interval, it is convenient to plot the function along this direction as a simple graph (see Fig. 2).

The values of f and f^+ of the function at points $\underline{x}$ and $\underline{x}^+$ are known; and so are its slopes, g_s and g_s^+, at these two points. We interpolate for the location of the minimum by choosing the "smoothest" curve satisfying the boundary conditions at $\underline{x}$ and $\underline{x}^+$, namely, the curve defined as the one which minimizes

$$\int_0^\lambda d\alpha \left(\frac{d^2 f}{d\alpha^2}\right)^2$$

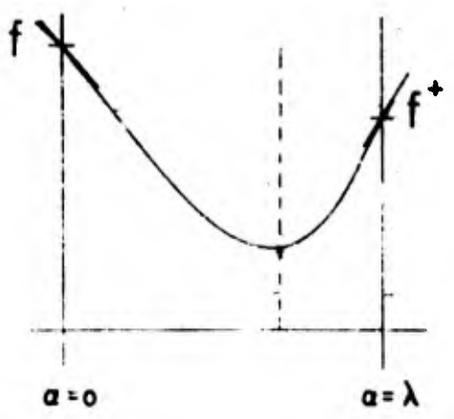

Fig. 2

Plot of f(x) along a one-dimensional interval.

over the curve. This is the curve formed by a flat spring fitted to the known ordinates and slopes at the end points, provided the slope is small. The resulting curve is a cubic, and its slope at any α ($0 \leq \alpha \leq \lambda$) is given by

$$g_s(\alpha) = g_s - \frac{2\alpha}{\lambda}(g_s + z) + \frac{\alpha^2}{\lambda^2}(g_s + g_s^+ + 2z), \qquad (5.1)$$

where

$$z = \frac{3(f - f^+)}{\lambda} + g_s + g_s^+ .$$

The root of Eq. (5.1) that corresponds to a minimum lies between 0 and 1 in virtue of the fact that $g_s < 0$ and either $g_s^+ > 0$ or $z < g_s + g_s^+$. It can be expressed as

$$\alpha_{min} = \lambda(1 - a) ,$$

where

$$a = \frac{g_s^+ + Q - z}{g_s^+ - g_s + 2Q} \qquad (5.2)$$

and

$$Q = (z^2 - g_s g_s^+)^{1/2} .$$

The particular form of Eq. (5.2) is chosen to obtain maximum accuracy, which might otherwise be lost in taking the difference of nearly equal quantities. The amount by which the minimum in f is expected to fall below f^+ is given by

$$\int_{(\lambda - a\lambda)}^{\lambda} d\alpha\, g_s(\alpha) = \frac{1}{3}(g_s^+ + z + 2Q)\, a^2 \lambda \quad . \qquad (5.3)$$

The anticipated change is new compared with what would be expected from a perpendicular step. On the basis of the metric $h^{\mu\nu}$, the step to the optimum point in the (N-1)-dimensional surface perpendicular to s^μ through $x^{+\mu}$ is given by

$$-h^{\mu\nu}\, g_\nu^+ + \frac{g_s}{\ell}\, s^\mu \longrightarrow t^\mu \tag{5.4}$$

The change in f to be expected from this step is $\frac{1}{2} t^\mu\, g_\mu^+$. Hence, the decision whether to interpolate for the minimum along $\underline{s}$ or to change $\underline{x}$ by use of Eq. (5.4) is made by comparing $g_t^+ = t^\mu\, g_\mu^+$ with expression (5.3).

The purpose of allowing for this option is to improve the speed of convergence when the function is not quadratic. Consider the situation of Fig. 3. The optimum point between $\underline{x}$ and $\underline{x}^+$ is point A. However, by going to point B, a greater improvement can be made in the function. When the behavior of the function is described by a curving valley, this option is of particular value, for it enables successive iterations to proceed around the curve without backtracking to the local minimum along each step. However, if evaluation of the function at this new position does not give a better value than that expected from the interpolation, then the interpolated position is used. Should the new position be better as expected, it is then desired to modify $h^{\mu\nu}$ to incorporate the new information obtained about the function. The full step taken is stored at s^μ, and its squared length is the sum of the squares of the step along $\underline{s}$ and the perpendicular step, i.e., $s^\mu = -g_t^+ + \lambda^2 \ell$. The change in the gradient resulting from this step is stored at $g_{\mu s}$ and these quantities are used in the section "Dress" in a manner to be described.

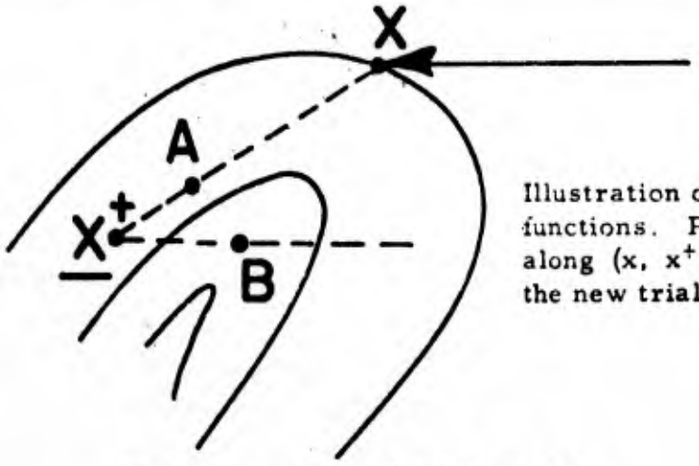

Fig. 3

Illustration of procedure for nonquadratic functions. Point A is the optimum point along (x, x^+); point B is the location for the new trial.

For the interpolated step, we set

$$a x^\mu + (1 - a)\, x^{+\mu} \longrightarrow t^\mu \tag{5.5}$$

By direct use of the x^μ instead of the s^μ greater accuracy is obtained in the event that a is small. After making this interpolation, we proceed to "Fire."

6. FIRE: CHART 3

The purposes of this section are to evaluate the function and its gradient at the interpolated point and to determine if the local minimum has been sufficiently well located. If so, then the rate of change of gradient is evaluated (or, more accurately, λ times the rate of change) by interpolating from its values at $\underline{x}$, $\underline{x}^+$, and at the interpolated point.

If the function were cubic, then f at the interpolated point would be a minimum, the component of the gradient at this point along $\underline{s}$ would be zero, and the second derivative of the function at the minimum along the line would be $2Q/\lambda$. However, as the function will generally be more complicated, none of these properties of f and its derivatives at the interpolated point will be exactly satisfied. We designate the actual value of f and its gradient at the interpolated point by $\bar{f}$ and $\bar{g}_\mu$. The component of $\bar{g}_\mu$ along $\underline{s}$ is $s^\mu \bar{g}_\mu = \bar{g}_s$. Should $\bar{f}$ be greater than f or f^+ by a significant amount ($> \epsilon$), the interpolation is not considered satisfactory and a new one is made within that part of the original interval for which f at the end point is smaller.

From the values of the gradient g_μ, $\bar{g}_\mu$, and g^+_μ at three points along a line, we can interpolate to obtain its rate of change at the interpolated point. With a quadratic interpolation for the gradient, we obtain

$$(\bar{g}_\mu - g_\mu)\frac{a}{1-a} + (g^+_\mu - \bar{g}_\mu)\frac{1-a}{a} \longrightarrow g_{\mu s} \tag{6.1}$$

where $\frac{1}{\lambda} g_{\mu s}$ is the rate of change of the gradient at the interpolated point The component of $g_{\mu s}$ in the direction of s, namely, $s^\mu g_{\mu s} = g_{ss}$, can be expressed as

$$\bar{g}_s\left(\frac{a}{1-a} - \frac{1-a}{a}\right) + 2Q \longrightarrow g_{ss} \tag{6.2}$$

If the interpolated point were a minimum, then $\bar{g}_s = 0$ and $g_{ss} = 2Q$.

An additional criterion imposed upon the interpolation is that the first term on the left of Eq. (6.2) be smaller in magnitude than Q. Among other things, this insures that the interpolated value for the second derivative is positive. If this criterion is not fulfilled, no interpolation is made, and the matrix $h^{\mu\nu}$ is changed in a less sophisticated manner.

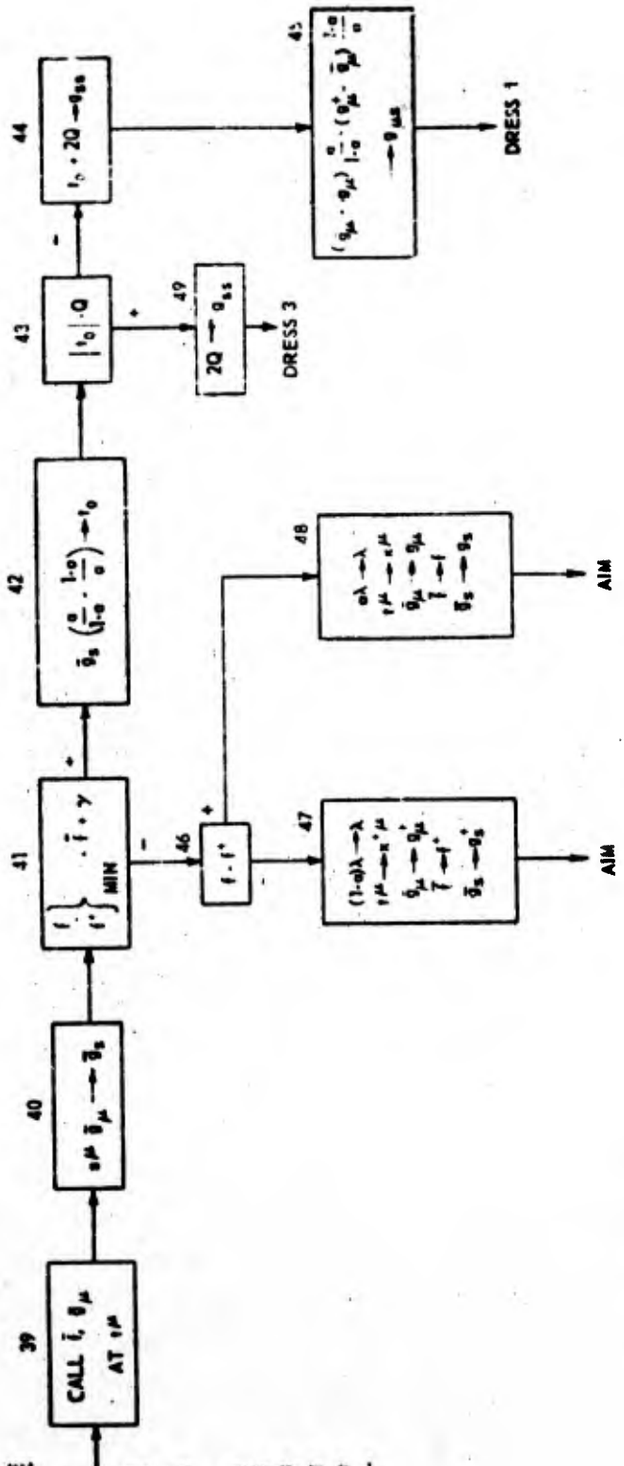

CHART 3: FIRE

7. DRESS. CHART 4

The purpose of this section is to modify the metric $h^{\mu\nu}$ on the basis of information obtained about the function along the direction $\underline{s}$. The new $h^{\mu\nu}$ is to have the property that $(h^{\mu\nu})' g_{\nu s} = \lambda s^{\mu}$, and must retain the information which the preceding iterations had given about the function.

If the vector $h^{\mu\nu} g_{\nu s} = t^{\mu}$ were in the direction of s^{μ}, then it would be sufficient to add to $h^{\mu\nu}$ a matrix proportional to $s^{\mu} s^{\nu}$. If t^{μ} is not in the direction of s^{μ}, the smallest squared length for the difference between s^{μ} and $(h^{\mu\nu} + \alpha s^{\mu} s^{\nu}) g_{\nu s}$ is obtained when $\alpha = \frac{\lambda}{g_{ss}} - \frac{1}{\ell}$. For this value of α, the squared length of the difference is $t_0 - \frac{g_{ss}}{\ell}$ where t_0 is the square length of $\underline{d}$, namely, $h^{\mu\nu} d_{\mu} d_{\nu}$. When this quantity is sufficiently small ($< \epsilon$), the matrix $h^{\mu\nu}$ undergoes the change:

$$h^{\mu\nu} + \left(\frac{\lambda}{g_{ss}} - \frac{1}{\ell}\right) s^{\mu} s^{\nu} \longrightarrow h^{\mu\nu} \tag{7.1}$$

The corresponding change in the determinant of $h^{\mu\nu}$ is

$$\frac{\lambda \ell}{g_{ss}} \Delta \longrightarrow \Delta \tag{7.2}$$

When the vectors t^{μ} and s^{μ} are not sufficiently colinear, it is necessary to modify $h^{\mu\nu}$ by a matrix of rank two instead of one, i.e.,

$$h^{\mu\nu} - \frac{t^{\mu} t^{\nu}}{t_0} + \frac{\lambda}{g_{ss}} s^{\mu} s^{\nu} \longrightarrow h^{\mu\nu} \tag{7.3}$$

Then the change in the determinant of $h^{\mu\nu}$ is

$$\frac{\lambda g_{ss}}{t_0} \Delta \longrightarrow \Delta \tag{7.4}$$

After the matrix is changed, the iteration is complete; after printing out whatever information is desired about this part of the calculation, a new iteration is begun. This is repeated until the function is minimized to within the accuracy required

8. STUFF: CHART 5

The purposes of this section are to test how well the function has been minimized and to test how well the matrix $h^{\mu\nu}$ approximates $\left\| \frac{\partial^2 f}{\partial x^{\mu} \partial x^{\nu}} \right\|$ at the minimum. This is done by displacing point $\underline{x}$ from the location of the minimum in a random direction.

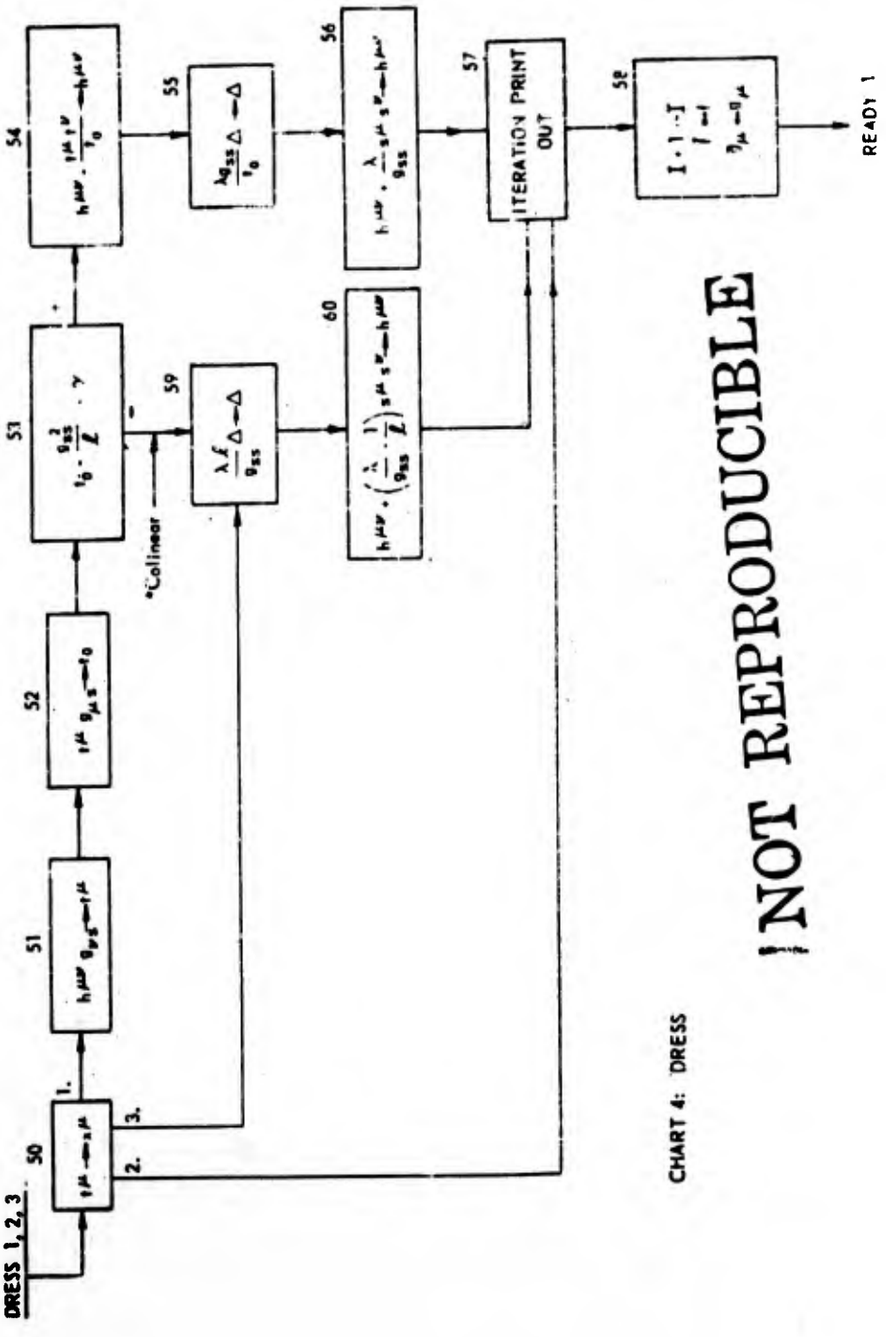

CHART 4: DRESS

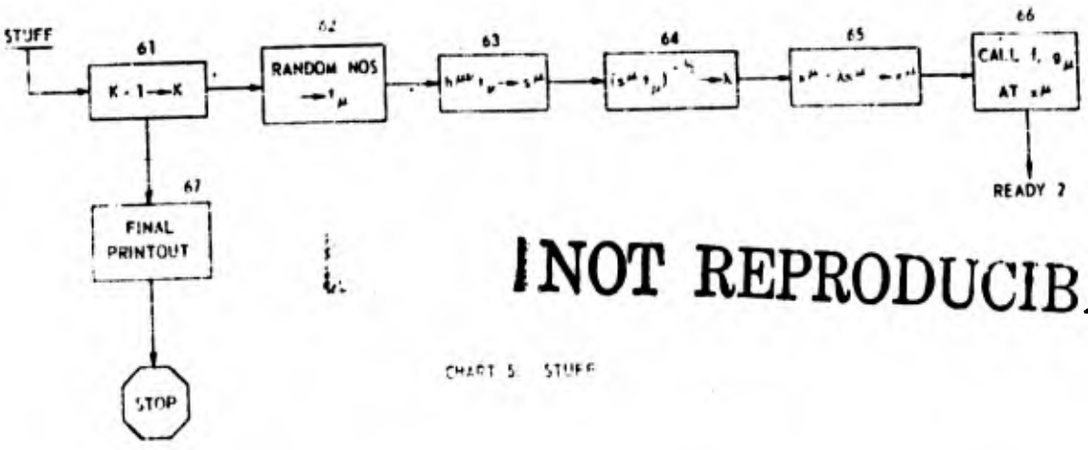

CHART 5 STUFF

The displacement of point $\underline{x}$ is chosen to be a unit length in terms of $h^{\mu\nu}$ as the metric. When $h^{\mu\nu} = \left\| \frac{\partial^2 f}{\partial x^\mu \partial x^\nu} \right\|^{-1}$, such a step will increase f by half the square of the length of the step.

If the direction were to be randomly distributed, then it would not be satisfactory to choose the range of each component of t_μ independently; rather, the range for the t_μ should be such that $h^{\mu\nu}\, t_\mu\, t_\nu$ is bounded by preassigned values. However, this refinement has not been incorporated into the charts nor the computer program. The length of the step has been chosen equal to one so that the function should increase by $\frac{1}{2}$ when each random step is taken.

Significance of $h^{\mu\nu}$:

We examine a least-squares analysis to illustrate how the initial trial value for $h^{\mu\nu}$ is chosen, and what its final value signifies. In this case, the function to be minimized will be chosen to be $\chi^2/2$, where χ^2 is the statistical measure of goodness of fit. The function $\chi^2/2$ is the natural logarithm of the relative probability for having obtained the observed set of data as a function of the variables χ^μ being determined.

The matrix $h^{\mu\nu} = \left\| \frac{\partial^2 f}{\partial x^\mu \partial x^\nu} \right\|^{-1}$ then specifies the spreads and correlations among the variables by

$$\langle \Delta x^\mu \Delta x^\nu \rangle = \frac{\int d^N x\, (x^\mu - \langle x^\mu \rangle)(x^\nu - \langle x^\nu \rangle) e^{-\chi^2/2}}{\int d^N x\, e^{-\chi^2/2}}$$

$$\approx h^{\mu\nu} \qquad (8.1)$$

The diagonal elements of $h^{\mu\nu}$ give the mean-square uncertainty for each of the variables, while the off-diagonal elements determine the correlations among them. The full significance of this matrix (the error matrix) is to be found in various works on statistics.[5] It enables us to determine the uncertainty in any linear function of the variables, for, if $u = a_\mu x^\mu$, then

$$\langle u \rangle = a_\mu \langle x^\mu \rangle$$

$$\langle (\Delta u)^2 \rangle = a_\mu a_\nu (\langle x^\mu x^\nu \rangle - \langle x^\mu \rangle \langle x^\nu \rangle)$$

$$= a_\mu a_\nu h^{\mu\nu} \tag{8.2a}$$

If u is a more general function of $\underline{x}$, then if in a Taylor expansion about the value of $\underline{x}$ derivatives higher than first can be ignored, we have

$$\langle u(\underline{x}) \rangle = u(\langle \underline{x} \rangle)$$

$$\langle \Delta u(\underline{x}) \rangle^2 = \frac{\partial u}{\partial x^\mu} (\langle \underline{x} \rangle) \frac{\partial u}{\partial x^\nu} (\langle \underline{x} \rangle) h^{\mu\nu} \tag{8.2b}$$

If it is possible to estimate the accuracy with which the variables are determined, the use of such estimates in the initial trial value of $h^{\mu\nu}$ will speed the convergence of the minimization procedure. Suppose, for example, that to fit some set of experimental data, it is estimated that the variables x^μ have the values:

$$x^1 = 3.0 \pm 0.1$$
$$x^2 = 28.0 \pm 2$$
$$x^3 = 10^4 \pm 10^2 \tag{8.3}$$

Then, the initial values for x^μ and $h^{\mu\nu}$ would be

$$x^\mu = (3.0 \quad 28.0 \quad 10^4)$$

$$h^{\mu\nu} = \begin{pmatrix} 0.01 & 0 & 0 \\ 0 & 4 & 0 \\ 0 & 0 & 10^4 \end{pmatrix} \tag{8.4}$$

If this estimate is even correct to within a couple of orders of magnitude, the number of iterations required to locate the minimum may be substantially less than that for some more arbitrary choice, such as the unit matrix.

If it is desired to impose linear constraints on the variables, this can be readily done by starting with a matrix $h^{\mu\nu}$ which is no longer positive definite, but which has zero eigenvalues. For the constraints

$$a_\mu x^\mu = \alpha$$

$$b_\mu x^\mu = \beta, \text{ etc.,} \tag{8.5}$$

the matrix $h^{\mu\nu}$ must be chosen so that

$$h^{\mu\nu} a_\nu = 0$$

$$h^{\mu\nu} b_\nu = 0 \tag{8.6}$$

and the starting value for x^μ must satisfy Eq. (8.5). For example, if x^3 is to be held constant, all elements of $h^{\mu\nu}$ in the third row and third column are set equal to zero and x^3 is set equal to the constant value.

When constraints are imposed, instead of setting Δ equal to the determinant of $h^{\mu\nu}$ (=0), it is set equal to the product of the non-zero eigenvalue of $h^{\mu\nu}$. Then, except for round-off errors, not only will the conditions (8.6) be preserved in subsequent iterations, but also Δ will continue to equal the product of non-zero eigenvalues.

Though Δ is not used in the calculations, its value may be of interest in estimating how well the variables have been determined, since $\sum_\mu h^{\mu\mu}$ gives the sum of the eigenvalues of $h^{\mu\nu}$, while Δ gives their product. The square root of each of these eigenvalues is equal to one of the principal semiaxes of the ellipse formed by all $\underline{x}$ for which $f(\underline{x})$ exceeds its minimum value by $\frac{1}{2}$.

9. CONCLUSION

The minimization method described has been coded for the IBM-704 using Fortran. Experience is now being gathered on the operation of the method with diverse types of functions. Parts of the procedure, not incorporating all of the provisions described here, have been in use for some time in least-squares calculations for such computations as the analysis of π-P scattering experiments,[6] for the analysis of delayed neutron experiments,[7] and similar computations. Though full mathematical analysis of its stability and convergence has not been made, general considerations and numerical experience with it indicate that minima of functions can be generally more quickly located than in alternate procedures. The ability of the metric, $h^{\mu\nu}$, to accumulate information about the function and to compensate for ill-conditioned $g_{\mu\nu}$ is the primary reason for this advantage.

The author wishes to thank Dr. G Perlow and Dr. M. Peshkin for valued discussions and suggestions, and Mr. K. Hillstrom for carrying out the computer programming and operation.

APPENDIX *

If we have the gradient of the function at a point in the neighborhood of a minimum together with $\underline{G}^{-1}$, where $\underline{G} = \left\| \frac{\partial^2 f}{\partial x^\mu \partial x^\nu} \right\|$, then, neglecting terms of higher order, the location of the minimum would be given in matrix notation by

$$\xi = x - \underline{G}^{-1} \nabla \tag{1}$$

In the method to be described, a trial matrix is used for $\underline{G}^{-1}$ and a step determined by Eq. (1) is taken. From the change in the gradient resulting from this step, the trial value is improved and this procedure is repeated. The changes made in the trial value for $\underline{G}^{-1}$ are restricted to keep the hunting procedure "reasonable" regardless of the nature of the function. Let $\underline{H}$ be the trial value for $\underline{G}^{-1}$. Then the step taken will be to the point

$$x^+ = x - \underline{H} \nabla \tag{2}$$

The gradient at x^+, ∇^+, is then evaluated. Let $D = \nabla^+ - \nabla$ be the change in the gradient as a result of the step $S = x^+ - x = -H \nabla$. We form the new trial matrix by

$$H^+_{\mu\nu} = H_{\mu\nu} + a(\underline{H} \nabla^+)_\mu (\underline{H} \nabla^+)_\nu \tag{3}$$

The constant a is determined by the following two conditions:

1. The ratio of the determinant of $\underline{H}^+$ to that of $\underline{H}$ should be between R^{-1} and R, where R is a preassigned constant greater than 1. This is to prevent undue changes in the trial matrix and, in particular, if $\underline{H}$ is positive definite, $\underline{H}^+$ will be positive definite also.

2. The non-negative quantity

$$\Delta = D \underline{H}^+ D + S (\underline{H}^+)^{-1} S - 2 S \cdot D \tag{4}$$

is to be minimized. This quantity vanishes when $S = \underline{H}^+ D$. The a which satisfies these requirements, together with the corresponding Δ, as functions of $N = \nabla^+ H \nabla^+$ and $M = \nabla^+ H \nabla$, are as follows: (8)

---

*The following method is a description of a simplified method embodying some of the ideas of the procedure presented in this report.

Range of M	a	Δ
$M < -N/(R-1)$	$1/(M-N)$	0
$-N/(R-1) < M < N/(R+1)$	$(1/RN) - (1/N)$	$(N - M + MR)^2/RN$
$N/(R+1) < M < NR/(R+1)$	$(N - 2M)/N(M - N)$	$4M(N - M)/N$
$NR/(R+1) < M < NR/(R-1)$	$(R/N) - (1/N)$	$(M + NR - MR)^2/RN$
$NR/(R-1) < M$	$1/(M-N)$	0

(5)

The dependence of Δ on M is bell-shaped, symmetric about a maximum at $M = N/2$, for which $a = 0$ and $\Delta = N$.

After forming the new trial matrix $\underline{H}^+$, the next step is taken in accordance with Eq. (2) and the process repeated, provided that $N = \nabla^+ H \nabla^+$ is greater than some preassigned ϵ. When the gradient is constant, it can be written as

$$\nabla = \underline{G}(x - \xi). \tag{6}$$

If u is an eigenvector of $\underline{HG}$ with eigenvalue one, then it will be an eigenvector of $\underline{H}^+\underline{G}$ with eigenvalue one as well, since

$$\begin{aligned} \underline{H}^+\underline{G}u &= \underline{HG}u + a\,\underline{H}\nabla^+(\nabla^+\underline{HG}u) \\ &= u + a\,\underline{H}\nabla^+[\nabla\underline{HG}(1 - \underline{HG})u] \\ &= u \end{aligned} \tag{7}$$

Furthermore, when $\Delta = 0$,

$$\underline{H}^+\underline{G}S = \underline{H}^+ D = S \tag{8}$$

so that S becomes another such eigenvector. After no more than N steps (for which $\Delta = 0$), $\underline{H}$ will equal $\underline{G}^{-1}$ and the following step will be to the exact minimum.

The entire procedure is covariant under an arbitrary linear coordinate transformation. Under these transformations of x, ∇ transforms as a covariant vector, $\underline{G}$ transforms as a covariant tensor of 2nd rank, and $\underline{H}$ transforms as a contravariant tensor of 2nd rank. The intrinsic characteristics of a particular hunting calculation are determined by the eigenvalues of the mixed tensor $\underline{HG}$, and the components of the initial value of $(x - \xi)$ along the direction of the corresponding eigenvectors. Since successive steps will bring $\underline{HG}$ closer to unity, convergence will be rapidly accelerating even when $\underline{G}$ itself is irregular. Constraints of the form $b \cdot x = c$ can be improved by using an initial $\underline{H}$ which annuls b, i.e.,

$$\underline{H} \cdot b = 0 \quad ,$$

and choosing the initial vector x such that it satisfies $b \cdot x = c$. Then all steps taken will be perpendicular to b and this inner product will be conserved. For example, if it is desired to hold one component of x constant, all the elements of $\underline{H}$ corresponding to that component are initially set equal to zero.

REFERENCES

1. A. Cauchy, Compt. Rend. 25, 536 (1847).

2. M. R. Hestenes and C. Stiefel, J. Research Natl. B. 409-36 (1952).

3. See, for example, F. B. Hildebrand, Introduction to Analysis, McGraw-Hill Book Co., Inc., New York W. A. Nierenberg, Report UCRL-3816 (1957).

4. R. L. Garwin and H. A. Reich, An Efficient Iterative Method (to be published).

5. E. g., H. Cramer, Mathematical Methods of Statistics University Press, Princeton, New Jersey (1946).

6. Anderson and Davidon Nuovo cimento, 10, 1238 (1

7. G. J. Perlow (to be published)

8. When the function is known to be quadratic, the fir dispensed with, in which case $a = (M - N)^{-1}$, $\Delta = 0$.